AN INVESTIGATION INTO SATELLITE DRAG MODELING PERFORMANCE

BY

Stephen Russell Mance

Submitted to the graduate degree program in Aerospace Engineering and the Graduate Faculty of the University of Kansas in partial fulfillment of the requirements for the degree of Master's of Science.

Chairperson: Dr. Craig McLaughlin

Committee Members: Dr. David Downing

Dr. Shahriar Keshmiri

Date Defended:_____

The Thesis Committee for Stephen Russell Mance certifies that this is the approved version of the following thesis:

AN INVESTIGATION INTO SATELLITE DRAG MODELING PERFORMANCE

Committee:

Chairperson: Dr. Craig McLaughlin

Dr. David Downing

Dr. Shahriar Keshmiri

Date Approved:_____

ABSTRACT

The errors in current atmospheric drag modeling are the primary source of error for orbit determination for objects in low Earth orbit (LEO) at lower altitudes in periods of high solar activity. This is a direct result of significant advancements in conservative force modeling in the form of high accuracy geopotential models. When these new geopotential models are applied to orbit determination packages, the majority of the error source shifts to non-conservative forces such as solar radiation pressure, Earth albedo, Earth infrared (IR), and atmospheric drag. During periods of high solar activity, the density of the atmosphere is highly variable due to interactions with the Sun and the upper atmosphere. These variations are very difficult for empirical density models to estimate and cause significant errors in deriving precise orbits. For this reason, increasing the accuracy and fidelity of atmospheric density models is crucial in order to further increase the accuracy of orbit determination during these times.

If equipped, on-board accelerometers can provide measurements of the non-conservative accelerations that a spacecraft encounters along its orbit. A very accurate approximation of the force on a spacecraft due to atmospheric drag can be found by accounting for all other non-conservative forces and considering the remainder to be drag. Accuracy is reduced when using that force to find the density of the atmosphere due to the nature of the drag equation. The drag coefficient (C_D) is used to balance the acceleration due to drag and the density of the atmosphere. Determining the value of

the drag coefficient is arduous for most applications. To make the process easier, the projected area (A) and mass (m) terms in the drag equation are often lumped together with C_D to form what is called the ballistic coefficient, C_DA/m. This is actually the inverse of the traditional definition of the ballistic coefficient. By using this term, the uncertainties in the projected area and mass can be lumped in with the drag coefficient.

Approximating the ballistic coefficient using two line element sets (TLE) was one objective of this research. TLEs are based on radar and optical observations and are thus are not nearly as accurate as other tracking methods, but are advantageous because of the multitude of satellites cataloged over the last several decades. The method of ballistic coefficient estimation presented here can be used quickly and without significant resources since TLEs are widely available. The results of this study indicate the ballistic coefficients generated for spacecraft in orbits less than 500 km in the 2001-2004 time period were within 8.2% of ballistic coefficients derived from analytical methods when using the analytical ballistic coefficients as truth. For satellites around 800 km or above, the ballistic coefficients generated were over 100% from those derived using analytical methods.

Creating corrections to existing density models has become a popular way of capturing these variations. Several techniques have been devised to generate these corrections in the past few decades. This thesis utilizes corrections to the NRLMSISE-00 empirical model of the atmosphere generated using the dynamic calibration of the atmosphere (DCA) technique. These corrections, along with the

NRLMSISE-00 empirical model, are implemented into GEODYN, NASA's precision orbit determination and parameter estimation program, to create three GEODYN versions; an unmodified GEODYN with the MSIS-86 atmospheric model, a version using the NRLMSISE-00 model, and a version using the DCA corrections. Any improvements using these new density routines will provide a direct benefit to orbit estimation which, in turn, improves science data.

In this thesis, the GEOSAT Follow-On (GFO), Starlette, Stella, and Geo-Forschungs-Zentrum-1 (GFZ-1) satellites were processed with the three versions of GEODYN in the waning of the most recent solar maximum. The results show that the NRLMSISE-00 empirical model can capture slightly more variations in the atmosphere than the previous MSIS-86 model, especially in high solar activity conditions. The DCA corrections produced results similar to the NRLMSISE-00 model, but after an investigation into the drag coefficient estimated through GEODYN, a more detailed investigation is necessary to determine the validity of these results. This is likely due to the altitude or time period of the satellites chosen for processing being outside the range of the DCA corrections to the NRLMSISE-00 routine.

ACKNOWLEDGEMENTS

First and foremost I would like to thank my adviser, Dr. Craig McLaughlin for the opportunity to conduct research under his advising. He provided many important didactic discussions in which I gained an enormous amount of understanding through his pedagogy. I would also like to thank Dr. Shahriar Keshmiri and Dr. David Downing for serving on my committee and providing valuable insight and feedback.

The researchers at NASA GSFC and SGT Inc. provided an invaluable experience by allowing me to visit and receive in-depth training on the GEODYN software package. While I was there, Frank Lemoine provided me with many insightful discussions and through his patience and guidance I was able to accomplish a great deal. Steve Klosko, Dave Rowlands, Doug Chinn, and Nikita Zelensky also provided many useful suggestions and instruction.

I would like to thank Kansas NASA EPSCoR for providing the funding which made much of this research possible through a Partnership Development Grant and also DOD EPSCoR. I also acknowledge Matthew Wilkins and Chris Sabol for their contribution of the test cases which verified the NRLMSISE-00 model and for their generous suggestions.

A portion of this research was provided by the Air Force Research Laboratory's Space Scholar program. I would also like to acknowledge several AFRL researchers including Chin Lin for providing a research topic, Sam Cable for

providing HASDM data, and Eric Sutton and Frank Marcos for many valuable discussions.

Lastly, I would like to thank all of those close to me. My family and friends have been extremely supportive of my efforts and I would not be in the place I am today without them.

TABLE OF CONTENTS

NOMENCLATURE

Symbol	Definition	Units
A	Satellite Projected Area	m^2
a_D	Acceleration due to drag	m/s^2
b_1	Daily DCA Coefficient	~
b_2	Daily DCA Coefficient	~
BC	Ballistic Coefficient	m^2/kg
C_D	Drag Coefficient	~
F	Wind Factor	~
h	Altitude	km
i	Inclination	deg
m	Mass	kg
Δn_M	Mean Mean Motion	rad/sec
n_M	Mean Motion	rad/sec
r	Distance from Center of Earth	km
t	Time	sec
v	Velocity	km/sec
w	Angular Velocity of the Earth's Rotation	rad/sec
X	Satellite State Vector	~

Greek Letter	Definition	Units
μ	Gravitational Parameter	m^3/s^2
ρ	Atmospheric Density	kg/m^3
ρ_m	Model Density	kg/m^4

Abbreviations	Definition
ANDE-RR	Atmospheric Neutral Density Experiment Risk Reduction
CHAMP	Challenging Mini-Satellite Payload
CNES	Centre National d'Etudes Spatiales
DCA	Dynamic Calibration of the Atmosphere
DORIS	Doppler Orbitography and Radiopositioning Integrated by Satellite
EGM	Earth Gravity Model
EUV	Extreme Ultra-Violet
FCal	Fence Calibration
GEODYN	Geodynamics
GEOSAT	Geodynamics Satellite
GFO	GEOSAT Follow-on
GFZ	GeoForschungsZentrum
GGM	GRACE Gravity Model
GPS	Global Positioning System
GRACE	Gravity Recovery and Climate Experiment
GSFC	Goddard Space Flight Center

HASDM	High Accuracy Satellite Drag Model
ILRS	International Laser Ranging Service
IR	Infrared
LEO	Low Earth Orbit
MAA	Mock ANDE Active
MSIS	Mass Spectrometer Incoherent Scatter
NASA	National Aeronautical and Space Administration
NOAA	National Oceanic and Atmospheric Administration
NORAD	North American Aerospace Defense Command
NRL	Naval Research Laboratory
OPR	Once Per Revolution
POD	Precision Orbit Determination
SGP4	Simplified General Perturbations Satellite Orbit Model 4
SLR	Satellite Laser Ranging
SO	Space Objects
SSN	Space Surveillance Network
STAR	Spatial Triaxial Accelerometer for Research
STARSHINE	Student Tracked Atmospheric Research Satellite for Heuristic International Networking Experiment
T/P	TOPEX/Poseidon
TDRSS	Tracking and Data Relay Satellite System
TOPEX	Topography Experiment

TRANET	Tracking Network

LIST OF FIGURES

LIST OF TABLES

1 INTRODUCTION

1.1 Objectives

The overarching objective of this research is to improve and verify satellite drag models and to enhance current understanding of the effects the upper atmosphere has on satellites. This goal is achieved by testing atmospheric models on several satellites, and creating and verifying estimates of satellite ballistic coefficients. This research should improve prediction and determination for lower accuracy orbits which would improve catalog maintenance. This research also has the potential to allow for an increase in the accuracy of orbit determination (OD) by providing advances that will be advantageous to OD software in the form of increased accuracy.

1.2 Motivation

Density in the upper atmosphere remains one of the foremost uncertainties when processing a low Earth orbit (LEO) satellite's position. At altitudes less than 1000 km, satellites encounter an appreciable acceleration due to atmospheric drag. The atmosphere that causes this force is highly variable, and is greatly affected by the Sun and its complex cycle. The Sun heats up the atmosphere through extreme ultra-violet (EUV) radiation, which causes the upper layers to be pushed higher. In addition, the Sun releases charged particles, or ions, which are then subject to interaction by the Earth's magnetic field. The Sun also progresses through an 11 year solar cycle, causing periods when the intensity of these effects is increased

significantly. These effects make understanding and modeling solar and geomagnetic activity crucial to density modeling.

Drag estimation is further complicated when predicting the interaction between the atmosphere and the spacecraft. At satellite altitudes, the atmosphere consists of free floating particles, and can no longer be considered a continuum fluid. This means that typical approaches to estimating the drag force must be modified. Drag estimation for satellites requires as much knowledge as possible of the atmosphere any given spacecraft is traveling through. This includes the density of the neutral particles, charged particles, the constituents of the atmosphere and precise knowledge of the spacecraft's position, geometry, and attitude. These effects are increased with lower satellite mass, higher satellite area, and lower orbit.

Several atmospheric models have been created over the years. Two popular models are the Naval Research Laboratory's (NRL) NRLMSISE-00 model which is the latest of the Mass Spectrometer Incoherent Scatter (MSIS) family of models [Ref. 1], and the High Accuracy Satellite Drag Model (HASDM) which is derived from the Jacchia family of models [Ref. 2]. A listing and brief history of the atmospheric models can be found in Vallado [Ref. 3]. These models provide estimates of many atmospheric parameters, but with so much variability, capturing the small scale changes the atmosphere undergoes is difficult. Many techniques have been developed to fine tune atmospheric models to include these variations. One such technique is dynamic calibration of the atmosphere (DCA). HASDM uses this method by employing calibration satellites to provide better spatial and temporal resolution [Ref.

2]. Corrections using similar techniques have been created for other models, including NRLMSISE-00 [Ref. 4, 5]. These correction techniques are essential to estimating atmospheric parameters with high precision.

By understanding and fine tuning the process of modeling and predicting atmospheric density, errors in OD may shrink for some satellites. This is partly due to recent advancements in modeling the geopotential forces satellites experience, making atmospheric drag the primary source of error for satellites in certain regimes. Advances in this field will also directly benefit satellites carrying sensors that require a high degree of OD accuracy, for example satellite altimeters whose ability to provide accurate results is directly dependent on precise knowledge of the spacecraft's orbit. Additionally, more accurate atmospheric models will increase accuracy of satellite orbit prediction.

1.3 Precision Orbit Determination Challenges

Orbit determination refers to the process of obtaining knowledge of a satellite's motion relative to the center of the Earth in a specified coordinate system [Ref. 6]. This state estimation process incorporates observations influenced by random and systematic errors using a mathematical model which is not exact. Precision orbit determination (POD) is essential for many science missions to return accurate results. This is especially true in the case of satellite altimeters where the accuracy of the data returned is solely based on the precision of the estimated orbit. POD requires mathematical models which represent the forces experienced by the

spacecraft to be as accurate as possible. Some of the forces experienced by a spacecraft are summarized from Reference 3.

1.3.1 Geopotential Forces

An orbiting spacecraft does not experience a constant acceleration of gravity along its orbit due to the non-spherical nature of the Earth. In order to account for this, potential functions can be used to represent the acceleration due to gravity from an aspherical body on a spacecraft. The potential function is developed with spherical harmonic functions to represent the Earth's non-spherical shape. A description of this technique is detailed in Reference 3. This process provides a rudimentary approximation of the geopotential forces a satellite will experience. To generate a more precise estimation of the gravity field, satellite-derived gravity fields become necessary.

The fidelity of spherical harmonic functions is expressed as two numbers representing the degree and order of the function. The degree and order define the associated Legendre functions, and determine how many terms can be computed to represent the geopotential of the Earth. These values can be compared to two dimensional curve-fitting techniques where higher degree polynomials will be able to represent a given data set with less error. Also similar to curve-fitting, the higher the degree/order of the spherical harmonic, the more computational resources are required to process the function.

There have been significant improvements in estimating potential coefficients to the spherical harmonic expansion of the Earth's gravitational potential over the years. These improvements are predominately accomplished by extending the highest degree in the expansion by utilizing satellite data, and increasing the accuracy of the coefficients that improves geographic coverage. The work done for the Earth Gravity Model (EGM) EGM96 achieved estimations of 30'x30' anomalies (arcmin) and degree-and-order 360 using satellite tracking data, satellite altimeters and surface gravity data [Ref. 7]. This model combined data from various sources, including satellite-to-satellite tracking through Global Positioning System (GPS) and Tracking and Data Relay Satellite System (TDRSS), and conventional satellite tracking data through Satellite Laser Ranging (SLR), Tracking Network (TRANET), and Doppler Orbitography and Radiopositioning Integrated by Satellite (DORIS). Although the EGM96 model provided significant advances in spatial resolution, many areas like western China and Antarctica still included only sparse data or had virtually no terrestrial anomaly data.

Several satellites devoted to mapping the Earth's gravitational field have been launched in the past ten years. The Challenging Mini-Satellite Payload (CHAMP) (launched in 2000) and the Gravity Recovery and Climate Experiment (GRACE) (launched in 2002) have provided several widely available satellite-only gravity field models. The initial GRACE gravity models (GGM), designated as GGM01S and EIGEN_GRACE01S, were derived using 111 days of early GRACE data from April to November of 2002 and made available in July of 2003. These models produced

calibrated global RMS orbit errors of 2 cm uniformly over land and ocean for degree and order 70 [Ref. 8]. The newest GRACE gravity model, GGM02S, has reduced the orbit error due to geopotential modeling to approximately 7 mm when using a spherical harmonic of degree 70 [Ref. 9]. This model improves by a factor of two over the previous gravity models. Other models have been compiled based on CHAMP and GRACE science data, such as the models generated at the German Research Centre for Geosciences, GFZ Potsdam. The high resolution global gravity field model, EIGEN-CG01C, which uses degree and order 360 has been estimated to improve the overall accuracy of gravity field modeling to the 20 cm level [Ref. 10]. The improvements in gravity modeling have reduced the modeling errors of the conservative force considerably, shifting the major source of error to non-conservative forces.

1.3.2 Atmospheric Drag

Satellites in LEO with altitudes of 1000 km or less experience non-negligible accelerations due to atmospheric drag. This effect increases as the altitude lowers. Atmospheric drag comes into play when performing orbit determination, estimating a satellite's lifetime, and investigations into the nature of the upper atmosphere. A better understanding of the atmosphere provides advances in OD, and allows for technological advancements in maneuvering such as aerodynamic breaking.

Advances in conservative force modeling have shifted the majority of error in OD to the non-conservative forces such as drag, SRP, and Earth albedo. With refined

gravity models, drag becomes one of the largest sources of error for LEO regimes at lower altitudes [Ref. 11]. The atmosphere is influenced by many variations, which highly complicates the estimation process. These variations cause many inconsistencies in the atmospheric density and constituency. The largest factor influencing atmospheric variation is the Sun. The Sun has a heating effect on the atmosphere, both by direct EUV radiation, and by creating ionized particles that are then influenced by the Earth's magnetic field. The variations cause the atmospheric levels to rise and fall and create winds which can cause noticeable changes in accelerations due to drag on the spacecraft. During periods of solar maximum, errors become even more significant because both the density magnitude and variability increase. This means that in addition to a larger effect by drag forces, these forces are also more difficult to predict. Better modeling the density in the upper atmosphere (especially in periods of high solar activity) is crucial in order to improve OD for low Earth orbit (LEO) spacecraft.

At satellite altitudes, the atmosphere can no longer be considered a fluid. Collisions between molecules become more infrequent at these altitudes, and momentum exchanges between individual molecules and a spacecraft surface provide the force considered to be atmospheric drag. This assumption is known as the kinetic theory of gases, which helps to generate estimates of the drag coefficient, C_D, used in the estimation of accelerations due to atmospheric drag on a spacecraft [Ref. 12]. The details and challenges of this process are described in a subsequent section.

The major time-varying influences that cause changes in the Earth's atmosphere summarized from Reference 3 are:

- Diurnal variations
- 27-day solar-rotation cycle
- 11-year solar cycle
- Semi-annual/seasonal variations
- Cyclical variations
- Rotating atmosphere
- Winds
- Magnetic-storm variations
- Irregular short-periodic variations
- Tides

1.3.2.1 Diurnal variations

The atmosphere experiences variations that occur daily as the Earth rotates. As the Sun heats the Earth, the atmosphere heats up and the layers rise. This bulge lags the direction of the Sun by approximately 2-3 hours, becoming the most pronounced around 2:00-2:30 P.M. local time [Ref. 3]. The minimum also lags the Sun's direction, occurring around 4:00 A.M. every day. The bulge is generally centered on the equator, but does rise and fall in latitude based on the season. Due to this bulge, the latitude, local time and season are important when estimating forces due to atmospheric drag.

1.3.2.2 27-day solar-rotation cycle

The Sun rotates on its axis through a 27 day period. Any local activity experienced on the surface of the Sun will rotate with the Sun through this period. This rotation causes a fluctuation in the radiation levels experienced at the Earth as active regions rotate to face the Earth then retreat. There are significant problems modeling this variation due to uncertainties in determining the growth, stability and decay of the active regions of the Sun.

1.3.2.3 11-year solar cycle

The principal periodic variation of the Sun is the 11-year cycle. The solar radiation that reaches the Earth varies throughout the cycle. Solar maximum creates several complications in determining forces on the spacecraft by the large effect on the upper atmosphere. In addition to the increase in atmospheric variation, the solar radiation levels also rise slightly.

The term ‘sunspots’ originates from astronomers who observed dark spots on projections of the Sun’s light through a telescope. The sunspots tend to occur in groups and appear predominately in solar latitudes between 5 and 30 degrees [Ref. 13]. The cycles have shown tremendous variability over the centuries. The Sporer and Maunder minima of the 15th and 17th centuries had exceptionally low sunspot counts which lasted for decades. These variations about the cycles create difficulties in predicting the Sun’s behavior.

The solar cycle causes a periodic variation of the amount of radiation, especially EUV, which reaches the Earth. Since the EUV cannot be directly measured on the Earth, the radiation from the sun at the 10.7 cm wavelength is used as a proxy. This F10.7 value also varies throughout the solar cycle.

1.3.2.4 Semi-annual/seasonal variations

As the Earth orbits the Sun, the distance between the two varies. When this is combined with the change in declination of the Sun throughout the year, small variations which last around six months are seen.

1.3.2.5 Cyclical variations

In addition to the 11-year cycle of sunspots, the Sun has an 11-year cycle which follows the sunspot cycle. The minima of this cycle does not occur exactly between the maxima. A maximum in this cycle, which varies from cycle to cycle, takes six to seven years for a full recovery. The cause of this cycle is thought to be related to the 11 year sunspot cycle.

1.3.2.6 Rotating atmosphere

Friction between the Earth and in the atmosphere causes the atmosphere to rotate with the Earth. This causes a time varying change in density which, as altitude decreases, the velocity increases due to an increase in friction.

1.3.2.7 Winds

The winds in the stratosphere and mesosphere are dominated by the Coriolis force [Ref. 13]. The result is a north-south pressure gradient due to solar heating, resulting in an eastward wind in winter and a westward wind in summer. The Sun's radiation causes winds to flow from the equator to the poles during the day, and the reverse at night. These geostrophic winds provide similar disturbances in the upper atmosphere, causing fluctuations in density by way of temperature variations.

1.3.2.8 Magnetic-storm variations

The ions created by the ionization of the Earth's atmosphere by the Sun's radiation are highly influenced by the Earth's magnetic field. Any changes in the magnetic field will cause slight changes in the density of the atmosphere. With high geomagnetic activity, a bulge will appear around the poles and propagate to the opposite pole. This effect becomes more significant as geomagnetic activity increases in periods of geomagnetic storms. The storms are caused by increases in the solar wind which is deflected around the Earth and to the poles by the Earth's magnetic field [Ref. 3].

1.3.2.9 Irregular short-periodic variations

A number of other disturbances with a small influence in atmospheric density exist and are often associated with transient geomagnetic disturbances. These include

random solar flares, variations of hydrogen currents in the atmosphere, and other small effects [Ref. 3].

1.3.2.10 Tides

Ocean tides and atmospheric tides cause some slight variations in atmospheric density. Tides caused by the Moon and the Sun move westward with periods corresponding to the lunar or solar day respectively. These perturbations cause thermospheric velocities of up to 200 m/s on a 24-hour period, driven largely by the solar tide. The temperature distribution centered at the equator creates winds in the thermosphere around 40 m/s during the day and around 120 m/s at night. The smaller winds during the day are a result of the drag force created by ions interacting with the Earth's magnetic field being higher during the day [Ref. 3].

1.3.3 Third-Body Perturbations

At higher altitudes, typically when the effects of atmospheric drag begin to diminish, perturbations from third bodies such as the Sun or Moon become noticeable. These forces are gravitational and thus conservative in nature and can be estimated using a disturbing-function solution. For more information on this formulation, see Reference 3.

1.3.4 Radiation Pressure Forces

Radiation pressure forces consist of solar-radiation pressure (SRP), Earth albedo, and Earth infrared (IR). Each of these are non-conservative forces, meaning that the mechanical work done in moving the spacecraft between two points is dependent on the path taken. This means that a model of the radiation pressure forces must be both time and spatially dependent.

Solar-radiation pressure becomes more dominant than atmospheric drag and the largest non-conservative force at altitudes in excess of 600-800 km. Solar radiation is one of the most difficult disturbing forces to model because of the Sun's constant variability. The sun progresses through an 11 year solar cycle, switching from solar minimum, where solar variations and solar storms are few, and solar maximum, where intense solar storms cause many difficulties in modeling and predicting variations. In addition to the difficulties modeling the Sun's behavior, there are many more difficulties modeling its effect on a satellite. Finding the acceleration imparted to a spacecraft from the Sun's radiation requires first determining the:

- Sun's precise location
- Satellite's precise position
- Exact value of the solar-radiation pressure
- Effective, time varying, cross-sectional area exposed to the radiation
- Correct, time varying coefficients that model the satellite's reflectivity

Earth albedo is the reflection of the Sun's radiation off the Earth back on a satellite. Pressure caused by this reflection is around 30% of the pressure force generated by SRP [Ref. 3]. Earth also emits infrared energy at about 237 W/m^2 [Ref. 3] and can be a measurable acceleration on some spacecraft at certain altitudes.

In order to solve for the acceleration on spacecraft caused by the radiation pressure forces, many orbit determination programs must model the geometry of the satellites as either a collection of flat plates, or in many cases as a box-wing structure due to the nature of the satellite/solar array design. An example of this modeling technique is presented in Reference 14. This allows the ability to assign different emissivity coefficients to specific parts of the spacecraft. This modeling technique also provides the capability to define shadowing as well as diffuse and specular reflectivity coefficients; which are essential to finding the overall acceleration due to radiation pressure.

1.3.5 Magnetic Field

Charged particles in the Earth's magnetic field can cause perturbations on a spacecraft, depending on the amount of charge and the electric field inherent to the spacecraft. This is due to the Lorentz force which describes the force caused by electromagnetic fields interacting with each other. This force does not change the semi-major axis of the orbit, but will create a torque on the spacecraft. The magnetic field is also modeled as a spherical harmonic positive gradient of the potential

function to be consistent with the geopotential function. For more information on the representation of this field potential, consult Reference 3.

1.3.6 Tides

Traditionally the term 'tides' refers to ocean tides, although tides actually include solid Earth, ocean, pole, and atmospheric tides. Tides are the result of gravitation distortion caused by other body effects (i.e. the Sun or Moon distorting the Earth). Determining this effect is a very complicated process and has only recently been studied as new computational and observational resources have become available. The tides are a function of many periods:

- The Earth's diurnal motion
- The Earth's rotation
- The Moon's motion

All of these periods have repetitive frequency so a harmonic expression is commonly used to represent the tidal potential. The tidal potential itself is not directly observable, but can be derived from the vertical and horizontal components of gravity [Ref. 3].

Solid Earth tides typically have the largest perturbing effect of all tides, the majority of which is caused by the Moon. Complications arise when considering the Earth as a non-uniform body with an interior structure which consists of both liquid and solid matter. The pole tides refer to the phenomenon of the Earth's rotation causing a tide due to a centrifugal effect. This is generally taken into account in the

coefficients of the solid Earth tide. With the increase in tracking precision over the years, many satellites have provided advances in estimation of solid Earth tides [Ref. 3].

Ocean tides cause a change in mass distribution due to gravitational attraction with the Sun and Moon. The effects of ocean tides on spacecraft are claimed to be only 10-15% of solid Earth tides [Ref. 15]. In general, ocean tides cannot be distinguished from solid Earth tides. Since ocean tide models are more uncertain than solid Earth models, the ocean tides are estimated in the presence of a fixed solid Earth tide model [Ref. 16]. Data returned by the TOPEX/Poseidon (T/P), launched in 1992 and operational until 2006, has provided altimeter returns with an orbit accuracy of 1.5 cm in the radial direction when utilizing the GRACE gravity field model GGM02C and tracking data [Ref. 17]. This is an order of magnitude better than the planned radial orbit accuracy of 13 cm, due largely to the refined gravity models. The follow on radar altimeter satellite to T/P, Jason-1, has achieved orbit accuracy in the radial direction of 1 cm [Ref. 18]. The Navy's GEOSAT Follow-On (GFO) satellite has radial orbit accuracy down to the 5 cm level for the precise orbits. The main goal of GFO is to perform satellite altimetry on the Earth's oceans. In doing so, GFO has helped to improve ocean tide models. Atmospheric tides have little effect on geopotential perturbations, but create difficulties when modeling drag accelerations.

1.3.7 Thrust

Thrust is considered an acceleration that causes a perturbation on a spacecraft's orbit. Differences in commanded thrust firings and actual thrust generated are generally small but not negligible. Motor firings do not occur instantaneously, and have anomalies due to variations in mass flow rate or specific impulse. For short, impulsive thrusts of five minutes or less, numerical-propagation is often used to advance the satellite to the time of the maneuver, then the velocity change is added to the velocity vector, where the numerical propagation is continued using the new velocity.

1.4 Satellite Drag Coefficients

Any time atmospheric drag is translated into density or vice versa, the effects of the drag acceleration must be separated from the drag coefficient. This becomes increasingly more important to accelerometer satellites measuring all non-conservative accelerations on a spacecraft. The density is found by modeling all radiation pressure forces and considering the remainder to be atmospheric drag. This provides an extremely accurate estimation of the acceleration due to drag on the spacecraft. This accuracy is reduced when translating this acceleration into density due to the nature of the relationship between drag acceleration and density. Consider the drag equation:

$$a_D = -\frac{1}{2}\rho v^2 \frac{C_D A}{m} \tag{1.1}$$

In order to solve for the density, ρ, all of the other quantities must be well known. The velocity relative to the atmosphere, v, can be determined with a high degree of certainty in most applications. The mass, m, of the spacecraft is also typically well known. The projected area, A, is often difficult to calculate. If the spacecraft has any consistent orientation, or is spherical, the problem becomes easier, but for satellites with complex geometry the process is much more arduous.

In Eq. **(1.1)**, the fraction $C_D A/m$ is known as the ballistic coefficient (BC). This is actually the inverse of the traditional definition of the ballistic coefficient. Lumping the drag coefficient in the BC is frequently more convenient than finding values for each term individually. In doing so, the need to find the orientation of the satellite over time, as well as the extent of difficulties discussed above with determining C_D is alleviated. In order to determine BC in most cases, density values must be known first, then BC values and density corrections may be found simultaneously and the process might be iterated [Refs. 19, 20].

The drag coefficient, C_D, is very difficult to separate from density. Historically, three types of drag coefficients have been analyzed; fixed drag coefficients, fitted drag coefficients, and physical drag coefficients [Ref. 21]. A fixed drag coefficient of 2.2 has been frequently used throughout the years from studies based on laboratory measurements in the mid 1960s [Ref. 22]. Using fixed values of C_D alleviates some of the difficulties in processing and creating atmospheric density models. Fitted drag coefficients are frequently used in precise orbit determination with the help of an atmospheric model. Physical drag coefficients are based on the

interactions of the incoming molecules on the spacecraft and are directly related to the drag force.

In order to obtain accurate density measurements, C_D is often estimated analytically. Cook built much of the groundwork that has become the standard of analytical drag coefficient calculation today [Ref. 22]. This reference applies the concept of free-molecule flow to artificial satellites. Pressure sensors and mass spectrometers in orbit have returned enough data to enable realistic theoretical models of the gas-surface interaction that is used to calculate the physical drag coefficients [Ref. 21]. Determining the physical drag coefficient is challenging because C_D is a function of many factors [Refs. 22, 21, 23, 24, 25, 26, 27, 28, 29].

- Spacecraft geometry
- Material properties of the spacecraft surface
- Duration the spacecraft has been in orbit
- Atomic species of atmosphere
- Altitude regime
- Orbit inclination

Most of these factors are complications in predicting the adsorption or re-admittance of the molecules interacting with the spacecraft. The total momentum transfer is dependent on the direction of the incoming molecule, the type of collision (specular or diffuse), and the velocity of the incoming and reflected molecule. This means the geometry of the spacecraft in relation to the incoming flow must be known. The material properties and duration in orbit will govern how the molecules will

collide. Studies have shown that surfaces are contaminated by adsorbed molecules over the course of a satellite's lifetime [Ref. 30]. The drag coefficients are also highly dependent on the regime the satellite is in because the constituency of the upper atmosphere varies based upon both altitude and location [Ref. 31]. Different molecules impart different momentum to a spacecraft depending on the rate of adsorption or re-admittance of that molecule.

To complicate the estimation further, the atomic species change as a function of solar and geomagnetic activity. Sutton recently described some of the pitfalls in determining satellite drag coefficients for the CHAMP spacecraft [Ref. 32]. Sutton showed that the method Sentman [Ref. 33] uses is more accurate at predicting densities that match the High Accuracy Satellite Drag Model (HASDM) when modeling CHAMP normalized force coefficients than the theory based on Schamberg's [Ref. 34] method that Cook [Ref. 22] made popular. This implies that the hyperthermal assumptions employed by Schamberg are inadequate and accounting for random thermal variations of the atmosphere is important in modeling force coefficients for satellites such as CHAMP.

A recent study comparing physical drag coefficients with histories of the orbital decay of several satellites during the recent solar maximum was performed to take advantage of recent data on spheres and attitude stabilized satellites [Ref. 21]. The fitted drag coefficients were obtained from an analysis of the decay of the semi-major axis from two line element sets while modeling all principle orbital perturbations. The results of this study indicate spherical satellites modified by solar

cells or other objects provide difficulties in determining reliable drag coefficient values because of an often misreported area and shape change. The study also found that energy accommodation coefficients are typically higher at solar maximum and decrease slowly with an increase in altitude.

1.5 Atmospheric Density Models and Measurements

In order to perform precision orbit determination on satellites in low Earth orbit, force models must be used to account for the accelerations on the spacecraft. Forces due to atmospheric drag are generally the largest non-conservative perturbing forces satellites in LEO experience. For this reason, there has been much advancement over the years in atmospheric density modeling and correcting.

1.5.1 Models

Empirical density models have made significant advancements in the past 50 years. A good depiction of the progress and variety is shown in Reference 3, page 563. The models are categorized as either obtaining total density from satellite drag, or using temperature and composition from the ground and in-situ instruments to model the atmosphere.

1.5.1.1 Jacchia 1971

The Jacchia 1971 model was an update to the Jacchia 1970 model. The new model had a larger emphasis on capturing more variations. This was accomplished by

altering the analytical formulation used for Jacchia 1970. These changes also alleviated some numerical issues involving the helium-hydrogen layer which eliminated the necessity of introducing ad hoc variations for semiannual variations from temperature variations [Ref. 35]. In the model, the upper atmosphere is separated into a region from 90-125 km, and from 125 km up. Jacchia employs a fixed boundary condition at 90 km, and assumes mixing between 90 and 100 km, then diffuse equilibrium above 100 km. This model has remained the foundation of a number of other empirical models, including Jacchia-Roberts, Jacchia-Bowman, and HASDM.

1.5.1.2 MSIS-86

The MSIS-86 empirical model of the atmosphere was an upgrade from the MSIS-83 empirical model which was based on in situ data from seven satellites and several rocket probes, as well as five ground based incoherent scatter stations. MSIS-86 ranges upward from 90 km, and used temperature and composition data from the Dynamics Explorer satellite to improve resolution of the polar region over MSIS-83 [Ref. 36]. Newer terms were added to better represent seasonal variations. This better captured the density in both quiet and active magnetic conditions. The MSIS family relies on equations and tabulated coefficients as lookups to represent the variations in the atmosphere. For this reason, it is difficult for the routine to accurately model small-scale density variations.

1.5.1.3 NRLMSISE-00

The MSIS-86 model has since been upgraded into MSISE-90, [Ref. 37] which primarily extended MSIS-86 into the middle and lower atmosphere, and then NRLMSISE-00. NRLMSISE-00 extends from the ground to the exobase, and is a major upgrade of the Mass Spectrometer Incoherent Scatter Radar (MSIS) family of models. The model incorporates total mass density from satellite accelerometers and from orbit determination, includes temperature and incoherent scatter radar, allows for a new component, "anomalous oxygen," and includes molecular oxygen number density from solar ultraviolet occultation aboard the Solar Maximum Mission [Ref. 1]. These updates of the model allow for a more accurate prediction of drag forces on a spacecraft.

The MSIS series of models uses temperature as the core of the MSIS formulation. The model allows the user to compute both the total mass density provided by past generations of MSIS and an effective mass density, which includes anomalous oxygen. Until now, the model database has not included either drag measurements or satellite accelerometer data. The new NRLMSISE-00 includes these data sets. In a comparison table with NRLMSISE-00 and MSIS-90, NRLMSISE-00 has the smallest standard deviation when compared to the Jacchia-70 model [Ref. 1]. This is shown for a range of altitudes and for high and low geomagnetic activity.

1.5.1.4 HASDM

The High Accuracy Satellite Drag Model (HASDM) is an initiative started by the Air Force Space Battlelab in January 2001 to improve Air Force Space Command's ability to meet Space Surveillance Capstone Requirements for satellite trajectory prediction accuracy [Ref. 2]. HASDM estimates and predicts, in 3 hour updates, a global density field which is constantly varying. The model applies mostly to satellites in the <600 km altitude regime and HASDM can make predictions up to three days in advance.

HASDM uses the Dynamic Calibration of the Atmosphere (DCA) technique to generate corrections using 75 space objects (SO) orbiting in low Earth orbit. The SOs are tracked by the Space Surveillance Network (SSN) and consist of a range of orbital characteristics. The SOs are all in LEO altitudes of less than 600km and have a reasonably consistent frontal area. This procedure uses tracking data on these calibration satellites to determine corrections to the Jacchia 70 empirical density model [Ref. 38]. HASDM can make forecasts of several days in advance by performing this process in near-real time. The corrections themselves are spherical harmonics of two of the Jacchian temperature parameters which improve spatial resolution. The calibration satellites provide a spatial resolution not available from traditional empirical models of the atmosphere.

1.5.2 Corrections

Current atmospheric density models can not adequately estimate nor predict the short term variations that exist in the upper atmosphere. For this reason, many techniques have become available to capture these small scale variations. Using empirical atmospheric models as a baseline, corrections can be generated using various methods presented in this section. These corrections are created to fine-tune specific empirical models, and usually result in temporal and spatial improvements in density modeling.

1.5.2.1 Dynamic Calibration of the Atmosphere

The method for Dynamic Calibration of the Atmosphere was pioneered by Gorochov and Nazarenko in the early 1980's [Ref. 4]. Originally the corrections were determined around every 3 hours from a set of calibration satellites to supplement geomagnetic data. This technique is now typically performed using North American Aerospace Defense Command (NORAD) two line element sets which yield results around once per day. HASDM uses SSN tracking data, but this data is not generally available to the public [Ref. 2]. The DCA technique is significant because it permits the first breakthrough of the generally accepted 10-15% error in atmospheric models [Ref. 3]

As many as 477 space objects have been utilized to generate these corrections; however, recent work has shown that as few as 15-20 space objects are required to

generate a statistically optimal solution [Ref. 5]. The number of satellites used to generate the corrections is dependent upon a number of factors and is geared toward finding the optimal density correction using a minimal amount of computational resources. Knowing that changes in the estimated ballistic factor are predominantly caused by errors in the density model, the DCA method uses position and velocity observations of satellites as pseudo-observations of the atmosphere in order to reduce the scattering of ballistic factor estimates. Therefore corrections to the density model can be constructed by removing as much structure as possible from the estimates of ballistic factor.

Reference 39 describes a technique of generating time-dependent global corrections to the Jacchia 1970 atmospheric model using tracking data from four satellites. This work helped to pave the way for the corrections generated to the Jacchia 1970 atmospheric model that are incorporated into the High Accuracy Satellite Drag Model (HASDM). HASDM uses the DCA technique to generate corrections using 75 space objects (SO) in low Earth orbit (LEO). The SOs are all in altitudes of less than 600km and have a reasonably consistent frontal area. The HASDM implementation of DCA makes corrections to select parameters of a density model. The method uses the statistical uncertainties and observations of satellites directly to supply a single weighted differential correction across the calibration satellites [Ref. 38].

Yurasov and Nazarenko have recently used the DCA technique to correct the NRLMSISE-00 density model in the region of 200-600 km. The method relies on 39

carefully selected drag perturbed space objects [Ref. 40, 41]. This work has been summarized and is available in References 42, 43, 44 and 45. The drag data is produced using a minimization technique then tabulated as coefficients to a correcting equation [Ref. 40].

1.5.2.2 POE Density

Recent studies have advanced density modeling using the precision orbit ephemerides (POE) of several satellites to generate density corrections using accelerometer satellites for calibration [Ref. 46]. POE data consists of precise position and velocity vectors obtained from global positioning system (GPS) receivers and satellite laser ranging (SLR) observations. Corrections to several atmospheric density models were created using POE, with the largest improvement appearing in the Jacchia family of empirical models. This work improved density modeling over existing atmospheric models regardless of solar and geomagnetic activity levels.

1.5.3 Accelerometers

Utilizing accelerometers onboard spacecraft has become one of the primary methods of generating atmospheric density data. Accelerometers are capable of measuring the non-conservative accelerations on a spacecraft. These accelerations are then separated into drag and radiation pressure forces such as SRP, Earth albedo, and Earth IR. This can then be used to find density by modeling all radiation pressure

forces and considering the remainder to be atmospheric drag. This provides an extremely accurate representation of the drag force on a spacecraft created by atmospheric density. Atmospheric density data supplied using accelerometers yields high temporal resolution, but low spatial coverage at any given time. This is due to the few satellites flying with accelerometers on board for this kind of processing. The two main missions capable of these measurements are the CHAMP and GRACE satellites. These satellites fly at roughly the same altitude (300-400 km) in near-circular, polar orbits. This provides full coverage of the Earth, but only in their relatively small altitude regime.

Since beginning its mission almost ten years ago, CHAMP data has enabled many investigations into the nature of the atmosphere. Preliminary results on atmospheric studies were analyzed and presented as a number of papers in Reference 47. One of those papers details the process of replacing non-conservative force models with accelerometer data to derive precise orbits [Ref. 48]. The reference goes on to describe the importance of using external measurements to the accelerometer such as SLR in order to calibrate these high accuracy accelerometers. The reference also notes the problems associated with the accelerometers needing calibration at the poles where variations are high due to geomagnetic activity. These regions would benefit greatly from local SLR observations, but no stations capable of SLR exist near the poles.

Reference 49 describes some of the practical challenges deriving accelerometer densities creates when analyzing data gathered throughout a satellite's lifetime. The

accelerometer instrument must be corrected for maneuvers, specific events such as orbit raising, and instrumental bias before the total density can be returned. Reference 50 provides a detailed description of the CHAMP satellite and instrumentation on board, along with comparisons done from the accelerometer derived densities to several other density models.

1.6 Precision Orbit Determination Software

Two different orbit determination software packages are used in this research. The original goal of this research was to increase the accuracy in GFO's precise orbits using GEODYN. Since then, other satellites like Starlette, Stella, and GFZ-1 have been processed using GEODYN to support some of the discoveries made by processing GFO.

1.6.1 GEODYN

The information contained in this section is summarized from Reference 51. GEODYN is a precision orbit determination and geodetic/geophysical parameter estimation program which has been operational since 1985. The Planetary Geodynamics Branch at the National Aeronautical and Space Administration's (NASA) Goddard Space Flight Center (GSFC) produces orbits for many satellites using GEODYN. The orbit determination program is a batch, least-squares filter that processes numerous types of tracking data. GEODYN is the primary tool for space

geodesy applications and is used and supported on an international level. GEODYN has the capability to estimate:

- Position and velocity of tracking stations
- Plate tectonics
- Gravity field
- Time dependent gravity
- Geoid parameters
- Sea surface topography
- Ocean and earth tides
- Earth orientation parameters

In order to solve the orbit prediction problem, GEODYN uses Cowell's method which numerically integrates the satellite equations of motion in rectangular coordinates directly. Using the initial conditions of epoch position and velocity, GEODYN is equipped with models of the following acceleration-producing forces:

- Geopotential
- Luni-solar potential
- Planetary potential
- Radiation pressure
- Solid Earth and ocean tidal potential
- Atmospheric drag
- General acceleration

1.7 Satellites Analyzed

Nine satellites were analyzed using various methods presented in this thesis. One of the objectives of this research was to attempt to improve orbits for the GEOSAT Follow-on (GFO) satellite. This objective makes GFO stand out from the rest of the satellites analyzed for the second objective of this project which is ballistic coefficient analysis. The GFZ-1 satellite was also processed using GEODYN but not the BC method. Table 1.1 shows the characteristics of each of the satellites analyzed for all objectives.

Seven different satellites were analyzed for the ballistic coefficient analysis portion of this research. Most satellites processed are in near circular orbits and cover a range of typical LEO altitudes in order to determine the performance in different regimes. The majority of the satellites were chosen because there has been previous work done in determining BCs using various methods. The BC values generated by those methods are used as a comparison for the BC results from this project.

Table 1.1 Satellites [Ref. 52]

Satellite	Perigee Alt. (km)	Eccentricity	Inclination (deg)	Mass (kg)	Launch Date	Decay Date
ANDE-RR (MAA)	400	0.007	51.6	52.04	21-Dec-06	25-Dec-07
CHAMP	474	0.00396	87.27	400	15-Jul-00	~
GFO	800	0.008	108	300	10-Feb-98	~
GFZ-1	398	0.000	51.6	20.6	19-Apr-95	23-Jun-99
GRACE-A	485	0.005	89	432	17-Mar-02	~
Starlette	812	0.0206	49.83	47	6-Feb-75	~
Starshine-2	380	0.002	39	40	5-Dec-01	26-Apr-02
Starshine-3	470	0.000066	67.048	91	30-Sep-01	21-Jan-03
Stella	802	0.0017	98.6	48	26-Sep-93	~

1.7.1 GEOSAT Follow-On (GFO)

Figure 1.1 GEOSAT Follow-On (GFO) [Ref. 53].

The primary mission of the GEOSAT Follow-On (GFO) spacecraft is to measure both relative and absolute ocean height through radar altimetry. GFO was launched on February 10, 1998 into a near circular, 800 km altitude, sun-synchronous orbit with an inclination of 108 degrees. GFO utilizes a 17-day exact repeat ground track to provide continuous ocean observations for both real-time and near-real-time measurements [Ref. 54].

The precursor to GFO was the U.S. Navy's GEOSAT mission which was launched on March 12, 1985 into an 800 km, 108 degree inclination orbit [Ref. 7]. The GEOSAT mission had a classified geodetic mission from March 31, 1985 to September 30, 1986 followed by a 17.05-day cycle exact repeat mission phase from November 8, 1986 to December 30, 1989 [Ref. 55]. The classified portion of the mission was declassified by the Navy in 1995, allowing for the National Oceanic and

Atmospheric Administration (NOAA) to produce geophysical data records for the entire GEOSAT mission in 1997.

Soon after deployment of GFO, the dual frequency GPS receivers on GFO were found to supply only limited data, and could not be used for precision orbit determination (POD). This presented a challenge in maintaining the designed accuracy of the altimeter. GFO is equipped with a single-frequency (13.5 Ghz) altimeter, a dual frequency water vapor radiometer, a dual-frequency Doppler beacon for operational tracking, and a laser retro reflector array for POD. Since the GPS receivers were found to be inadequate to derive orbits, both precise and operational orbits are determined through satellite laser ranging (SLR) as well as DORIS tracking in combination with altimeter crossovers [Ref. 54]

GFO was built for the U.S. Navy by Ball Aerospace and launched via a Taurus launch vehicle from Vandenberg Air Force Base. The satellite was declared operational on November 29, 2000 and has returned almost six years of altimeter data over 120 repeat cycles. NOAA is responsible for the distribution of GFO's altimeter data. The precise and operational orbits for GFO are determined at NASA GSFC using the GEODYN precision orbit determination and parameter estimation program.

Knowledge of the orbit is crucial to altimeter satellites, particularly in the radial direction since the only way to discriminate the changes in height (topography) of the ocean is the radial direction. The precision of the orbit is largely affected by the quality of the tracking data, and the fidelity of the force measurements. Traditionally, the major components of error for force modeling at 800 km are gravity, and non-

conservative forces. GEODYN currently uses the MSIS-86 density model in processing the orbits for GFO [Ref. 36]. GEODYN is also equipped with two tuned gravity models, PGS7727 and PGS7777b, produced specifically for GFO from the CHAMP mission data [Ref. 56]. Those gravity models reduce the error in the radial component of the orbit due to the conservative force model errors from 65.2mm (JGM-2, 1993) to 10.0mm (PGS7777b, 2003) [Ref. 54]. This provides an increase in the radial accuracy of the precise orbits to the 5 cm level.

1.7.2 CHAMP

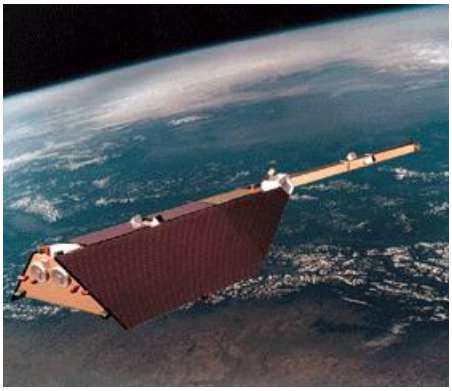

Figure 1.2 Challenging Minisatellite Payload (CHAMP) [Ref. 57].

The CHAMP satellite was launched on July 15, 2000 into a near-circular, 454 km orbit with 87.3 degree inclination. The main goal of the CHAMP mission is to study and understand the Earth as a system composed of solid, fluid, and gaseous parts which have complex interactions. The primary mission objectives are: mapping of the magnetic and gravity fields of the Earth and monitoring the ionosphere and troposphere, with a secondary objective to monitor thermospheric density. To achieve

those objectives, CHAMP carries a number of instruments; two fluxgate magnetometers, an Overhauser magnetometer, a digital ion-drift meter, a GPS receiver for orbit determination and limb sounding of the atmosphere, a laser retro-reflector array, and the Spatial Triaxial Accelerometer for Research (STAR) [Ref. 50].

1.7.3 GRACE

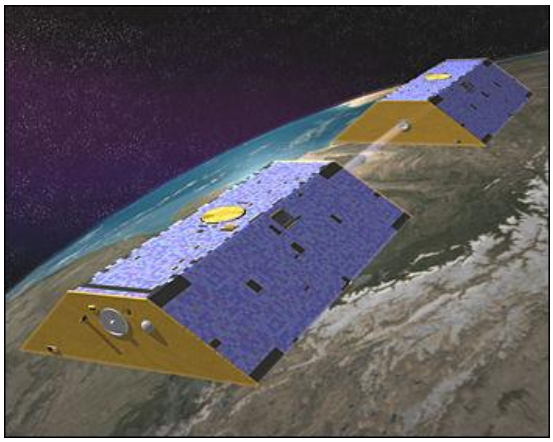

Figure 1.3 Gravity Recovery and Climate Experiment (GRACE) [Ref. 58].

The two GRACE satellites were launched on March 17, 2002 into near-circular orbits of 500 km altitude, with an inclination of 89.5 degrees. The primary objective is to map the global gravity field with a spatial resolution of 400 km to 40,000 km every thirty days. The designed mission lifetime was 5 years, but has already surpassed that, returning science data for over 8 years.

The two satellites are separated by approximately 220 km along track, and linked by a highly accurate inter-satellite, K-Band microwave ranging system [Ref.

8]. Each satellite carries GPS receivers, attitude sensors, and high precision accelerometers. The purpose of flying two satellites is to remove the effects of oscillator instability by combining the K-Band phase measurements during ground processing to produce an ionospheric-free ‘dual one-way’ measurement [Ref. 59]. As each satellite progresses along the orbit, the leading satellite will encounter all of the small-scale accelerations first, which changes the distance between the satellites. This change in distance is measured using the K-Band range measurements, and the effects of non-gravitational forces acting on the satellite are removed using the precise accelerometers that measure surface force acceleration. This process is used to determine the gravitational field components down to a few hundred kilometers. The precise time-tagging necessary for this mission is provided using the GPS receivers on each satellite.

1.7.4 ANDE-RR

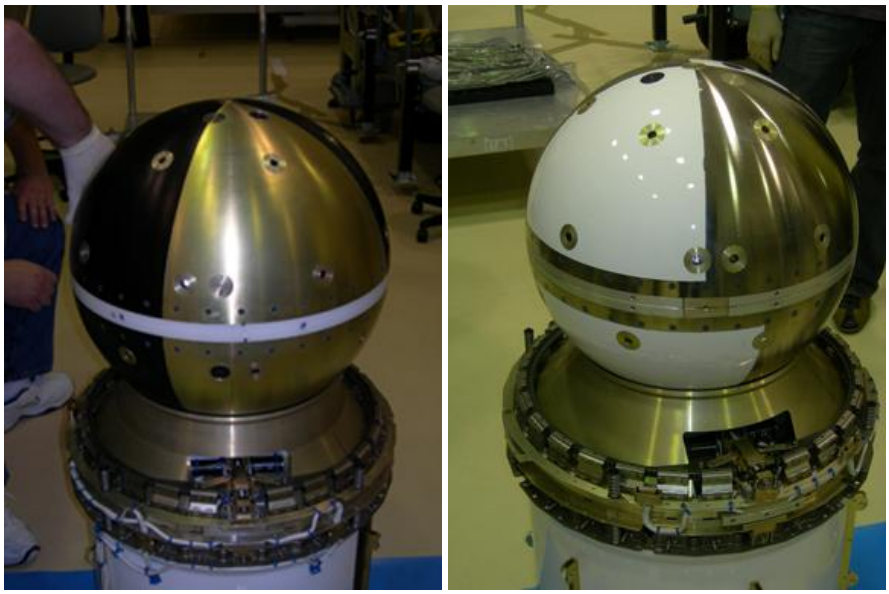

Figure 1.4 Atmospheric Neutral Density Experiment Risk Reduction (ANDE-RR) [Ref. 60].

The ANDE-RR mission was launched on December 9, 2006 aboard the Space Shuttle Discovery and deployed on December 21, 2006. The primary mission objective was to test the deployment mechanism aboard the Shuttle in order to prepare the ANDE satellites which were launched on July 30, 2009. The scientific objectives consist of: monitoring total neutral density along the orbit for improved orbit determination of resident space objects, monitor the spin rate and orientation of the spacecraft, and provide a test object for polarimetry studies [Ref. 61].

The mission consists of two spheres, the Mock ANDE Active (MAA) sphere and the Fence Calibration (FCal) sphere. Each of the satellites is fitted with retro-reflectors for satellite laser ranging. The International Laser Ranging Service (ILRS)

provides the SLR observations for the ANDE-RR satellites [Ref. 62]. The spherical nature of these satellites provides a constant and well determined cross section and surface properties which enhances the ability to recover atmospheric drag.

1.7.5 Stella/Starlette

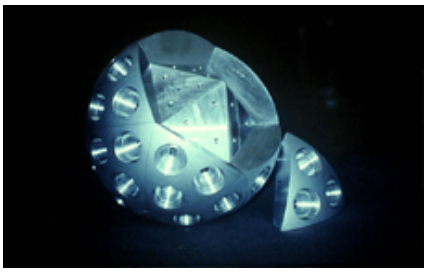

Figure 1.5 Starlette. [Ref. 63]

The Starlette satellite was launched by the French Centre National d'Etudes Spatiales (CNES) on February 6, 1975 into a 49.8 degree orbit with apogee and perigee heights of 1105 and 810 km respectively. The satellite has a radius of 12 cm and a weight of 47.295 kg. This low area to mass ratio was designed specifically to minimize the effects of non-gravitational forces and was achieved by using a core comprised primarily of uranium 238 [Ref. 64]. This high density, specular reflecting sphere has a skin of aluminum alloy containing a total of 60 corner reflectors for satellite laser ranging.

Figure 1.6 Stella. [Ref. 63]

The Stella satellite is a follow-on to the Starlette satellite. Stella was launched on September 26, 1993 into a near circular orbit with a perigee altitude of 802 km, 98.6 degree inclination, and eccentricity of 0.0017. The objectives of Stella mirror those of Starlette, as do the design. Stella is also a 12 cm radius sphere with a mass of 48 kg and has 60 corner reflectors for SLR observations.

1.7.6 STARSHINE 2 & 3

The STARSHINE satellites are spherical student satellites that are optically reflective. The project's objective is to increase student participation and interest in space by allowing students an opportunity to polish the satellites many small, front surface, aluminum mirrors and provide the students the opportunity to take optical observations of the satellites. The U.S. Naval Research Laboratory performed the development and final assembly of the satellites. Students took part in measuring the magnitude of the daily decrease of the satellite's period by optical observations due to

sunlight reflection, and from there made rudimentary calculations of the force due to aerodynamic drag [Ref. 65].

Figure 1.7 STARSHINE 2 [Ref. 66].

STARSHINE-2 was deployed from the Space Shuttle Endeavor on December 16, 2001 into a 370 km, 51.6 degree near circular orbit. The satellite had 858 mirrors covering the outside of the satellite's surface. The satellite also had thirty one laser retro-reflectors, enabling SLR observations. STARSHINE-2 carried a cold gas thruster which provided a 5 degree per second rotation after the satellite was deployed from the shuttle. The satellite reentered the Earth's atmosphere on April 26, 2002.

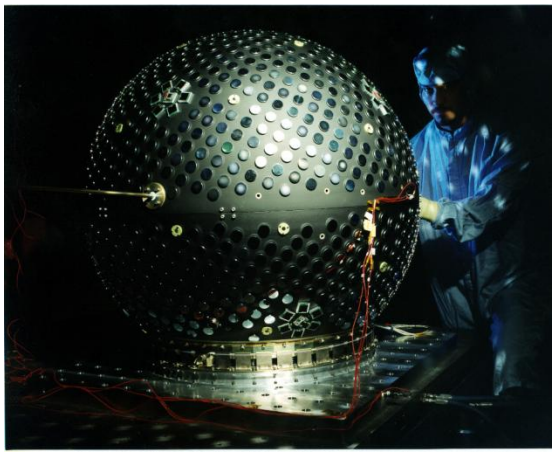

Figure 1.8 STARSHINE 3 [Ref. 67].

STARSHINE-3 was launched by a Athena I launch vehicle on September 29, 2001 into a 470 km near-circular orbit with 67 degree inclination. STARSHINE-3 was the largest of the STARSHINE series so far, with a radius of 0.47m and a mass of 91 kg. The satellite also had thirty one laser reflectors in enable SLR observations, and 1500 mirrors that were polished by approximately 40,000 students. The satellite was spun at a rate of 5 degrees per second at launch, but that spin rate decayed to nearly zero after its third month in orbit. STARSHINE reentered the Earth's atmosphere on January 21, 2003, nearly two years earlier than predicted due to increased solar activity.

1.7.7 GFZ-1

Figure 1.9 GFZ-1 [Ref. 68].

The GeoForschungsZentrum-1 (GFZ) satellite was launched from the MIR space station on April 19, 1995 into a 398 km, near circular orbit with an inclination of 51.6 degrees. GFZ-1 is a spherical satellite approximately 21 cm in diameter with a launch mass of 20 kg. The satellite was tracked using its 60 corner reflectors using SLR until the satellite reentered the atmosphere on June 23rd, 1999. The SLR tracking data for this satellite is sparser than other satellites at higher altitudes because of the effect of the Earth's atmosphere on the spacecraft. As the satellite decays, the tracking passes become shorter. This is coupled with the difficulty of predicting the satellite's orbit due to the variable nature of the atmosphere. Even with these complications, tracking data is available for this spacecraft until shortly before its demise. This demonstrated some of the possibilities and difficulties of tracking an object so close to the earth.

2 METHODOLOGY

This thesis consists of an evaluation of the NRLMSISE-00 empirical atmospheric model as well as corrections to that model using the DCA technique. A subsequent study was performed on estimating satellite ballistic coefficients using TLEs. These two avenues of research allow for an evaluation of the performance and application of atmospheric density models. This chapter will cover some of the techniques and methods of evaluation used in these studies.

2.1 TLE Processing Method

The Space Surveillance Network (SSN) has an extensive database of two line elements (TLEs) since they began collecting routinely over 40 years ago. The TLEs are calculated on the order of twice per day using radar or optical observations by the SSN and give all orbital elements required to determine an orbit. The TLEs are determined from several routine observations of LEO objects per day using a low-order analytic solution to Newton's second law for a realistic gravitational potential and a dissipative atmospheric environment called the general perturbations method. A description of the TLE format is described in Reference 69 and reprinted here.

Data for each satellite consists of three lines in the following format:

```
AAAAAAAAAAAAAAAAAAAAAAAA
1 NNNNNU NNNNNAAA NNNNN.NNNNNNNN +.NNNNNNNN +NNNNN-N +NNNNN-N N NNNNN
2 NNNNN NNN.NNNN NNN.NNNN NNNNNNN NNN.NNNN NNN.NNNN NN.NNNNNNNNNNNNNN
```

Line 0 is a twenty-four character name.

Lines 1 and 2 are the standard Two-Line Orbital Element Set Format identical to that used by NORAD and NASA. The format description is:

Table 2.1 NORAD Two Line Element Set Format [Ref. 69]

Line 1	
Column	***Description***
01	*Line Number of Element Data*
03-07	*Satellite Number*
08	*Classification (U=Unclassified)*
10-11	*International Designator (Last two digits of launch year)*
12-14	*International Designator (Launch number of the year)*
15-17	*International Designator (Piece of the launch)*
19-20	*Epoch Year (Last two digits of year)*
21-32	*Epoch (Day of the year and fractional portion of the day)*
34-43	*First Time Derivative of the Mean Motion*
45-52	*Second Time Derivative of Mean Motion (decimal point assumed)*
54-61	*BSTAR drag term (decimal point assumed)*
63	*Ephemeris type*
65-68	*Element number*
69	*Checksum (Modulo 10)* *(Letters, blanks, periods, plus signs = 0; minus signs = 1)*
Line 2	
Column	***Description***
01	*Line Number of Element Data*
03-07	*Satellite Number*
09-16	*Inclination [Degrees]*
18-25	*Right Ascension of the Ascending Node [Degrees]*
27-33	*Eccentricity (decimal point assumed)*
35-42	*Argument of Perigee [Degrees]*
44-51	*Mean Anomaly [Degrees]*
53-63	*Mean Motion [Revs per day]*
64-68	*Revolution number at epoch [Revs]*
69	*Checksum (Modulo 10)*

All other columns are blank or fixed.

TLEs are not nearly as accurate as other tracking methods, but with so many objects being tracked, there is still significant potential for learning about the upper atmosphere. This potential was realized by many pioneers of the dynamic calibration of the atmosphere technique who used TLEs and other observations very similar to TLEs. Since then, TLEs have been used to generate corrections to several atmospheric density models.

Picone et al. developed a method to derive densities from TLEs using the Simplified General Perturbations Satellite Orbit Model 4 (SGP4) [Ref. 70]. This process uses the change in mean motion, n_M, to determine forces acting on the spacecraft.

$$\rho \cong \frac{\frac{2}{3}\mu^{\frac{2}{3}} n_M^{\frac{-1}{3}} \Delta n_M}{BC \int v^3 F dt} \tag{2.1}$$

Since the mean motion, n_M, and mean mean motion Δn_M are given or can be found with the TLEs and the gravitational parameter, μ, is well known, the remaining quantities must be determined. The velocity, v, is found by propagating the TLEs with the SGP4 propagator. This is then integrated with F, the wind factor. King-Hele suggests in Reference 71 that a good approximation of the wind factor is

$$F \cong \left(1 - \frac{rw}{v}\cos i\right)^2, \tag{2.2}$$

where r is the distance of the object from the center of the Earth, w is the angular velocity of the Earth's rotation, and i is the inclination of the orbit. All of these quantities are either well known, or can be obtained from the TLEs. The remaining

term in Eq. **(2.1)**, the ballistic coefficient (BC) suggests again the difficulty in determining densities using satellite observations since the BC must first be estimated in order to obtain accurate densities. This relies on some sort of analytical calculation, or previous work to achieve reasonable results with satellites of complex geometry. The result is a single density estimate for every two TLEs.

The method for processing two line elements (TLEs) into ballistic coefficients is based on the work by Picone et al. from Reference 70. This is accomplished by rearranging Eq. **(2.1)** to solve for BC to yield the following equation:

$$BC \cong \frac{\frac{2}{3}\mu^{\frac{2}{3}} n_M^{\frac{-1}{3}} \Delta n_M}{\oint \rho v^3 F dt} \tag{2.3}$$

The density is supplied by an atmospheric model, in this case HASDM, using the position obtained using the SGP4 propagator. It is then incorporated into the integral to provide a better estimate of what atmosphere the satellite encountered along its orbit. Along with the procedure for acquiring densities from TLEs, the BCs are estimated once per every two TLEs since they are determined by taking the average of the mean motion.

2.2 Orbit Determination

Orbit determination refers to the process of estimating the orbital characteristics of a satellite relative to the primary celestial body. This process can be performed on any orbiting body, either natural satellite or man-made. Most man-made satellites (hereafter referred to solely as satellites) generally have significantly

different size, mass, and orbital characteristics from natural satellites which increases the effects from nongravitational forces on the satellite's orbit. For satellites orbiting close to the central body, the point mass assumption is no longer valid due to the topography and constituency of the central body. This makes gravity variations one of the primary concerns when modeling forces on a satellite to perform orbit estimation. Information presented in this section has been summarized primarily from Reference 6. Additional information on orbit determination can be found in References 3 and 51.

The state of a dynamical system refers to the set of parameters necessary to predict the future motion of the system. In the case of a satellite, the minimum set of parameters to predict future motion are the position and velocity of the spacecraft at some epoch. This minimum set of parameters can be expanded to include dynamic and measurement model parameters to increase the estimation accuracy. The state of the system at time, t, is generally denoted as $\mathbf{X}(t)$. To estimate the state of the system at some time, t, the *a priori* state information is use in conjunction with differential equations that govern the system's motion integrated over time. The result of this process is not accurate enough for many applications because the initial state is never known exactly, and both the equations of motion and forces modeled are only approximated. To achieve a higher degree of accuracy, the spacecraft must be tracked or observed from stations with precisely known locations. The tracking provides an enhanced estimate of the satellite's state but is not exact because of the influence of random and systematic errors.

Using orbit determination, the predicted state will differ from the true state due to the following effects which appear in Reference 6.

1. *Inaccuracies in the estimated state vector (i.e. position and velocity vector) caused by errors in the orbit determination process, such as:*
    a. *Approximations involved in the method of orbit improvement and in the mathematical model,*
    b. *Errors in the observations,*
    c. *Errors in the computational procedure used in the solution process.*
2. *Errors in the numerical integration procedure caused by errors in the dynamical model and computer truncation and round off errors.*

GEODYN is an optimal orbit determination package in use by NASA GSFC. The term ‘optimal’ refers to the best estimate in a least squares sense. These packages provide instantaneous estimates of some key parameters in order to obtain higher accuracy. These are quantities like:

- Position and velocity
- Drag coefficient
- Local atmospheric density
- Solar radiation pressure coefficients
- Measurement biases
- Station position and biases

By allowing these parameters to be estimated using the software and by utilizing some of the recent advances in gravity field modeling, orbital errors have

shrunk for some satellites below the centimeter level [Ref. 18] when using accurate tracking methods such as GPS, satellite laser ranging, and Doppler tracking.

2.3 GEODYN Setup

GEODYN was used for analyzing the performance of the NRLMSISE-00 empirical atmospheric model and corrections to that model when compared to the MSIS-86 model using several satellites in various regimes. A version of the GEODYN version 0712 source code and canned GEODYN setups for the GFO satellite were provided by the Planetary Geodesy group at NASA's GSFC. GEODYN was compiled and the setups provided were used as a benchmark to validate the GEODYN program. The output matched all sample outputs provided to a reasonable degree using the comparison metrics described in the next section, so the program was considered to be compiled successfully. The gravity field model being used by GEODYN for all of the satellites processed for this research is the GRACE/LAGEOS based EIGEN-GLO4C global gravity field model. This gravity model is complete to degree and order 360 and resolves some anomalies from previous models [Ref. 72]. The ocean tides are modeled with the GOT99.2 ocean tide model derived from TOPEX/Poseidon altimetry [Ref. 73]. For processing GFO, a macromodel is used to model the accelerations from the radiation pressure forces and atmospheric drag [Ref. 54].

2.3.1 Atmospheric Modeling Upgrade

The original goal of upgrading GEODYN was to reduce orbit errors for the GFO spacecraft near solar max. This could be accomplished by reducing the error due to atmospheric drag modeling. To accomplish this, two new instances of GEODYN version 0712 were created and evaluated in addition to the original. After these new versions of GEODYN were created, the same test cases that were used to verify the original version of GEODYN were run using the modified versions. As expected, the results were not exactly the same as the original cases, but with help from researchers at NASA's GSFC, the routines were verified to be correctly implemented.

2.3.1.1 NRLMSISE-2000 Modification

The first modified version of GEODYN incorporates the NRLMSISE-2000 subroutine. This subroutine was obtained as FORTRAN code from the supplementary code to Reference 3. The routine was incorporated into GEODYN using the previous MSIS-86 driver as a template. In order to ensure the updated version of GEODYN produces results consistent with the NRLMSISE-00 model, the subroutine itself must be verified. A test protocol was developed consistent with previous work [Ref. 74] where a series of 21601 (several days worth of satellite data in five second increments) test cases were evaluated using the new subroutine. The resulting total density from the subroutine fell within 0.03% of the test protocol data. For the test protocol, only the daily averaged value of global geomagnetic proxy Ap were

utilized. The test protocol was designed in a manner consistent with how the density corrections were generated with only the daily Ap data being used. However, for maximum precision, GEODYN requires that all of the geomagnetic data be supplied (daily and 3-hourly). The results presented here utilize all the available geomagnetic data.

2.3.1.2 DCA Corrections Modification

The second modified version has the NRLMSISE-2000 subroutine and corrections using DCA supplied from Yurasov and Nazarenko [Ref. 40-41]. These corrections are tailored directly for the NRLMSISE-2000 model. The corrections used are valid from January 2000 to November 2003 up to a 600 km altitude. Due to these limitations, the application of DCA corrections to the GFO orbit is not expected to make a significant statistical difference in the GFO orbit error.

The drag data is produced using a minimization technique then tabulated as coefficients to the following equation [Ref. 40].

$$\left(\frac{\delta\rho}{\rho_m}\right) h,t \;=b_1\;\; t \;+b_2\;\; t \quad h-400\;\;/200 \tag{2.4}$$

Where b_1 and b_2 are daily coefficients generated by DCA, h is the altitude in km, and ρ_m is the model density. This equation, along with the capability to read in the coefficient data file, was added as a routine into GEODYN. The routine was also added in order to pave the way for a new set of corrections we plan to generate which will be extended to GFO's altitude using DCA. If a particular day does not have an

associated correction, the equation simplifies so that the NRLMSISE-00 density value is multiplied by unity and remains unchanged.

2.4 GEODYN Comparison Methods

Several metrics of comparison have been investigated in order to evaluate the performance of the modified versions of GEODYN. These comparison methods are used to determine the performance of each routine at estimating either the satellites state, or how well the new density models represent the drag on each satellite.

2.4.1 Orbit Overlaps

The duration through which a satellite's state is computed is traditionally referred to as an arc. Arcs can be any length of time, but are generally not longer than one week. The driving factor behind the duration of an arc is accuracy. As the length of time increases, the accuracy tends to decrease depending on the coverage of tracking data. However, the accuracy can also decrease if the arc is too short due to a limited amount of measurement data. Arcs are usually specified to be between any maneuvers or significant changes in attitude because of difficulties in estimation through these changes.

One way to show an improvement in force modeling is to compare orbit overlaps between adjacent arcs. When each arc is computed there are a number of time steps where the duration of the arc overlaps with adjacent computed arcs. During those overlaps, the prediction of the state will be slightly different from adjacent arcs,

which include the same time span. Small overlaps imply precision in the state estimate. The improvement of the drag model should be most notable in the along-track component of the position and velocity vectors since the drag force appears predominately in the along-track direction.

2.4.2 SLR RMS of Fit Residuals

All of the satellites processed with GEODYN for this research are equipped with retro-reflectors to enable satellite laser ranging observations. This SLR tracking provides range measurements with millimeter accuracy. This tracking accuracy translates into very precise orbit accuracy when sufficient coverage is achieved. There are many tracking stations all over the globe to assist in providing the high level of orbit accuracy. A listing of the stations and their corresponding locations is depicted in Figure 2.1. Most all of the SLR data are weighted at 10 cm, although some of the SLR stations are downweighted to between 60 cm and 1 meter depending on the accuracy in the station location and measurements [Ref. 54].

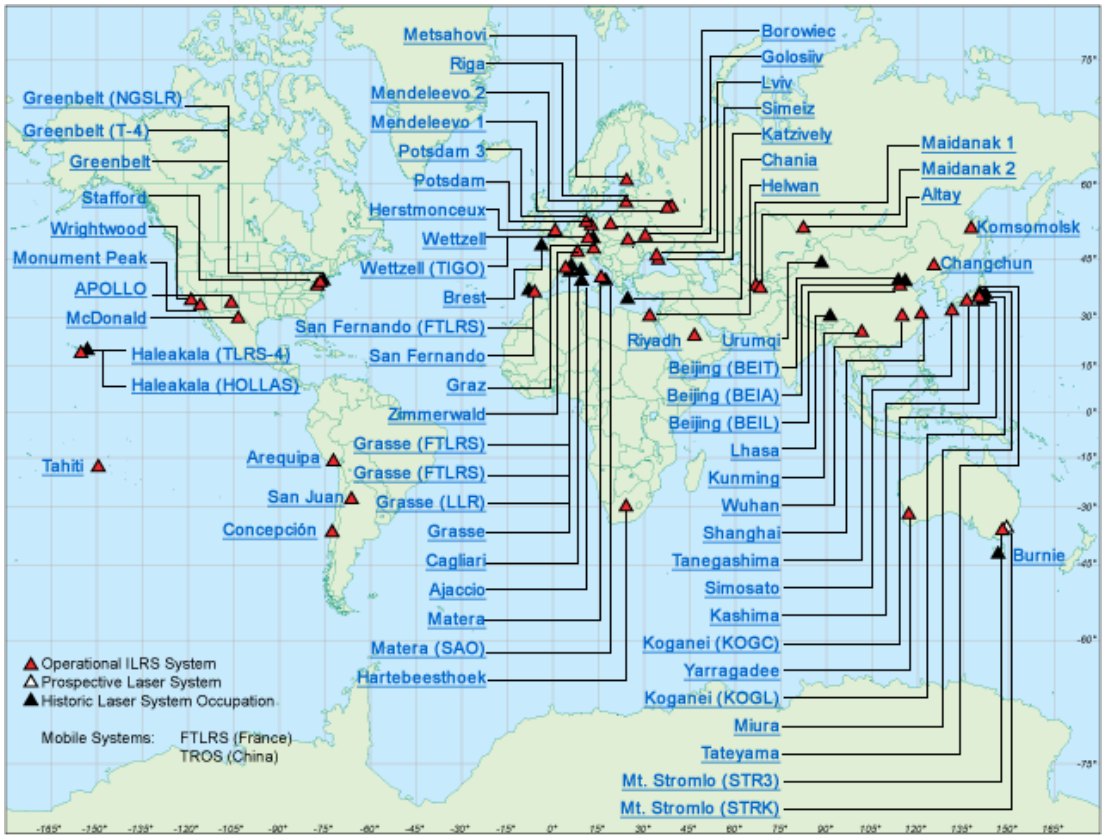

Figure 2.1 ILRS Satellite Laser Ranging Stations [Ref. 75].

The SLR RMS of fit for each set of runs is computed using GEODYN and represents the consistency of the orbit estimation to the observations. A decrease in the SLR RMS of fit indicates that the forces on the spacecraft that are modeled are a better representation of the actual forces on the spacecraft, and thus a decrease in error from that modeling technique. This translates to a smaller error in the position, which is measured by the SLR RMS of fit. The SLR RMS analysis is the best estimate of the orbit accuracy because the measurements are very precise.

2.4.3 Empirical Accelerations

In satellite orbit determination, all of the forces, both conservative and nonconservative, are modeled to the highest fidelity possible. However, since none of the force models are perfect, once per revolution (OPR) empirical accelerations have been estimated using GEODYN in the along-track and cross-track directions. These accelerations are typically made up of nonconservative forces. By estimating these accelerations, the orbit accuracy is increased significantly. The magnitude of the empirical accelerations will decrease if the force models are improved so they can also be used as a test of relative force model accuracy. However, some of the acceleration due to drag may be absorbed by the OPR acceleration modeling. If this is the case, looking at results from runs without estimations of OPR empirical accelerations is necessary to determine the performance of the new density routines more definitively.

2.4.4 Drag Coefficient Analysis

The setups for the GFO satellite specify the coefficient of drag to be estimated by GEODYN every eight hours. The value for the drag coefficient at each time step on the final iteration of each arc can be extracted from GEODYN to compare the relative strength of representing the drag force on the spacecraft for each version of GEODYN. This provides a valuable insight into the performance of each density model update because the drag coefficient acts as a scaling factor between the density

from the density model and estimated acceleration due to drag on the spacecraft. More variations in the modeled atmosphere which are not seen on the spacecraft will appear as variations in the drag coefficient modeling.

2.5 Solar and Geomagnetic Activity Bins

The atmosphere is the most variable in periods of high solar and geomagnetic activity. This variability can cause modeling errors due to atmospheric density to exceed those of solar radiation. For this reason, any improvements made in estimating a satellite's orbit by changes in atmospheric modeling should be most prominent in these periods. This also means that modeling atmospheric drag in periods of high solar activity are crucial to increasing orbit accuracy.

Solar activity has been split into four categories, or bins, in order to show comparisons at different levels. Improvements in the Elevated and High bins are expected to be more prominent if the atmosphere is better modeled. The same is true for the geomagnetic activity which has been binned into three categories. The convention for solar and geomagnetic activity levels follows that of Reference 1 and can be summarized as follows.

Solar Activity

- Low – ($F10.7 < 75$)
- Moderate – ($75 < F10.7 < 175$)
- Elevated – ($150 < F10.7 < 190$)
- High – ($F10.7 > 190$)

Geomagnetic Activity

- Quiet – (Ap < 10)
- Moderate – (10 < Ap < 50)
- Active – (Ap > 50)

3 TLE BALLISTIC COEFFICIENT PROCESSING

This chapter examines the TLE processing method which provides BC estimates for seven satellites. TLEs were obtained by special data requests from T.S. Kelso's TLE database website, www.celestrak.com, for all TLEs available for each of the seven satellites in the 2001 to 2008 time period. A program was designed to ingest this file format and store the information contained in each TLE. Some of the TLEs provided were found to have been corrupted and required removal. The reason for these 'bad' TLEs was most likely due to insufficient tracking coverage. The elements requiring removal were few, so most coverage was on the order of two TLEs per day.

The information in each TLE was used to propagate an orbit using the SGP4 propagator for the time period available. Details on the SGP4 propagator can be found in Reference 76 and 77. The propagated orbit returns a file containing latitude, longitude, along with a time stamp in thirty second steps. For longer duration satellites, one table was generated for each year of data. A single table was created for each of the shorter duration satellites whose lifetime was on the order of one year. The orbits for those satellites were propagated into one table each. The format of these tables was chosen as to be read natively by the HASDM routine developed and maintained by U.S. Air Force Space Command.

Using the propagated TLEs as inputs, the HASDM atmospheric density was computed for each time step in the propagated orbit table. This translated into a density value at each thirty second time step for each year-long orbit table used as an

input. The TLEs and HASDM densities were then used as inputs to the BC routine described in Section 2.1.

The BC routine included an outlier removal technique to take out all TLE predicted densities and TLE predicted BCs outside of two standard deviations from the mean. The number of outliers removed by this method were few, less than five TLEs for each year of data. Since the TLEs are averaged to produce results, the number of resulting BCs is equal to one less than the number of good TLEs. This translates into slightly less than two BCs per day, or on the order of ~600 BCs per year. Yearly averages of the BCs were taken for each satellite except satellites whose lifetime is on the order of one year. Most short-lived satellites were centered around one particular year, so that year was used as a designation for those satellites.

The averaged BC results are compared to BCs found in References 61 and 78-80. Reference 61 describes the drag coefficient modeling technique used in the preliminary processing of the ANDE-RR mission. This technique involves modeling the two spheres using 94 flat plates, 73 for the leading hemisphere and 21 for the trailing side. The computations for momentum accommodation were determined for each plate, then aggregated to create a total C_D. This C_D accounted for variations caused by atmospheric composition and surface temperature variations. The averaged value of C_D for the two ANDE-RR satellites MAA and FCal were 2.1123 with a standard deviation of 0.00763 and 2.1113 with a standard deviation of 0.00798 respectively. These values were compared to an analytical solution and to precise numerical integration and were found to be within 0.02%. The averaged drag

coefficient for the MAA sphere was used to calculate a ballistic coefficient using the precise values of mass and surface area and found to be 0.00594 m^2/kg.

Reference 78 details the estimation of drag coefficient values for the CHAMP and GRACE satellites. This method uses the HASDM atmospheric corrections to produce C_D values around 3.3 to 3.4. These new C_D values were compared against theoretical drag coefficients derived using Sentman's equation to achieve similar results. This produced BC values for CHAMP of 0.00444 for 2002-2003 and 0.00436 for 2004-2006. The GRACE satellites have average BC values of 0.00687 m^2/kg and 0.00686 m^2/kg from 2004-2006 for GRACE-A and GRACE-B respectively.

Reference 79 uses gas-surface interaction assumptions to approximate the drag coefficient for both the Stella and Starlette satellites. This process uses a paneling method to calculate the satellite's aerodynamics. Each surface panel is represented by its area, surface normal, molecular mass, solar absorptivity and diffusivity. Atmospheric density errors are removed by using two satellites at similar altitudes analyzed over a similar time. This produced BC values of 0.0023916 m^2/kg for both Stella and Starlette due to their identical construction.

Reference 80 analyzes the drag coefficient variability of a number of spherical satellites including the GFZ-1, and STARSHINE 2 and 3 spheres using Sentman's and Schamberg's methods. The averaged drag coefficients for STARSHINE-2 and STARSHINE-3 were found to be 2.15 and 2.01 respectively. This leads to BC values of 0.009831 m^2/kg and 0.01532 m^2/kg for STARSHINE-2 and -3 respectively. These values are computed using a quasi-specular computed model.

Table 3.1 Ballistic Coefficient Results

Satellite	Year	Avg. Perigee Alt. (km)	BC* (m^2/kg)	TLE BC (m^2/kg)	Standard Deviation	Error
ANDE-RR (MAA)[T]	**2007**	**285**	**0.00594[61]**	**0.005502**	**0.000721**	**7.4%**
CHAMP[O,T]	2001	419	~	0.0045101	0.001244	~
	2002	400	0.00444[78]	0.004373	0.000944	1.5%
	2003	397	0.00444[78]	0.0042737	0.0010809	3.7%
	2004	377	0.00436[78]	0.0039823	0.0009671	8.7%
	2005	357	0.00436[78]	0.0038747	0.0007799	11.1%
	2006	354	~	0.0036624	0.0008513	~
	2007	344	~	0.0032219	0.0005454	~
	2008	329	~	0.0029244	0.0005092	~
	AVG	**383**	**0.0044**	**0.00413**	**0.000943**	**6.20%**
GRACE-A[O,T]	2002	489	~	0.0059471	0.0014302	~
	2003	480	~	0.0061691	0.0019236	~
	2004	475	0.00687[78]	0.0061211	0.0025793	10.9%
	2005	471	0.00687[78]	0.0061733	0.0030615	10.1%
	2006	468	0.00687[78]	0.0055967	0.0030276	18.5%
	2007	467	~	0.0060615	0.0037735	~
	2008	465	~	0.0063411	0.0039947	~
	AVG	**472**	**0.00687**	**0.00596**	**0.002889**	**13.20%**
Starlette[T]	2001	809	0.0023916[79]	0.1101215	0.008214	4505%
	2002	809	0.0023916[79]	0.1153363	0.0081133	4723%
	2003	811	0.0023916[79]	0.1909776	0.0193067	7885%
	2004	809	0.0023916[79]	0.2461247	0.0374078	10191%
	2005	809	0.0023916[79]	0.394573	0.0582525	16398%
	2006	811	0.0023916[79]	0.2289547	0.0634547	9473%
	2007	809	0.0023916[79]	0.1187701	0.0633522	4866%
	2008	809	0.0023916[79]	0.1181203	0.0707538	4839%
	AVG	**803**	**0.002392**	**0.05824**	**0.041107**	**2335%**
STARSHINE 2[T]	**2002**	**313**	**0.009831[80]**	**0.010731**	**0.005208**	**9.16%**
STARSHINE 3[T]	**2002**	**402**	**0.01532[80]**	**0.014843**	**0.002516**	**3.11%**
Stella[T]	2001	803	0.0023916[79]	0.0083539	0.148405	249%
	2002	803	0.0023916[79]	0.0080232	0.123735	235%
	2003	803	0.0023916[79]	0.0208017	0.15689	770%
	2004	803	0.0023916[79]	0.0506063	0.204057	2016%
	2005	803	0.0023916[79]	0.0789344	0.311709	3201%
	2006	803	0.0023916[79]	0.0951942	0.201405	3880%
	2007	803	0.0023916[79]	0.0920246	0.0911225	3748%
	2008	803	0.0023916[79]	0.1119449	0.0814444	4581%
	AVG	**809**	**0.002392**	**0.19037**	**0.164846**	**7860%**

*Values in this column are obtained from their corresponding reference.

T - Theoretical, O - Observed

The data generated by this method along with BCs obtained from the other sources are listed in Table 3.1 for every satellite in every year computed. The error term in Table 3.1 refers to the percentage difference between the values obtained by the TLE method, to the values obtained by other methods described above. The AVG row is the average of all of the BCs generated for each satellite with a corresponding BC from another source.

The BCs generated between each good TLE were used as inputs to the TLE density routine to generate TLE derived densities which are essentially scaled to match the HASDM densities. This allows for a direct comparison with HASDM density values in order to validate the results of the TLE processing routine and to compare the relative variations of each density model.

Figures 3.1-3.10 show the resulting plots for five of the satellites analyzed, representing a range of altitudes. HASDM density values were averaged between TLEs to represent the same average density estimated by the TLE calculation. Both the HASDM density and the TLE density (utilizing the TLE BC generated) have been plotted individually in the first plot for each satellite, and together in the second plot for each satellite. This gives the opportunity to see trends in each data set. The selected plots cover either one year or, in the case of ANDE-RR and STARSHINE-3, an entire mission.

In the first plot for each satellite, the red line in the BC plot represents the average (shown in Table 3.1). The standard deviation is also displayed in blue to show the variation about the mean and can also be found in Table 3.1. Both the

HASDM density and the TLE density have been plotted individually in the first plot of each satellite, and together in the second plot for each satellite.

The TLE density trends from Figure 3.1 through Figure 3.8 are well correlated in most cases with HASDM densities. However, the TLE densities have much more variation about the trend. This is likely due to the absorption of all other forces on the spacecraft in the calculation of the TLE density. Also, some anomalies have been found as spikes like the final BC value in Figure 3.7 and one BC value in late June of Figure 3.3.This is most likely due to an inadequate outlier removal technique. All TLE density values outside of two standard deviations were removed from processing before the BC was calculated. Since the BC is not solely based on the TLE data, anomalies can still develop depending on the HASDM density values supplied in the calculation.

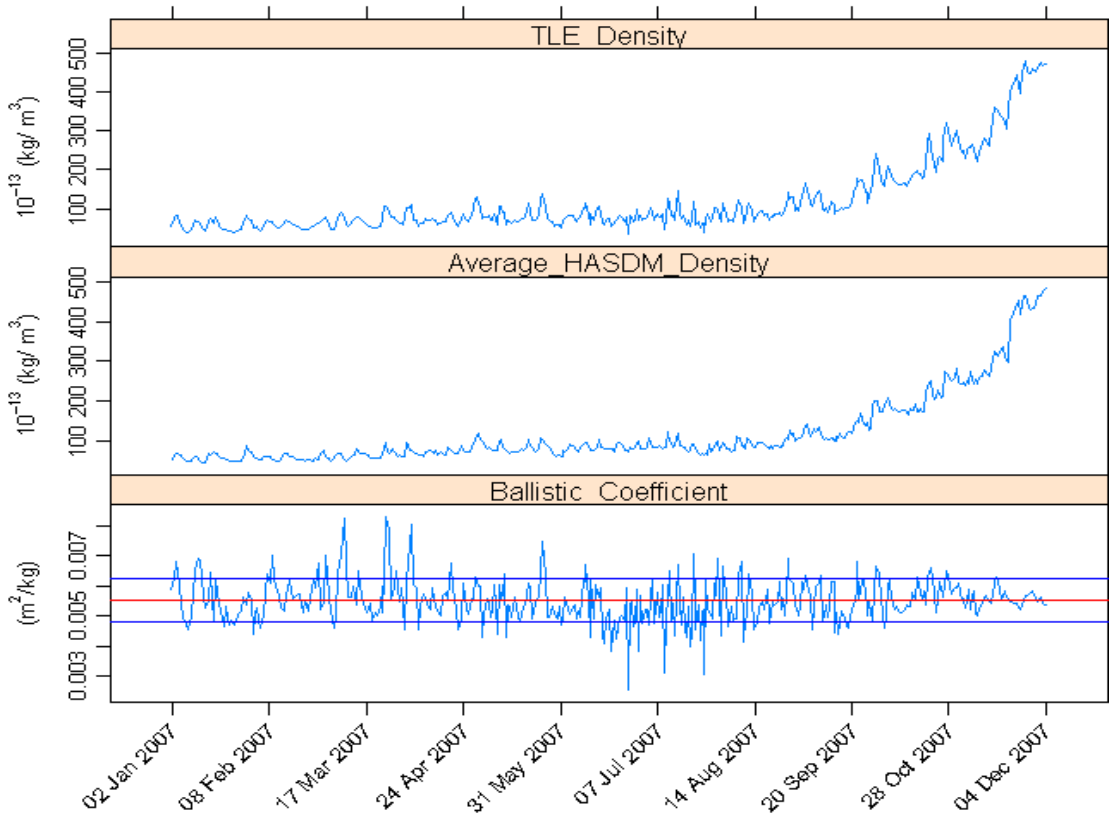

Figure 3.1 ANDE-RR (MAA) Ballistic Coefficient.

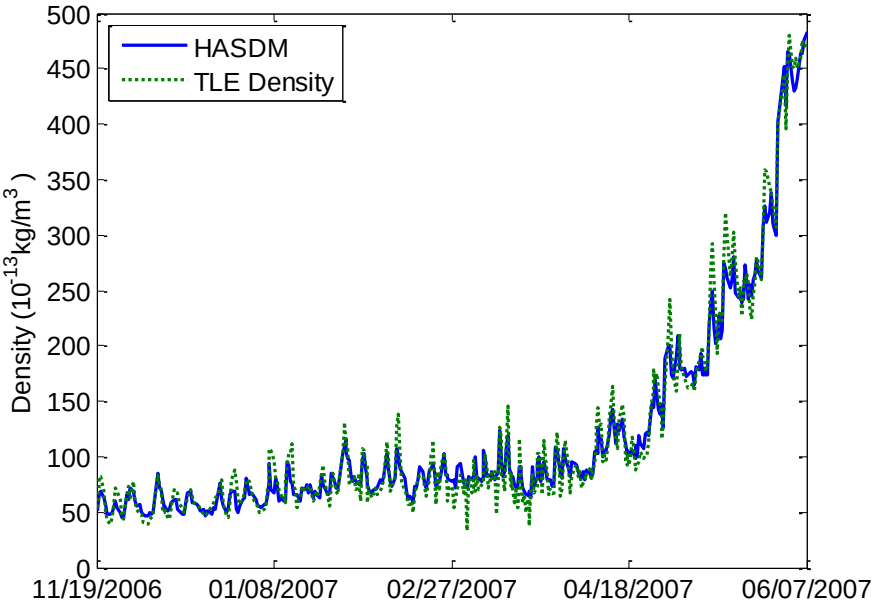

Figure 3.2 ANDE-RR (MAA) Density.

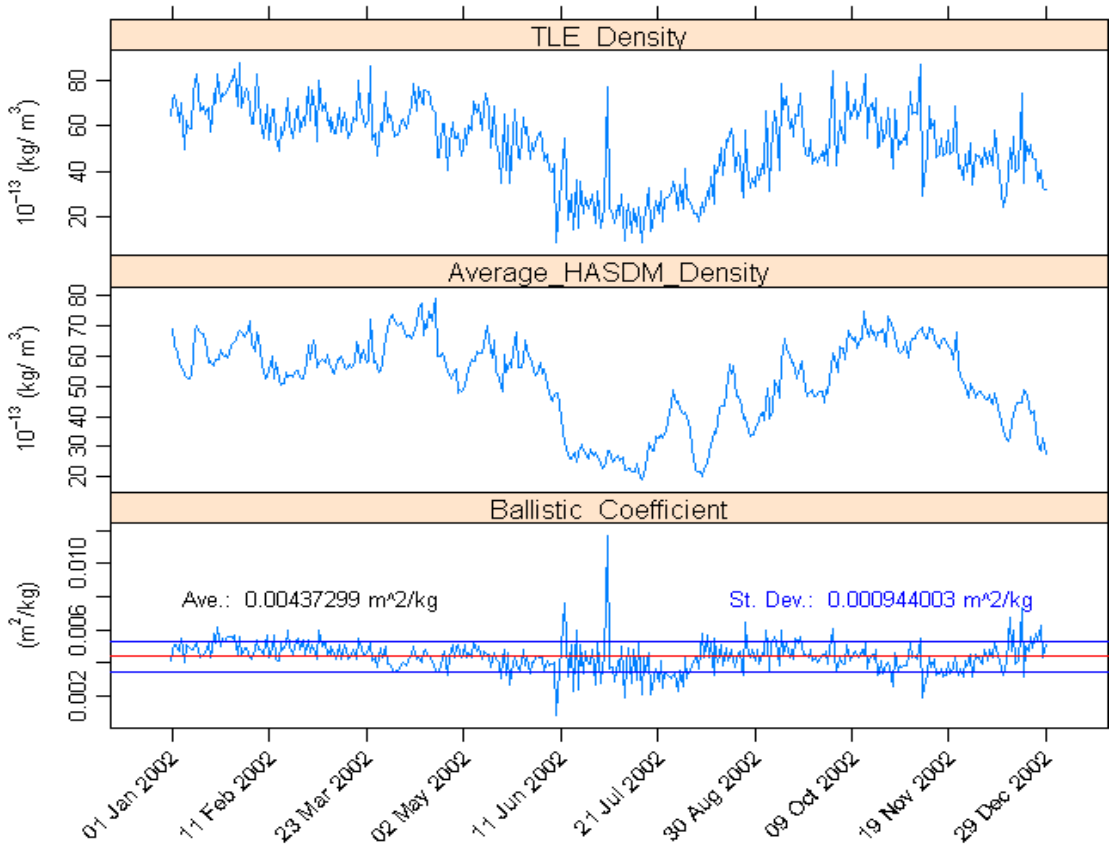

Figure 3.3 CHAMP 2002 Ballistic Coefficient.

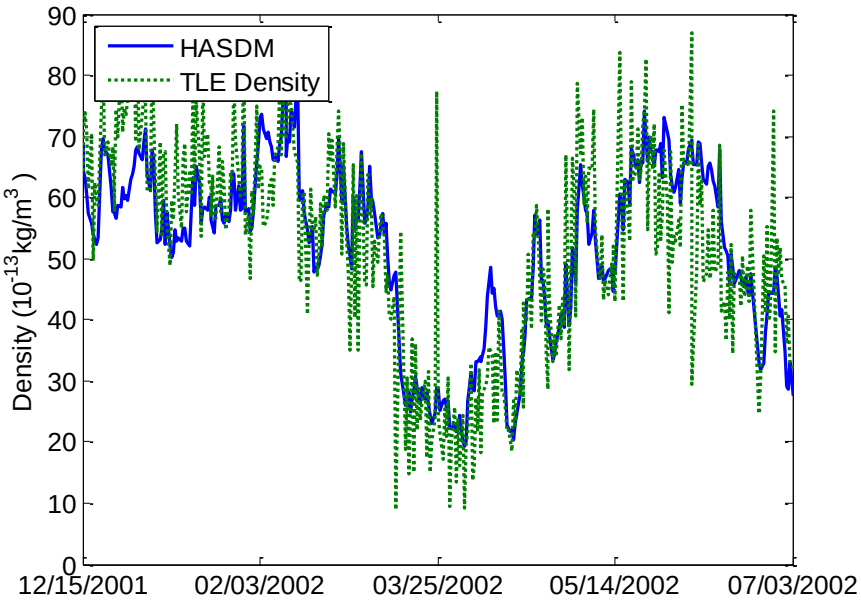

Figure 3.4 CHAMP 2002 Density.

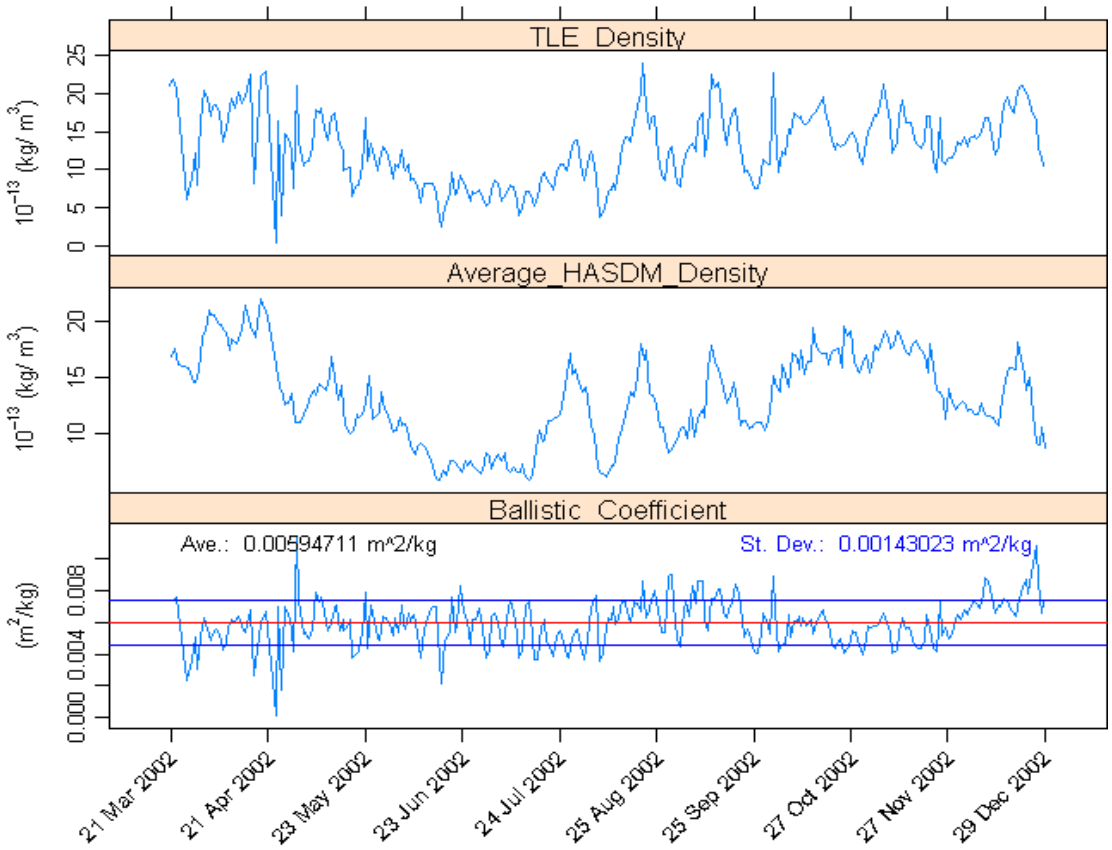

Figure 3.5 GRACE-A 2002 Ballistic Coefficient.

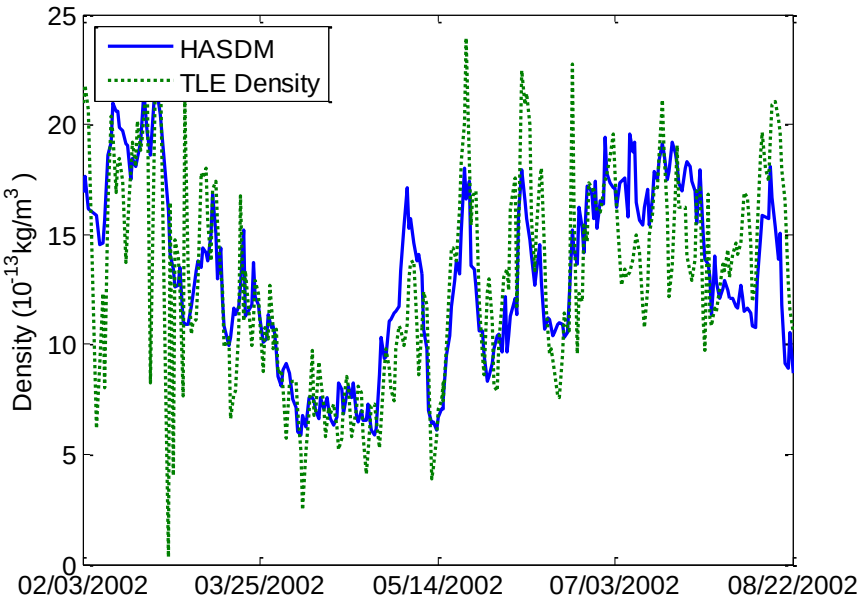

Figure 3.6 GRACE-A 2002 Density.

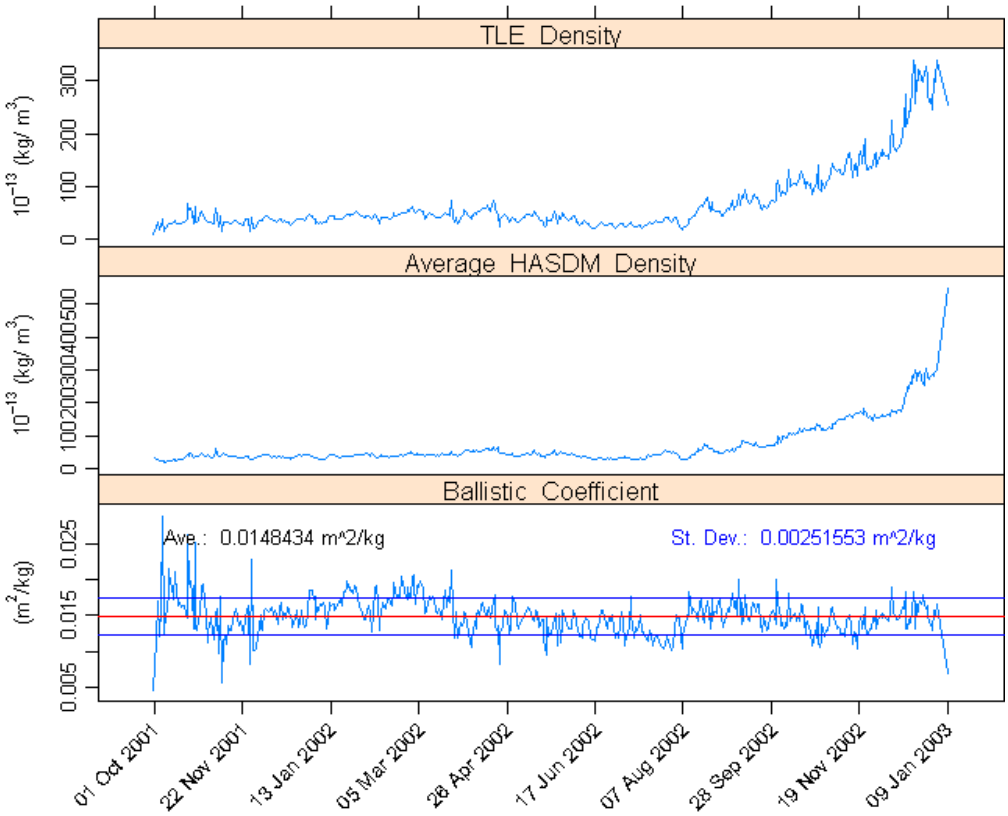

Figure 3.7 STARSHINE-3 Ballistic Coefficient.

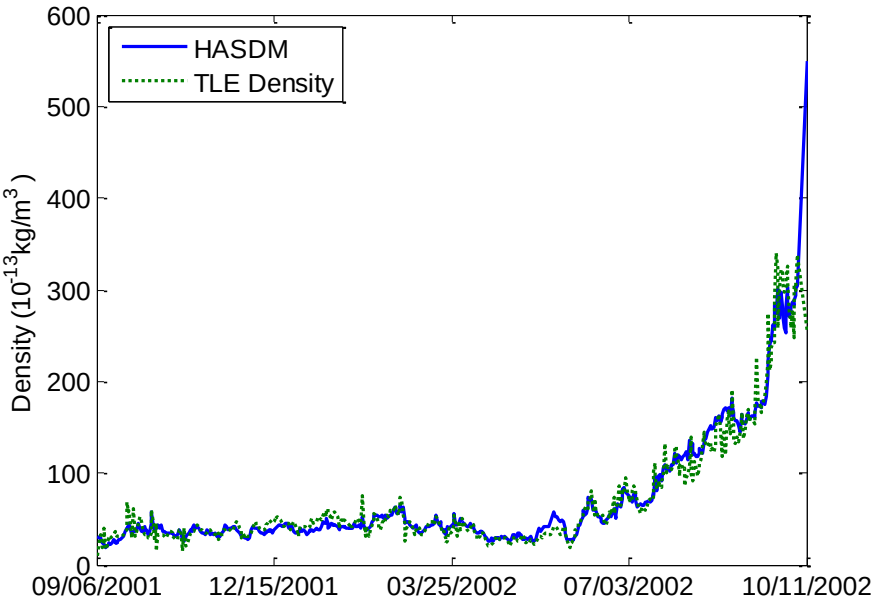

Figure 3.8 STARSHINE-3 Density.

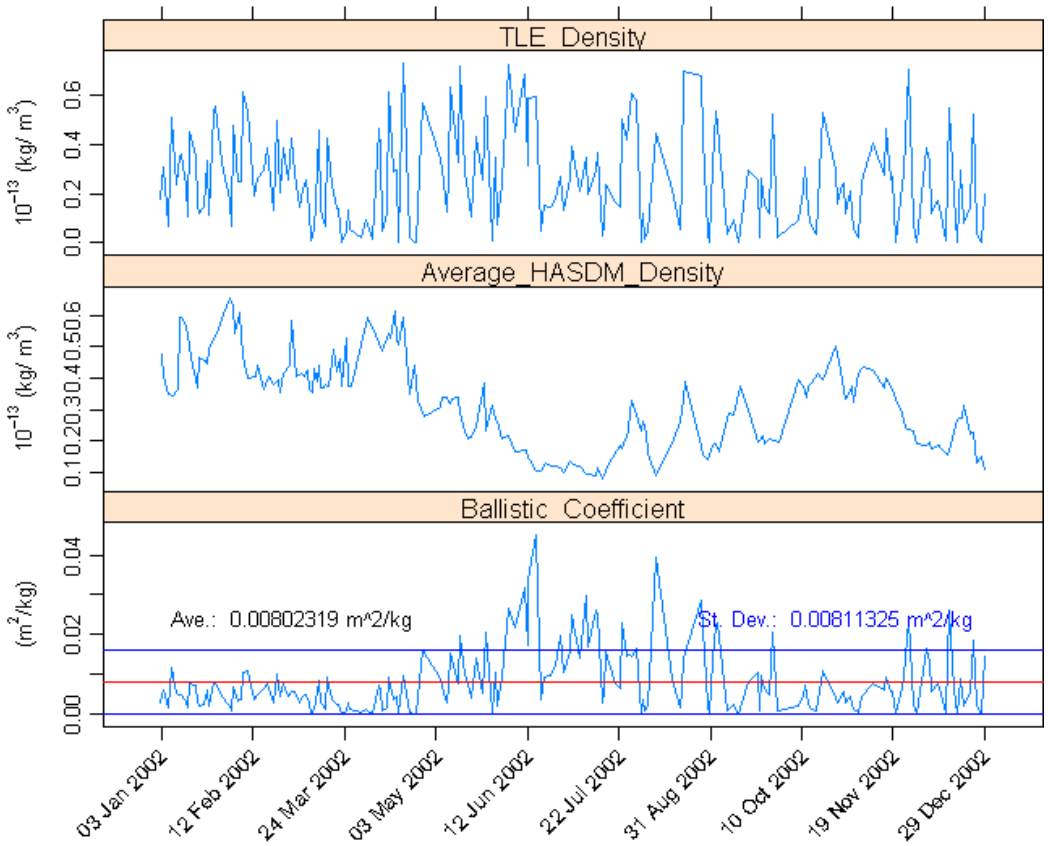

Figure 3.9 Stella 2002 Ballistic Coefficient.

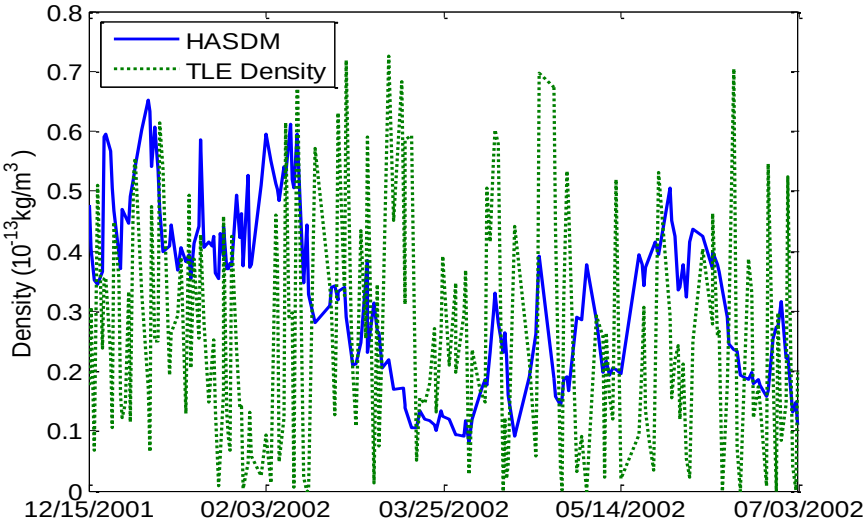

Figure 3.10 Stella 2002 Density.

Figure 3.9 and Figure 3.10 show the poor performance of this routine at Stella's higher altitude. The poor performance is likely due to a larger influence from other non-conservative forces like solar radiation pressure. Notice that the standard deviation for Figure 3.9 is higher than the actual BC value. All of the TLE densities for Stella and Starlette have tremendous variation and do not correlate well with the HASDM density averages. Additionally, the BCs predicted for Stella and Starlette are orders of magnitude larger than the values predicted by Harrison [Ref. 79].

The satellites which give the closest values to predicted BCs are the short-lived 'cannonball' satellites at low altitudes. ANDE-RR and the STARSHINE satellites produced BC values that averaged within 10% of values predicted using other methods when their entire mission duration was averaged. These satellites also show the best correlation between the TLE densities and the HASDM densities.

Comparing the BC results versus altitude and time is also a worthwhile investigation. The yearly averages for both BC and the BC error described above are displayed in Figure 3.11 through Figure 3.14. This provides some insight on the validity of this technique as a function of both time and altitude. In the plots showing BC error trends, only the cases that have corresponding BC values obtained through other sources are shown.

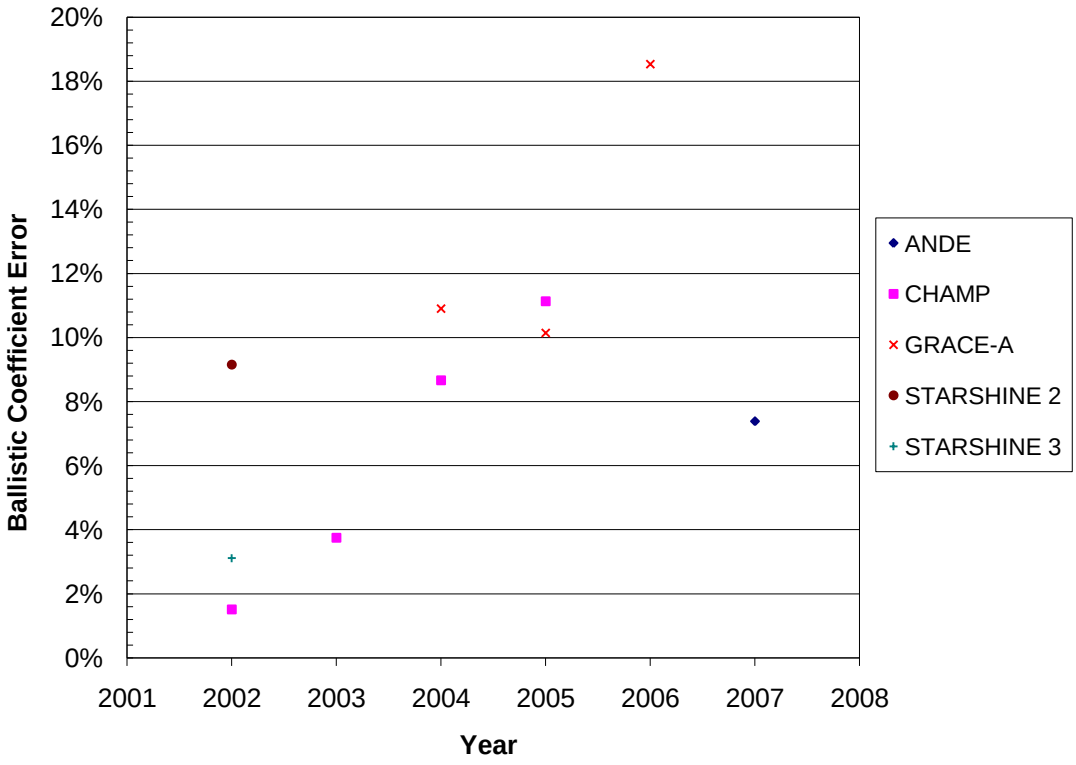

Figure 3.11 Ballistic Coefficient Error for Perigee Altitude < 500 km.

The data shown in Figure 3.11 indicate a positive slope of the error for both the CHAMP and GRACE-A satellites towards solar minimum. Table 3.1 and Figure 3.12 show that this error is due to decreasing BCs. The Stella and Starlette satellites trends in Figure 3.12 are deceptive and should be ignored in this analysis because the standard deviations on the BC values from Table 3.1 are on the same order as the BC values themselves. GRACE-A exhibits some degree of a downward slope while CHAMP shows a definite downward slope.

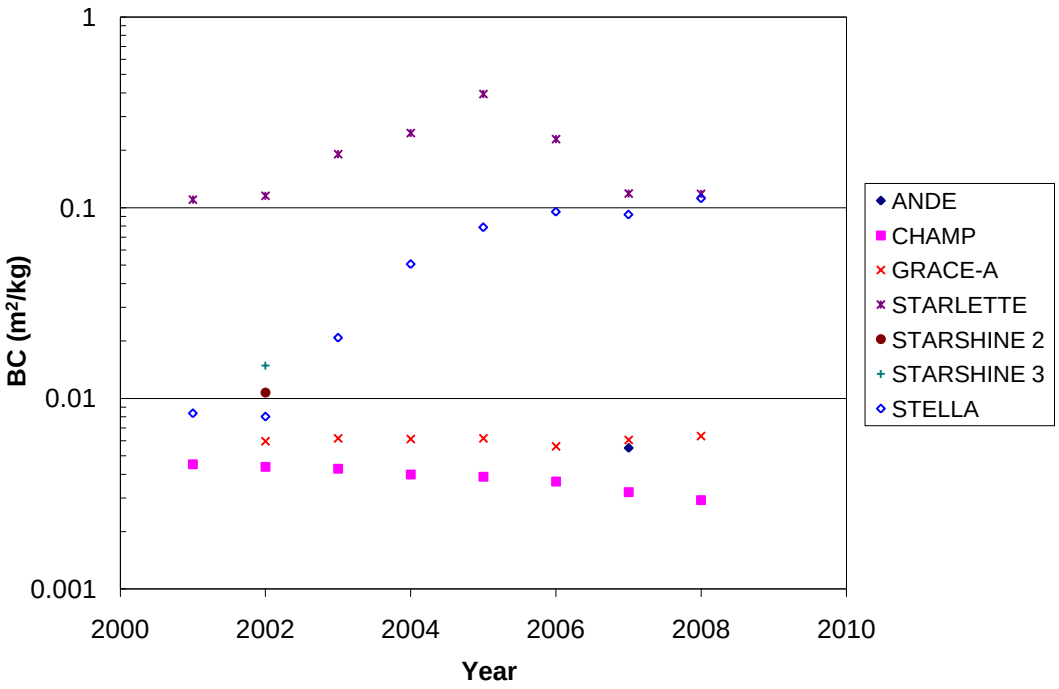

Figure 3.12 Ballistic Coefficient versus Year.

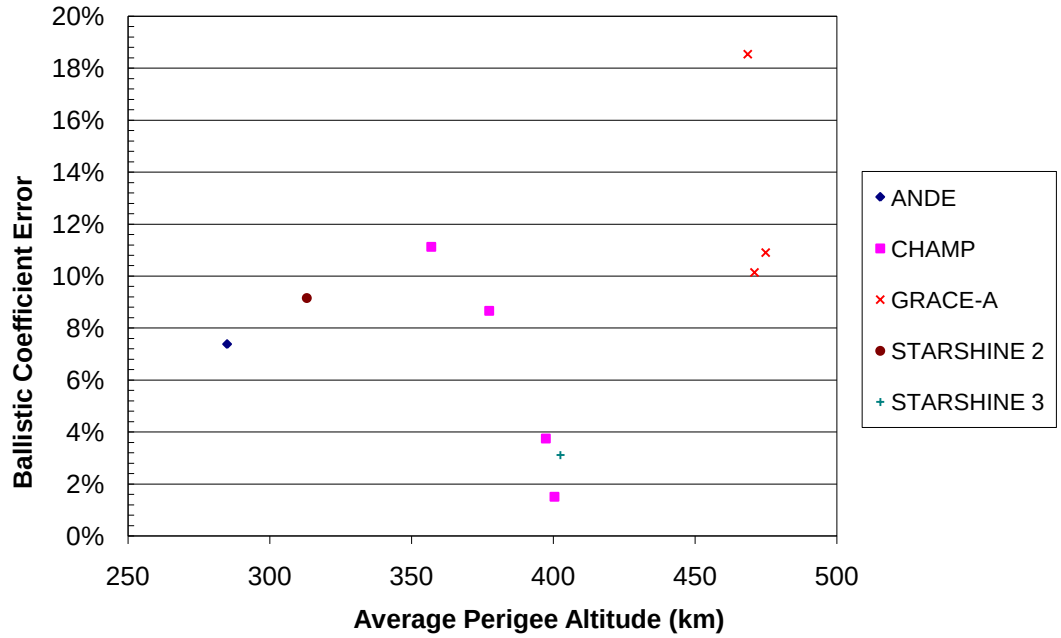

Figure 3.13 BC Error vs. Average Perigee Altitude for all Perigee Altitudes < 500 km.

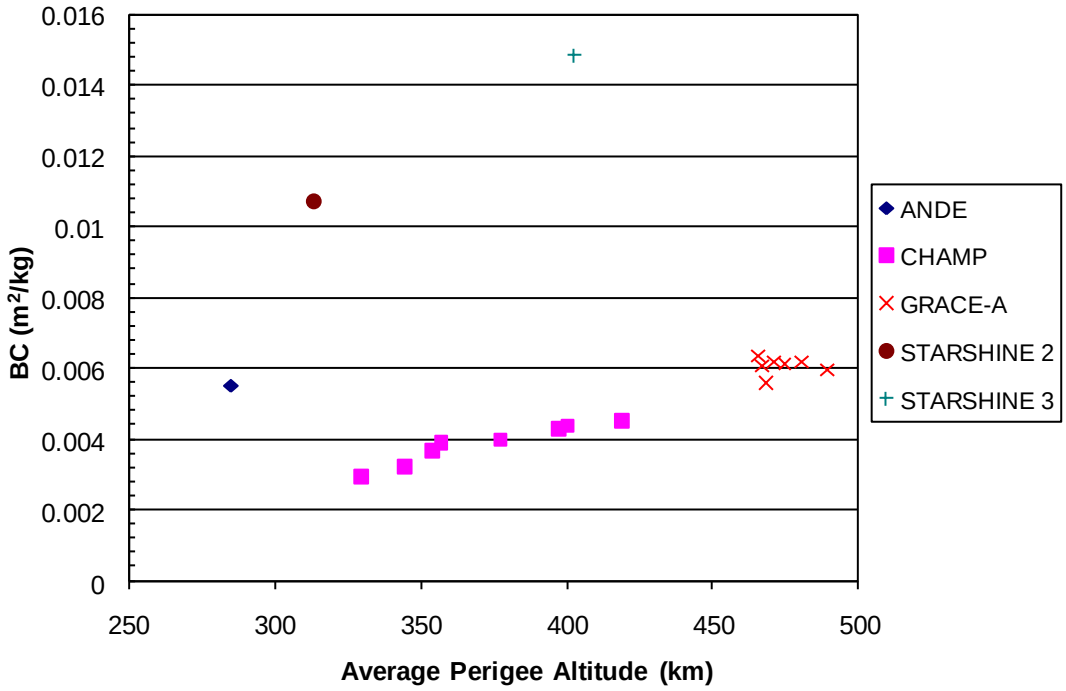

Figure 3.14 Ballistic Coefficient vs. Average Perigee Altitude for all Perigee Altitudes < 500 km.

Figure 3.13 and Figure 3.14 show the opposite trend from expected for the CHAMP satellite. The ballistic coefficient error was thought to increase with altitude because the contribution from other factors (solar radiation pressure, earth albedo, etc.) should be relatively higher; however this is not the case. The GRACE-A satellite at a slightly higher altitude does not seem to exhibit this behavior as much. The lower altitudes coinciding with the solar minimum could be one explanation of this phenomenon.

This decreasing trend is contrary to the decrease in mass over a satellite's lifetime due to station keeping and orbit raising maneuvers which would cause the BC to increase because it appears in the denominator of the BC formulation. The

decreasing BCs suggest the possibility that the HASDM density which appears in the denominator in Eq. **(2.3)** may be overestimating the density. However, there could be other possible explanations for this phenomenon. As the satellites approach solar minimum (going from 2000 to 2008), the Sun excites the atmosphere less, causing the atmosphere to push down to a lower altitude. This decreases the density the satellite is exposed to. According to Sutton [Ref. 32], using Sentman's formulation a decrease in density will cause a decrease in C_D. This will cause the BC to also decrease. Similarly, as the orbit decays, the satellites get lowered into more and more atmosphere. This causes the opposite effect, leading to a higher C_D and thus a higher BC.

4 GEOSAT FOLLOW-ON PROCESSING

The GEOSAT Follow-on spacecraft experienced difficulties due to faulty GPS receivers upon deployment which presented problems in maintaining the required radial accuracy of the satellite altimeter. To mitigate this, orbit determination performed using the GEODYN software package is supplied with SLR and DORIS observations, as well as tuned gravity models to reduce the radial error considerably. Since the science data returned by the altimeter is directly dependent on the knowledge of the spacecraft's orbit, any increase in accuracy of the spacecraft's position translates into a direct increase in the accuracy of the altimeter.

GFO is processed for this paper using three versions of GEODYN; the original 0712 version using the MSIS-86 atmospheric model, a modified version using the NRLMSISE-00 atmospheric model; and a modified version using the NRLMSISE-00 model and DCA corrections to the NRLMSISE-00 model [Refs. 40-41]. Each of these versions were run using setups obtained from NASA GSFC for the years 2000-2002 and 2005. The 2000-2002 time period was chosen because it is the height of the most recent solar maximum. The 2005 data set is used as a control to see performance at lower solar activity levels.

Initially, setups specifying GEODYN to estimate once per revolution (OPR) empirical accelerations were used. These setups were exact copies of those used for the precise orbits for GFO, so they returned the most accurate results. Improvements using these setups and the new versions of GEODYN would directly enhance the

altimeter science data and verify that the changes made by upgrading GEODYN are worthwhile. However, after an initial investigation with the results from these setups, only marginal improvements were obtained by the updates and did not show much consistency.

The small changes seen in the setups with OPR empirical accelerations estimated can become more pronounced if those accelerations are not estimated. If the empirical accelerations are not estimated, then the small changes in the spacecraft's velocity caused by forces on the spacecraft that are not modeled will cause significantly greater errors in the satellite's position over time. This allows for a better representation of any improvement made by changing force models.

This chapter covers an investigation into the performance of the two new versions of GEODYN created versus the original using two different sets of setups for the GFO spacecraft. These results are analyzed using several different metrics of comparison to determine whether the updates made to GEODYN are significant improvements.

4.1 Processing with Empirical Accelerations

The setups obtained from NASA GSFC specified for GEODYN to estimate empirical accelerations once per revolution (OPR). In satellite orbit determination, all of the forces, both conservative and nonconservative, are modeled to the highest fidelity possible. However, since none of the force models are perfect, once per revolution (OPR) empirical accelerations have been estimated in the along-track and cross-track directions. These accelerations are typically made up of nonconservative

forces. The estimation process absorbs some mismodeling of the forces on the spacecraft used in the determination of the orbits. Estimating these accelerations increases the accuracy of the orbits, and enables GFO to achieve the accuracy set forth in the mission objectives. The setups provided are the same setups used to produce the precise orbits which derive the altimeter data. Thus, any improvements in these cases will translate directly to improvements in the altimeter returns.

4.1.1 Empirical Accelerations Analysis

The magnitude of the estimated empirical accelerations will decrease if the force models are improved so they can be used as a test of relative force model accuracy. Improvements in atmospheric drag modeling will occur predominately in the along-track direction (direction along the satellite's orbit). The along-track accelerations were extracted from GEODYN output and plotted against both daily Ap and the F10.7 solar flux proxy to show correlations with solar and geomagnetic activity. High solar or geomagnetic activity will cause higher empirical accelerations to be estimated. This is primarily due to the difficulty in capturing the true variations in atmospheric density during these periods of high activity. The empirical accelerations will decrease compared to the original GEODYN version when the accelerations due to atmospheric drag are a better representation of the forces on the spacecraft, thus reducing the amplitude of estimated OPR empirical accelerations. The results of this analysis are displayed in Figure 4.1 through Figure 4.8. Note that each plot has a different scale.

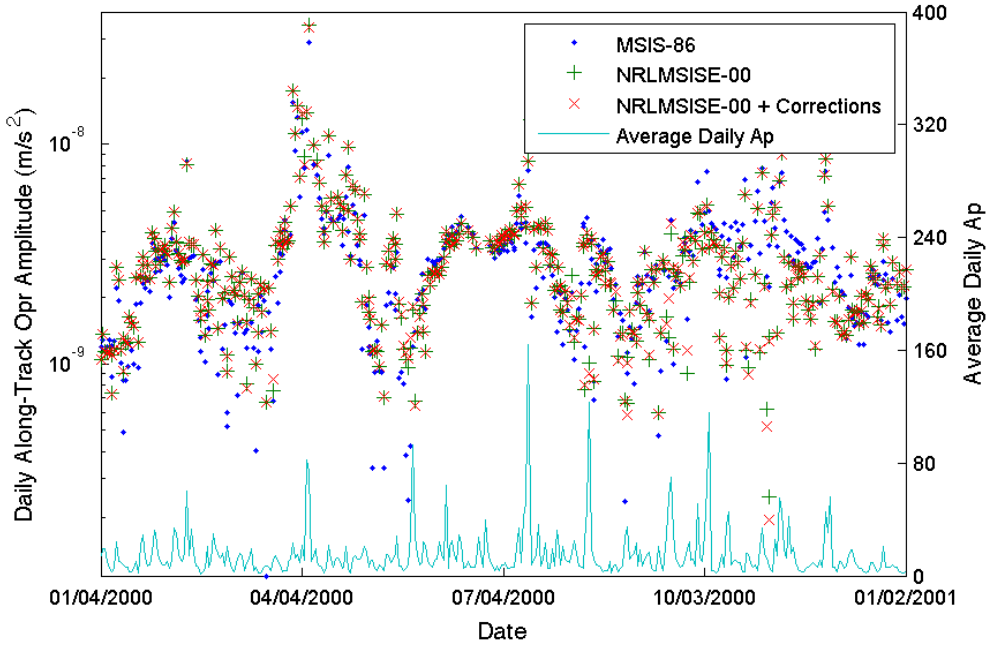

Figure 4.1 2000 GFO Daily Along-Track Accelerations with Ap.

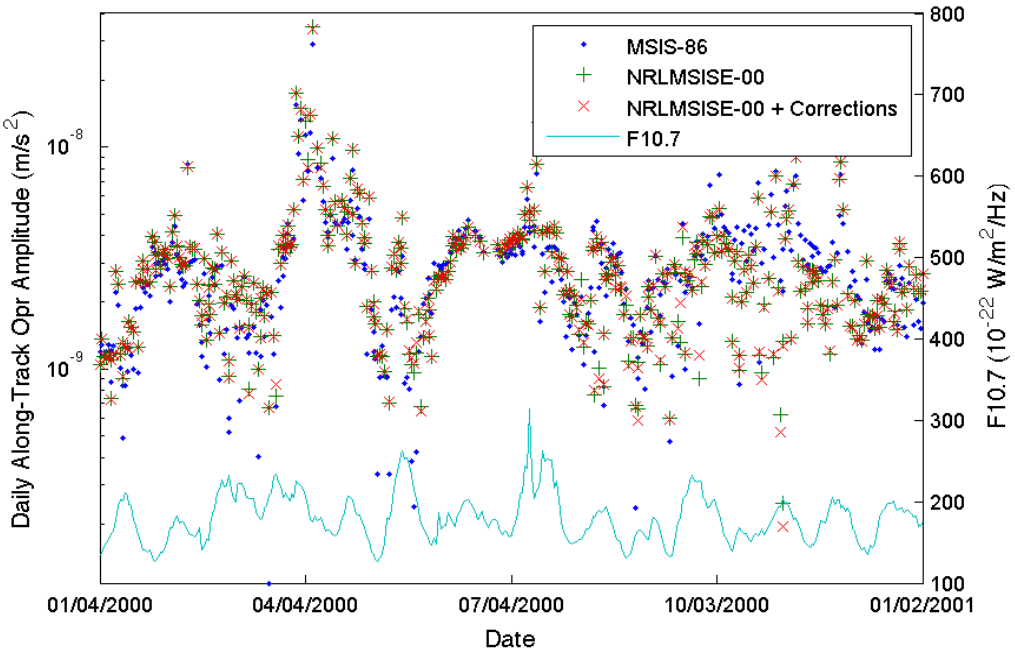

Figure 4.2 2000 GFO Daily Along-Track Accelerations with F10.7.

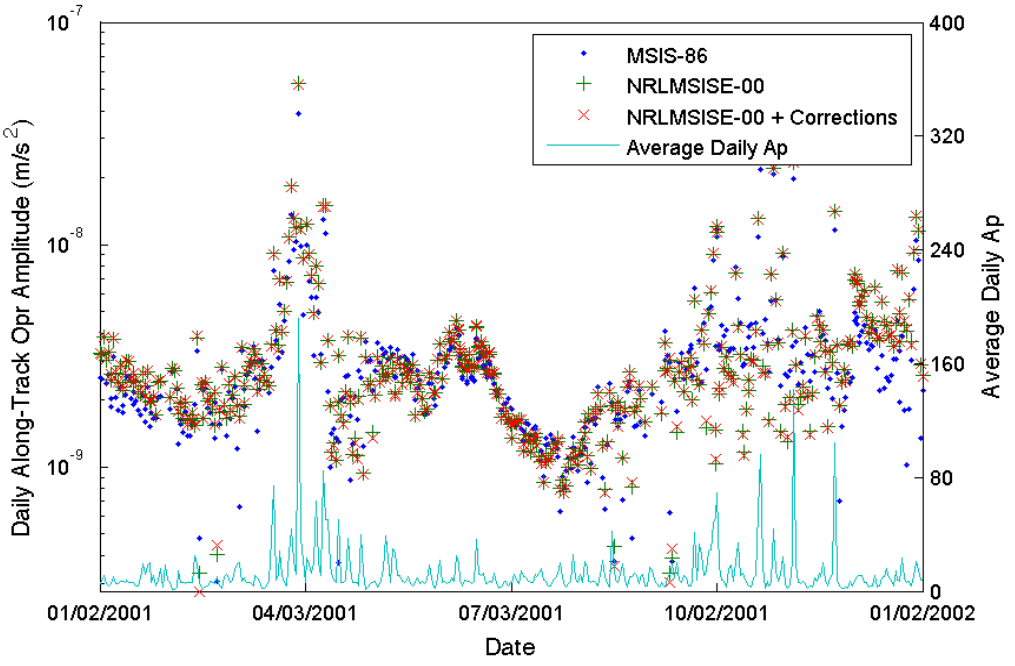

Figure 4.3 2001 GFO Daily Along-Track Accelerations with Ap.

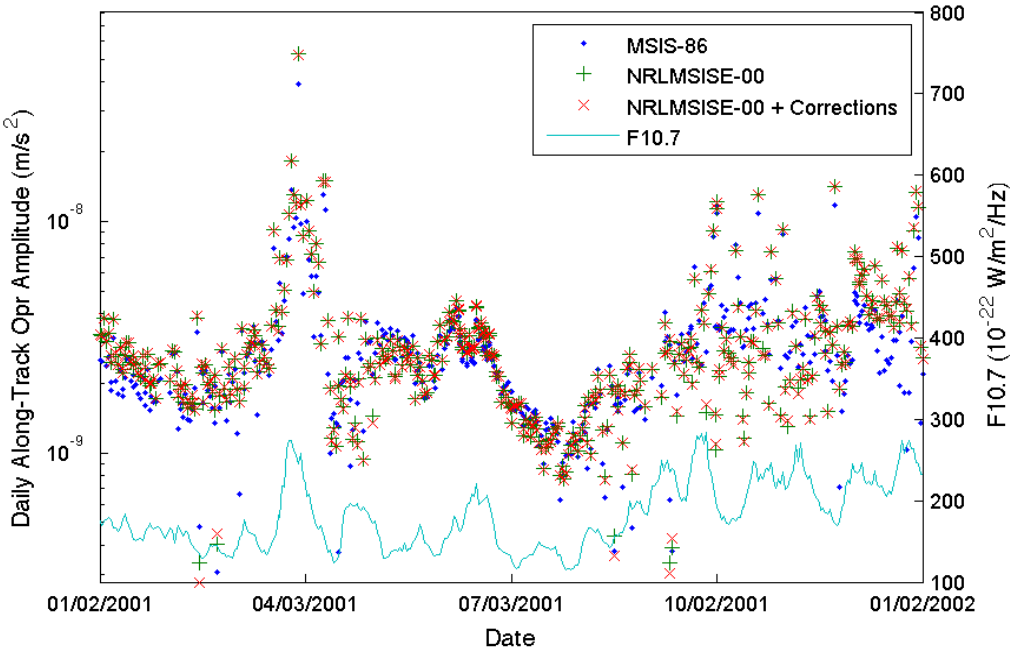

Figure 4.4 2001 GFO Daily Along-Track Accelerations with F10.7.

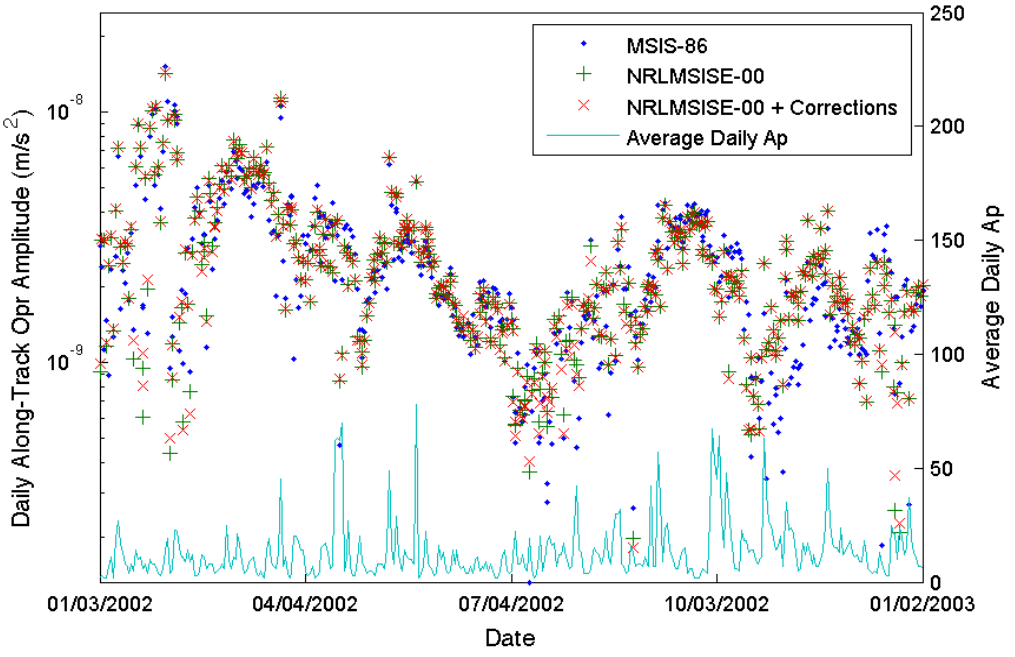

Figure 4.5 2002 GFO Daily Along-Track Accelerations with Ap.

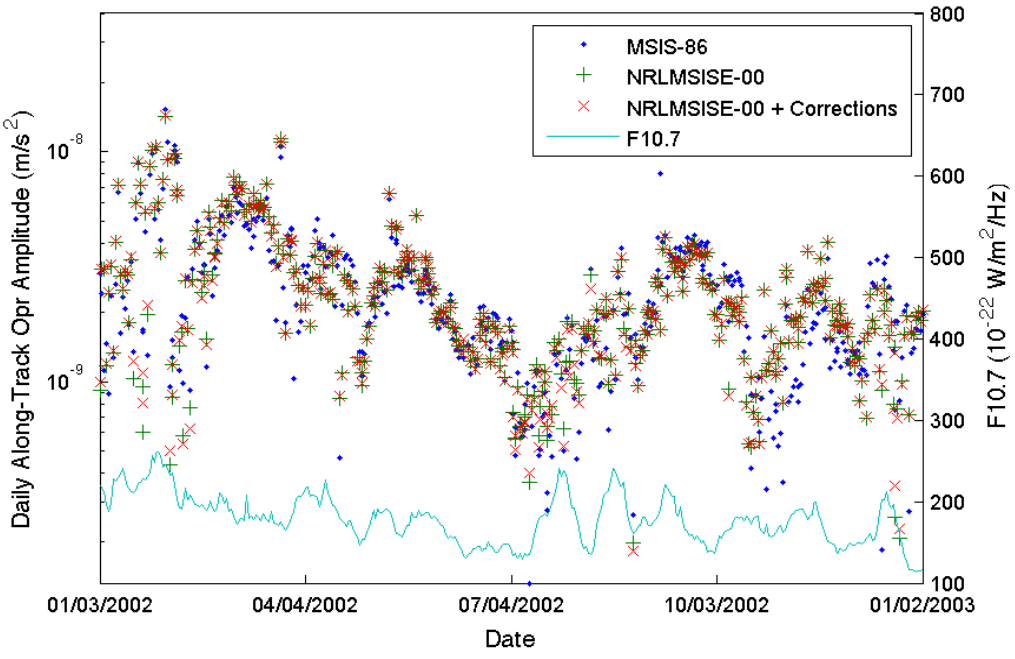

Figure 4.6 2002 GFO Daily Along-Track Accelerations with F10.7.

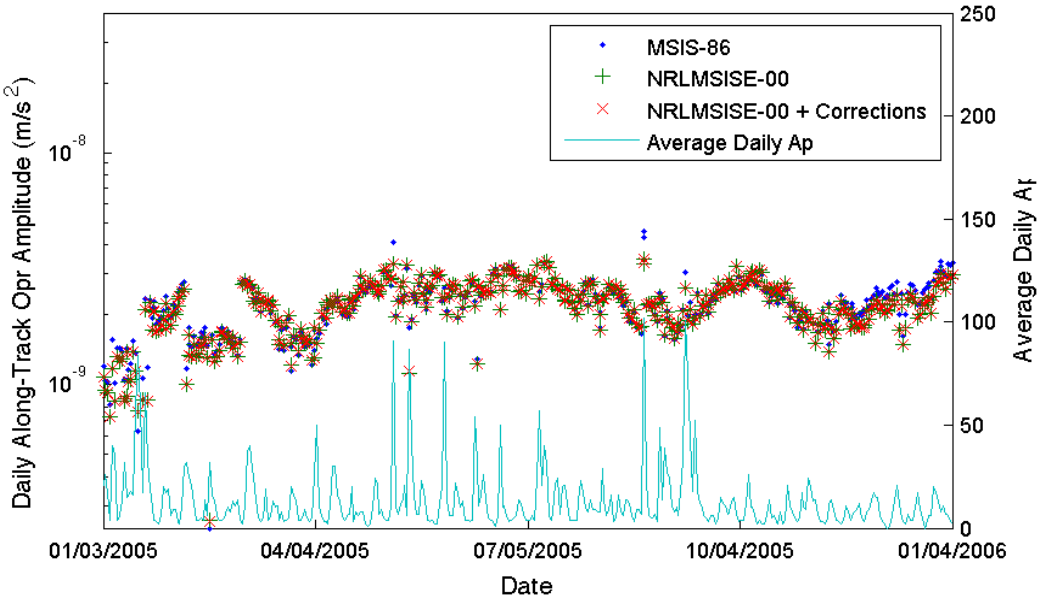

Figure 4.7 2005 GFO Daily Along-Track Accelerations with Ap.

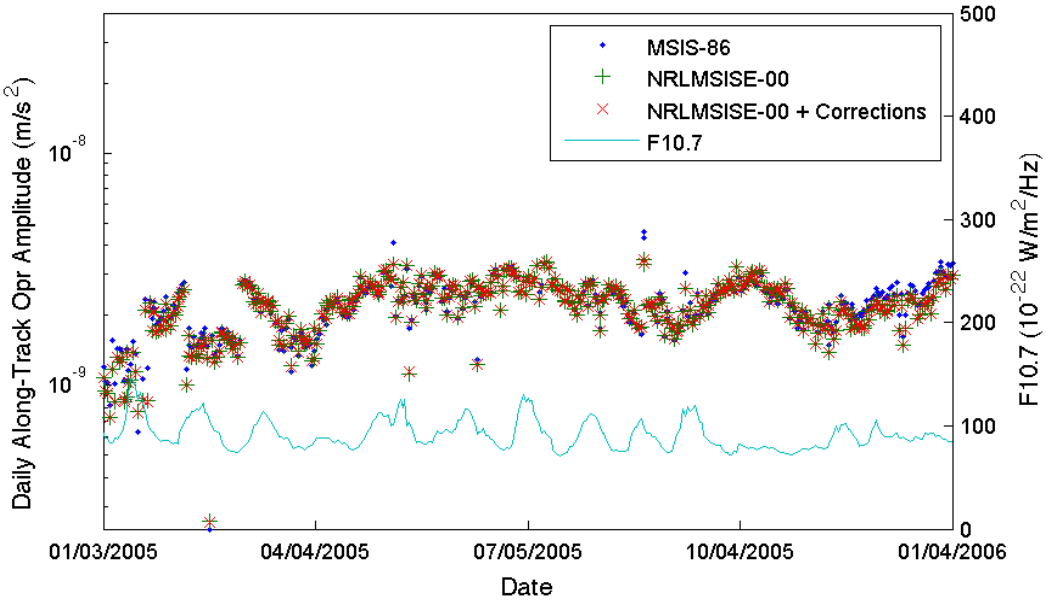

Figure 4.8 2005 GFO Daily Along-Track Accelerations with F10.7.

The along track accelerations show correlation with both F10.7 and Ap. Spikes of Ap can be seen in Figure 4.5 and coincide with better performance with the new density models. The spikes in 2001 match the higher Ap values in Figure 4.3, and the trend of the accelerations matches the trend in F10.7 in Figure 4.4. The high deviation region in late March of 2001 of Figure 4.3 and Figure 4.4 also matches both the solar flux peak, and peak in Ap. There are regions that appear to show an improvement according to these figures like the early and later parts of 2005 seen in Figure 4.7 and Figure 4.8, but overall, the empirical accelerations seem to roughly match the previous density routine.

In order to show a more quantitative comparison, yearly averages of the empirical accelerations are taken to determine if the force modeling has improved. The results are shown in the following tables. The orange cells indicate the best performance of the density models.

Table 4.1 GFO Yearly Average of Daily OPR Along-Track Empirical Accelerations (m/s^2).

Year	MSIS-86	NRLMSISE-00	NRLMSISE-00 + DCA
2000	1.661E-08	1.635E-08	1.676E-08
2001	1.733E-08	1.756E-08	1.708E-08
2002	8.456E-09	8.620E-09	8.696E-09
2005	4.103E-09	4.106E-09	4.115E-09

Table 4.2 GFO Yearly Average of Daily OPR Cross-Track Empirical Accelerations (m/s^2).

Year	MSIS-86	NRLMSISE-00	NRLMSISE-00 + DCA
2000	3.051E-09	3.154E-09	3.158E-09
2001	3.089E-09	3.417E-09	3.413E-09
2002	2.617E-09	2.696E-09	2.690E-09
2005	2.254E-09	2.197E-09	2.197E-09

The along-track empirical acceleration produced mixed results. There are cases where the yearly average of the along-track accelerations improve over MSIS-86 (2000 with NRLMSIS and 2001 with the corrections). These cases are interesting because the two years which have been improved are the most effected by high solar activity. Although, these changes are small and may be negligible. The cross-track accelerations did not show any improvements and most changes were small. This is expected for the changes in drag modeling investigated.

The data has been binned by solar activity level in Table 4.3 to determine if a correlation with high solar activity and performance with the different routines is visible. The convention follows that of Picone et al. and can be summarized as follows [Ref. 1].

- Low – (F10.7 < 75)
- Moderate – (75 < F10.7 < 175)
- Elevated – (150 < F10.7 < 190)
- High – (F10.7 > 190)

In order to have set divisions between the levels, moderate has been chosen to be binned in this paper spanning from 75<F10.7<150.

There seems to be a slight improvement during high and low solar activity, with the updated density model and the corrections. The cross-track component is not seen to exhibit any improvements.

Table 4.3 GFO Average of Daily OPR Empirical Accelerations by Solar Activity (m/s^2).

Solar Activity Level	Direction	Density Routine		
		MSIS-86	NRLMSISE-00	NRLMSISE-00 + DCA
Low Solar Activity (F10.7 < 75)	Along-track	3.247E-09	3.239E-09	3.238E-09
	Cross-track	2.360E-09	2.383E-09	2.383E-09
Moderate Solar Activity (75 < F10.7 < 150)	Along-track	5.845E-09	5.964E-09	6.057E-09
	Cross-track	2.094E-09	2.063E-09	2.061E-09
Elevated Solar Activity (150 < F10.7 < 190)	Along-track	8.464E-09	8.563E-09	8.534E-09
	Cross-track	2.828E-09	2.945E-09	2.938E-09
High Solar Activity (F10.7 > 190)	Along-track	2.439E-08	2.422E-08	2.412E-08
	Cross-track	3.654E-09	3.981E-09	3.987E-09

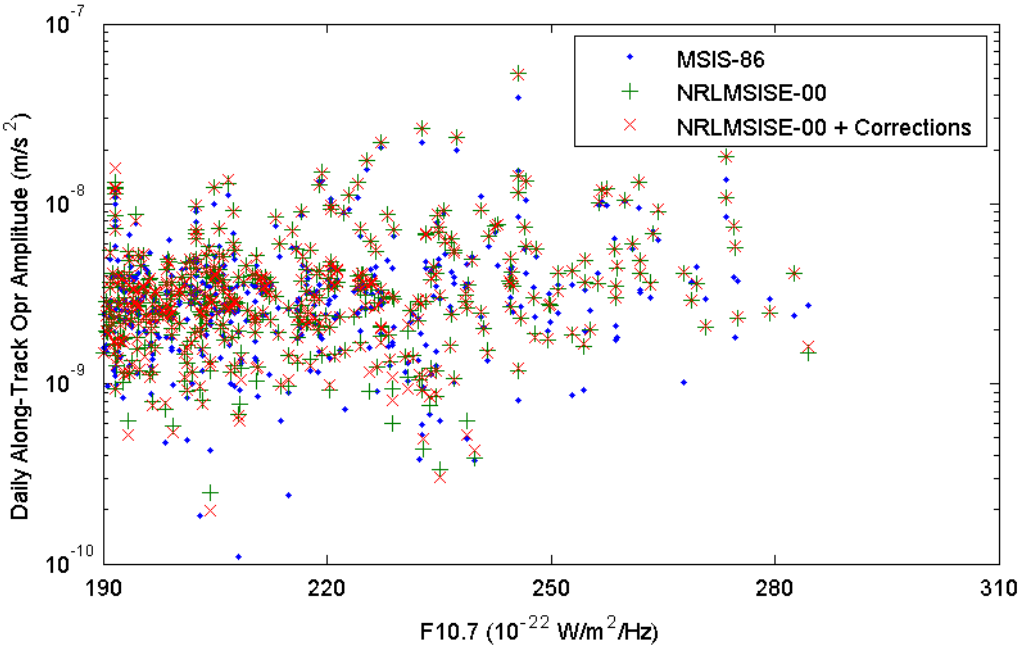

Figure 4.9 GFO Daily Along-Track Accelerations vs. F10.7.

In order to visualize the performance at high solar activity, Figure 4.9 is created to see if any of the along-track components were improved. Again, there does not seem to be any consistent improvement. Some of the data points at high solar flux have been improved, where some have not. There are few outliers in this plot, suggesting the averages in this activity level are a reasonable representation of the performance of the new force models.

Table 4.4 GFO Average of Daily OPR Empirical Accelerations by Geomagnetic Activity (m/s^2).

Solar Activity	Direction	Density Routine		
		MSIS-86	NRLMSISE-00	NRLMSISE-00 + DCA
Quiet Ap (Ap < 10)	Along-track	9.468E-09	9.552E-09	9.461E-09
	Cross-track	2.501E-09	2.516E-09	2.515E-09
Moderate Ap (10 < Ap < 50)	Along-track	1.366E-08	1.355E-08	1.366E-08
	Cross-track	2.760E-09	2.953E-09	2.952E-09
Active Ap (Ap > 50)	Along-track	1.645E-08	1.746E-08	1.749E-08
	Cross-track	6.152E-09	6.733E-09	6.730E-09

The same comparison as Table 4.3 has been created with geomagnetic activity instead of solar activity and the result is displayed in Table 4.4. The data was binned according to the following convention described by Picone et al. and summarized as follows [Ref. 1].

- Quiet – (Ap < 10)
- Moderate – (10 < Ap < 50)
- Active – (Ap > 50)

The performance in the active region does not seem to improve over MSIS-86 at all. There are some conditions where the corrections perform better, but the changes are slight.

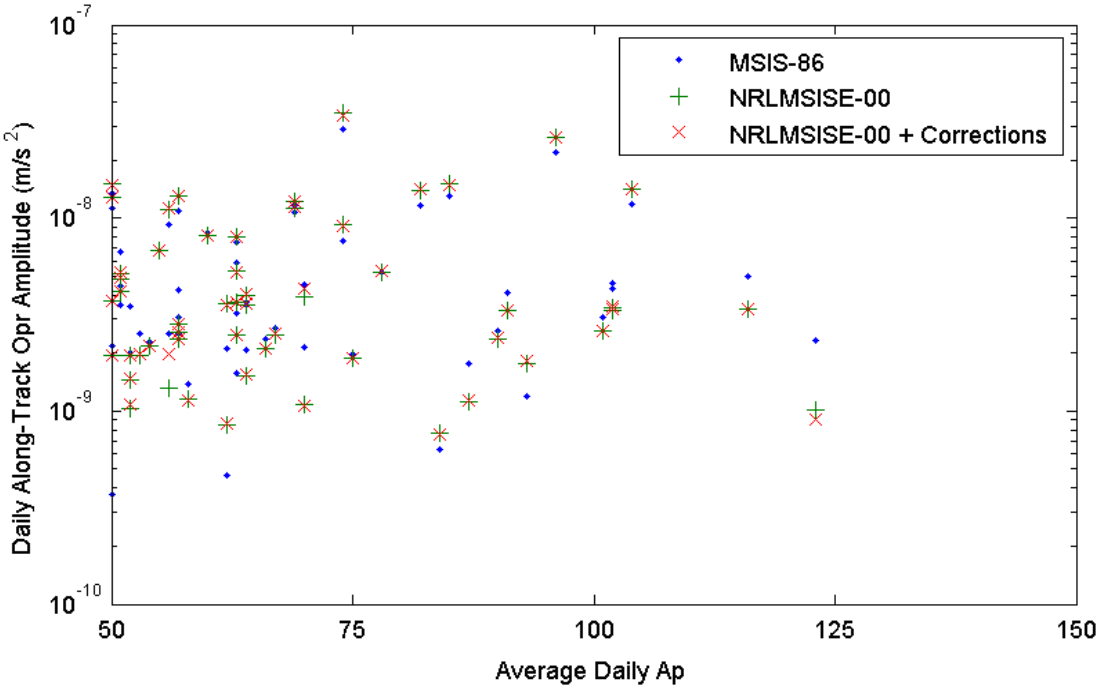

Figure 4.10 GFO Daily Along-Track Accelerations vs. Ap.

The along-track empirical accelerations have been plotted versus geomagnetic activity and displayed in Figure 4.10. Some of the highest geomagnetic activity points show some of the most improvement, but most are slightly worse. Again, there are no outliers throwing off these values, so the averages are good representations of the performance of each routine.

4.1.2 SLR RMS of Fit

Since modeling all forces on a spacecraft perfectly is impossible, there are inevitably differences between observations, estimated orbits, and the true trajectory. Small differences between observations and the estimated orbit are indicative of an accurate orbit. The root mean square (RMS) value of the differences in range measurements from SLR stations to the predicted orbit is especially important in this case because SLR observations are the main measurement source for GFO due to faulty GPS receivers. By comparing these RMS values for each arc using all versions of GEODYN, a significant insight to the performance of each density model can be discovered since any decrease in the SLR RMS of fit will represent an improvement in density modeling.

After running all GFO data sets including estimates of empirical accelerations, the SLR RMS of fit values for 2000, 2001, 2002, and 2005 were extracted and plotted in Figure 4.11 through Figure 4.14. Note that each plot has a different scale. The figures do not seem to indicate any consistent trends one way or the other. In each figure, there are some instances where one routine is significantly better or worse than another, but for the most part they have comparable results. There are also few outliers, which signifies that any averaging done with these data sets will be representative of the actual performance.

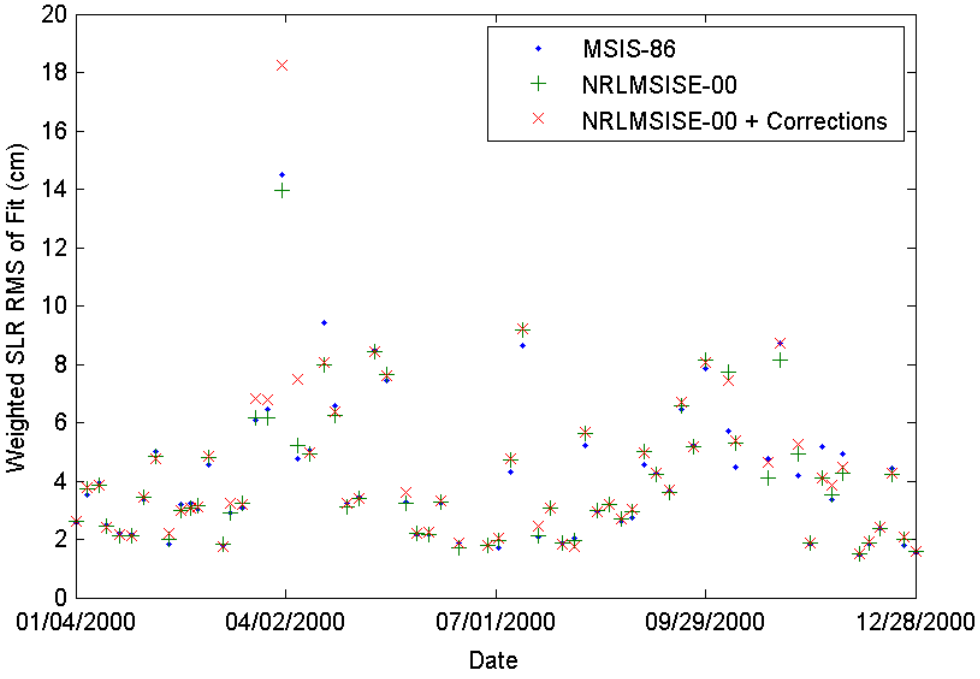

Figure 4.11 2000 GFO SLR RMS of Fit.

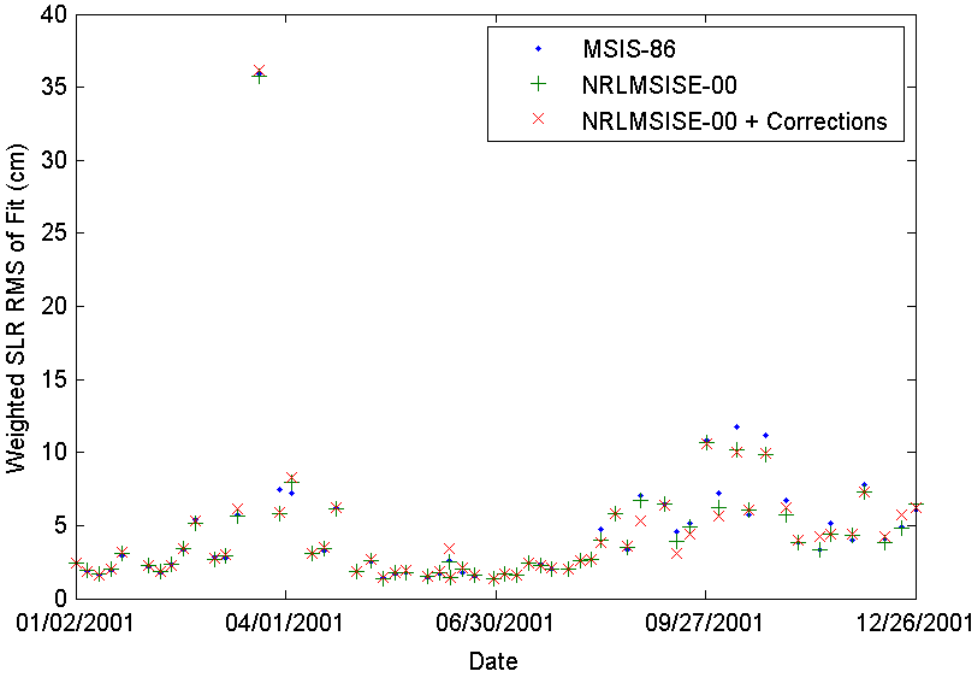

Figure 4.12 2001 GFO SLR RMS of Fit.

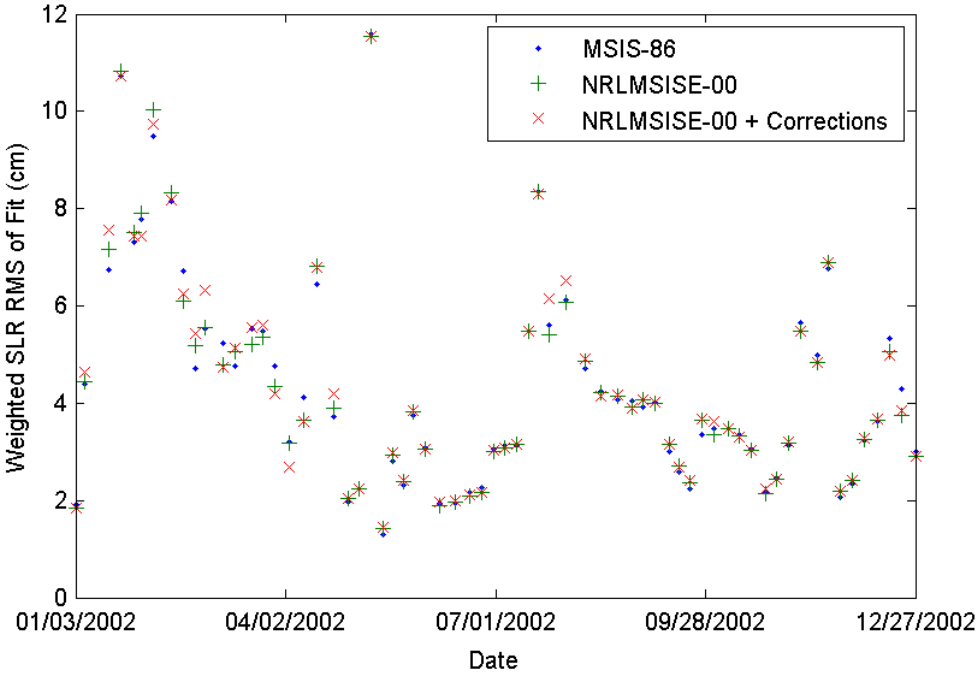

Figure 4.13 2002 GFO SLR RMS of Fit.

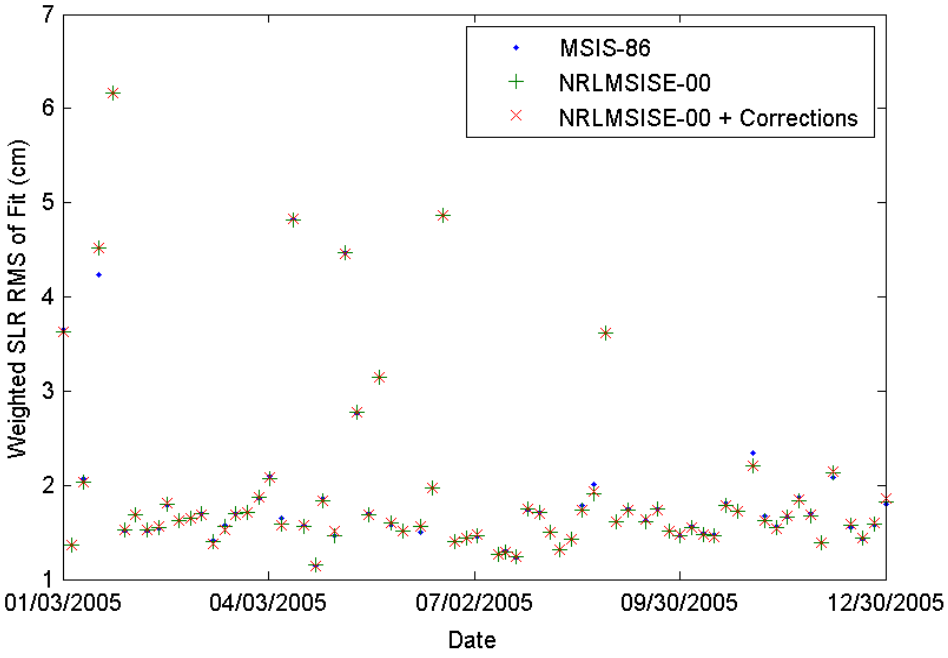

Figure 4.14 2005 GFO SLR RMS of Fit.

Table 4.5 GFO Yearly Average of Daily SLR RMS of Fit (cm).

Year	MSIS-86	NRLMSISE-00	NRLMSISE-00 + DCA
2000	4.023	4.041	4.209
2001	3.780	3.679	3.708
2002	4.049	4.052	4.093
2005	1.950	1.948	1.950

The yearly averages for each set of SLR RMS values are displayed in Table 4.5. Each set achieves averages within only a millimeter or two of the others, but in 2001 and 2005 the NRLMSISE-00 model has the smallest RMS. Changes on this level do not imply any significant improvement or worsening.

In order to determine a correlation between solar activity level and density routine performance, the SLR residuals were averaged in four categories of solar activity level. The result of this averaging is displayed in Table 4.6.The results are consistent with the yearly averages in that they show negligible change (~1mm). The DCA corrections provided no improvement over the MSIS-86 model when averaged this way.

Table 4.6 GFO SLR RMS of Fit Average Arranged by Solar Activity (cm).

Solar Activity	MSIS-86	NRLMSISE-00	NRLMSISE-00 + DCA
Low Solar Activity (F10.7 < 75)	1.490	1.494	1.495
Moderate Solar Activity (75 < F10.7 < 150)	2.261	2.268	2.276
Elevated Solar Activity (150 < F10.7 < 190)	4.245	4.220	4.296
High Solar Activity (F10.7 > 190)	5.570	5.500	5.648

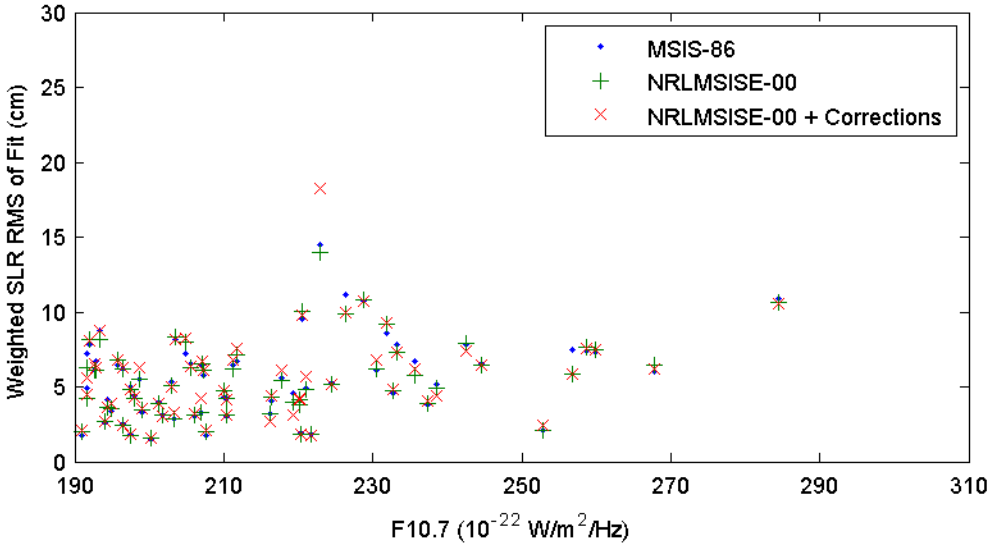

Figure 4.15 GFO SLR RMS of Fit vs. F10.7.

In order to show whether the SLR residuals were reduced more with higher solar flux, Figure 4.15 was generated. The figure plots only the SLR residuals at high solar activity (F10.7 > 190), and shows a correlation between higher solar flux and higher SLR residuals. However, the figure shows that the corrections do not consistently improve the SLR residuals at high solar activity.

Table 4.7 GFO SLR RMS of Fit Average Arranged by Geomagnetic Activity (cm).

Geomagnetic Activity	MSIS-86	NRLMSISE-00	NRLMSISE-00 + DCA
Quiet Ap (Ap < 10)	3.607	3.624	3.672
Moderate Ap (10 < Ap < 50)	3.881	3.807	3.898
Active Ap (Ap > 50)	3.509	3.454	3.489

Another significant correlation is the performance with geomagnetic activity. In order to show this comparison, the data was binned by geomagnetic activity according to the convention described previously. Table 4.7 shows a slight improvement in moderate and active Ap conditions, but both are on the order one millimeter and are thus not particularly significant.

Figure 4.16 was generated to show the correlation between the SLR residuals and active geomagnetic activity (Ap > 50). One data point at ~67 Ap has likely caused the average of active geomagnetic activity bin to be slightly exaggerated. This data point is also seen in the high solar activity plot near F10.7 ~ 193×10^{-22} W/(m^{2}Hz).

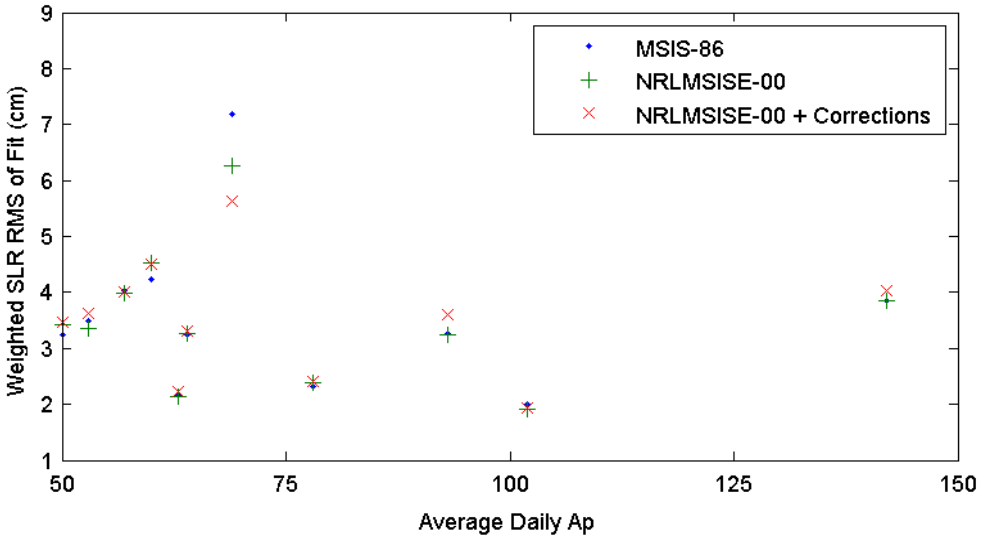

Figure 4.16 GFO SLR RMS of Fit vs. Active Ap.

4.1.3 Altimeter Crossover RMS of Fit

Since GFO is in an exact repeat ground track orbit, every 17 days GFO passes over the same geographic location. Being an altimeter satellite, consistency checks can be done by examining the altimeter returns from the same location GFO has passed over in recent history. These are typically locations where GFO crosses over an ascending pass where a recent descending pass has been or vice versa.

The altimeter crossovers for each arc have been averaged using the same method as the SLR values and tabulated in Table 4.8. The addition of the new routines shows no improvement, but the yearly averages do not change more than 1 mm.

Table 4.8 GFO Yearly Average of Daily Altimeter Crossover RMS of Fit (cm).

Year	MSIS-86	NRLMSISE-00	NRLMSISE-00 + DCA
2000	8.048	8.092	8.128
2001	7.459	7.494	7.498
2002	7.439	7.469	7.471
2005	6.543	6.542	6.542

Table 4.9 GFO Altimeter Crossovers Average Arranged by Solar Activity (cm).

Solar Activity Level	MSIS-86	NRLMSISE-00	NRLMSISE-00 + DCA
Low Solar Activity (F10.7 < 75)	6.731	6.733	6.733
Moderate Solar Activity (75 < F10.7 < 150)	6.989	7.001	7.001
Elevated Solar Activity (150 < F10.7 < 190)	8.202	8.214	8.242
High Solar Activity (F10.7 > 190)	9.214	9.295	9.303

The altimeter crossovers have also been subjected to the same binning with respect to solar activity as the SLR residuals. The result of this is displayed in Table 4.9. Again, the averages are not improved by the new density routines, but the change is still less than 1 mm. Similar to the SLR residuals, the routine with the DCA corrections are slightly worse than without the corrections.

Table 4.10 GFO Altimeter Crossovers Average Arranged by Geomagnetic Activity (cm).

Geomagnetic Activity	MSIS-86	NRLMSISE-00	NRLMSISE-00 + DCA
Quiet Ap (Ap < 10)	7.812	7.873	7.856
Moderate Ap (10 < Ap < 50)	8.058	8.082	8.078
Active Ap (Ap < 50)	8.255	8.184	8.180

To show a trend with the altimeter crossovers and the geomagnetic activity conditions described previously, averages of all altimeter crossovers were taken for

each condition and for each density routine. Table 4.10 shows good correlation between a rise in Ap and a rise in the altimeter crossover residuals. The table does suggest that both the corrections and NRLMSISE-00 by itself improved the altimeter crossovers in active geomagnetic activity, but again these improvements are on the order of one millimeter.

4.1.4 Orbit Overlaps

Table 4.11 GFO Yearly Average of RMS of Orbit Overlap Position Components (cm).

Density Routine	Direction	Year			
		2000	2001	2002	2005
MSIS-86	Along-track	26.4	12.1	14.8	6.5
	Cross-track	14.1	7.1	7.1	5.7
	Radial	2.8	1.7	2.1	1.0
	Total	32.6	15.4	17.6	9.23
NRLMSISE-00	Along-track	25.0	13.1	14.0	6.5
	Cross-track	14.9	7.1	7.1	5.7
	Radial	2.7	1.7	2.0	1.0
	Total	31.8	16.4	16.8	16.8
NRLMSISE-00 + DCA	Along-track	25.5	13.1	14.1	6.5
	Cross-track	14.6	7.2	7.1	5.7
	Radial	2.8	1.7	2.0	1.0
	Total	32.0	16.3	16.8	9.18

The orbit overlaps for 2000-2002 and 2005 were computed for each data set (original MSIS-86, NRLMSISE-00 and NRLMSISE-00 with DCA) for a total of 12 sets. To easily compare the results of these overlaps, the yearly average for each set of overlaps was found (generally on the order of 50 per year). The resulting values are displayed in Table 4.11. For 2000 and 2002, the along track component of the RMS

of position orbit overlaps are improved slightly by the addition of the new density routine or the new density routine with the corrections, as evident in Table 4.11. The total position orbit overlap in Table 4.11 shows improvement in every year except 2001.

4.2 Processing with Empirical Accelerations Removed

The setups obtained from NASA GSFC were modified to remove the estimation of along-track and cross-track empirical accelerations. This was accomplished by removing the ACCEL9 input cards in the setup files. By not estimating the empirical accelerations, any effects due to force modeling errors will become more pronounced. This is especially true of non-conservative forces like atmospheric drag. The performance of removing the empirical accelerations can be compared to the runs with empirical accelerations to determine if the routines improved similarly.

After modifying the setups, the same GFO arcs were run for 2000-2002 and 2005. Since the estimation of empirical accelerations is the only change between the two sets of runs, a comparison of the relative improvements from each setup type can be made. Ideally, if the updated density routines show increased accuracy with the empirical acceleration estimation removed then they are a better representation of the forces due to atmospheric drag imposed on the spacecraft.

Each metric of comparison from the previous section is also examined here with exception of the empirical accelerations. In addition to the previous comparison studies, the drag coefficient estimated using GEODYN is also analyzed.

4.2.1 SLR RMS of Fit

Similarly to the previous section, the SLR RMS of fit values were extracted from the GEODYN summary output file and analyzed. This time, the values are plotted in Figure 4.17 through Figure 4.24 against both F10.7 and Ap to examine the performance knowing the influence from the other major sources of non-conservative forces. Each data point is located at the beginning of an arc. The arcs are typically one week in duration, so the solar or geomagnetic activity immediately following each data point will be included in the computation of that arc.

The RMS values are much larger than the previous section, which is expected after removing the estimated OPR accelerations which soak up some of the error each revolution. The original MSIS-86 routine exhibits consistently lower SLR RMS values for 2000. This is a significant discovery because 2000 is a period of high solar activity (near solar max) and a period where the performance was thought to have the largest potential to improve accuracy with the updated density routines.

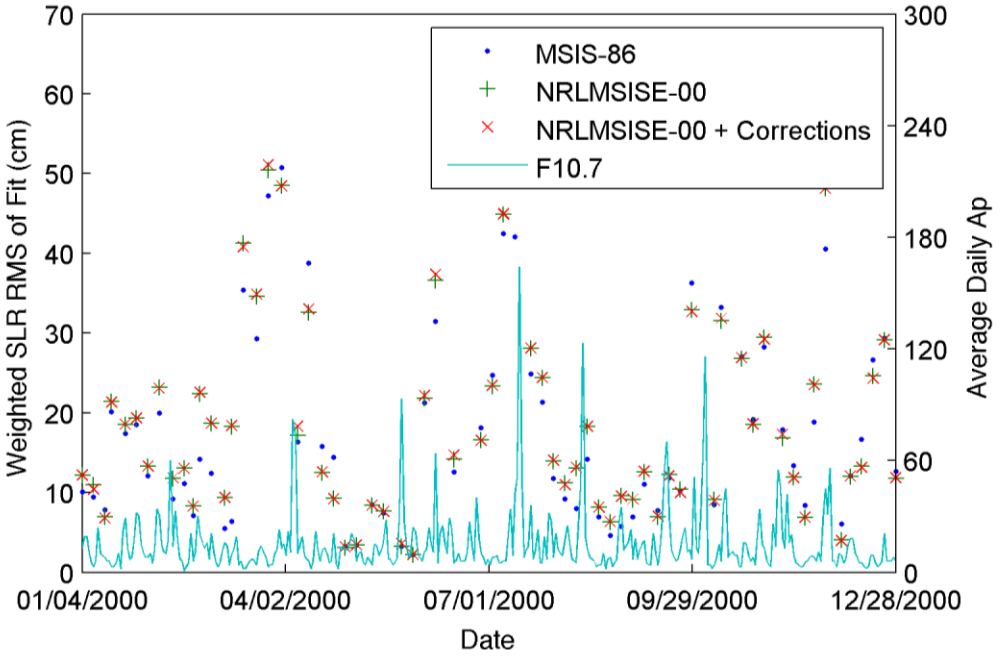

Figure 4.17 2000 GFO SLR RMS of Fit with Ap.

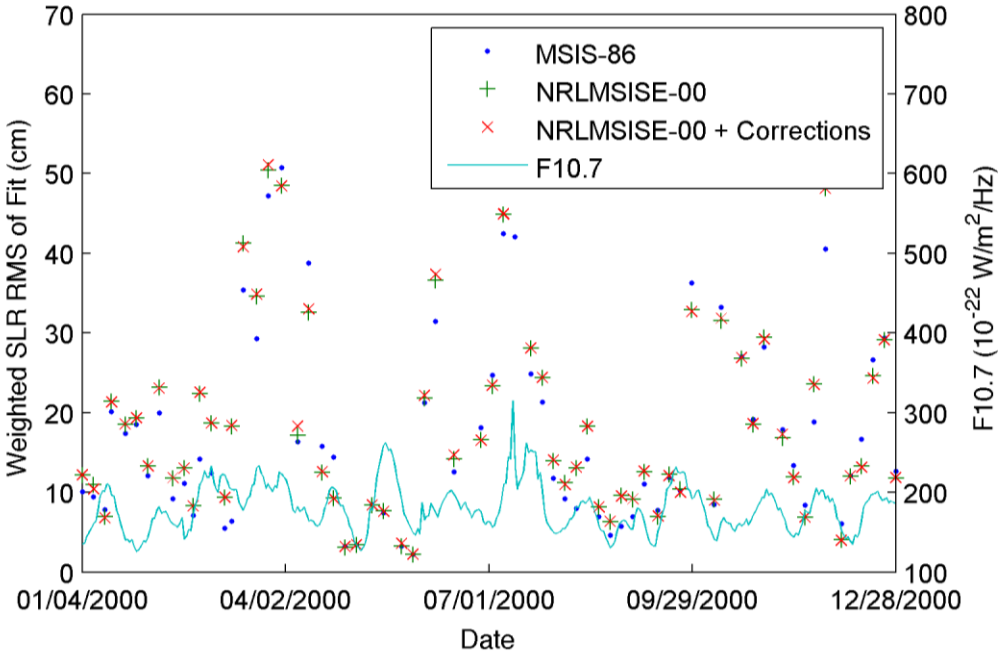

Figure 4.18 2000 GFO SLR RMS of Fit with F10.7.

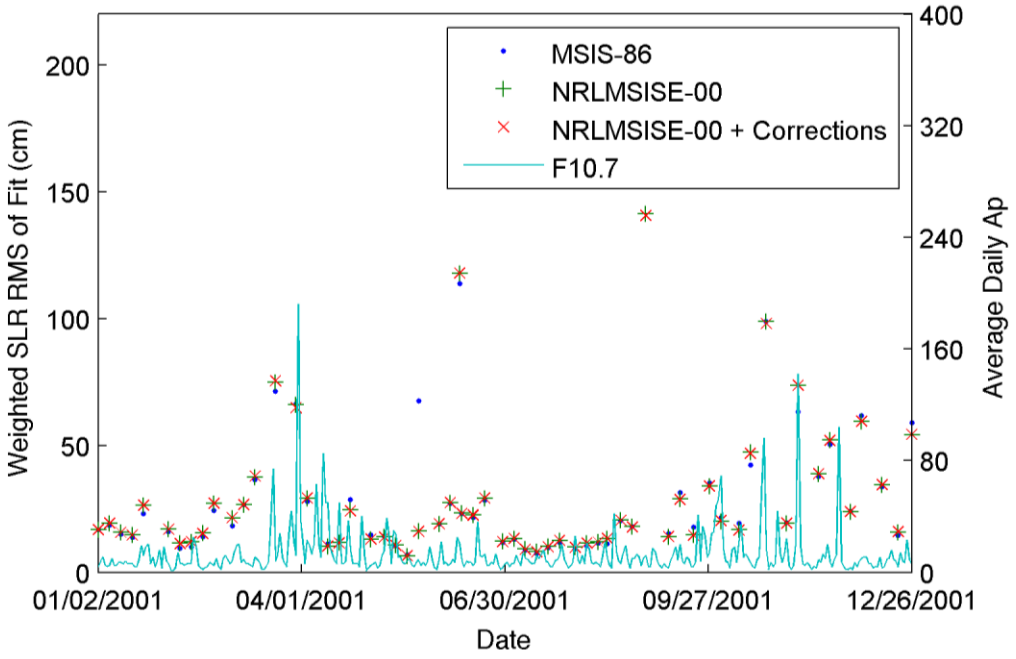

Figure 4.19 2001 GFO SLR RMS of Fit with Ap.

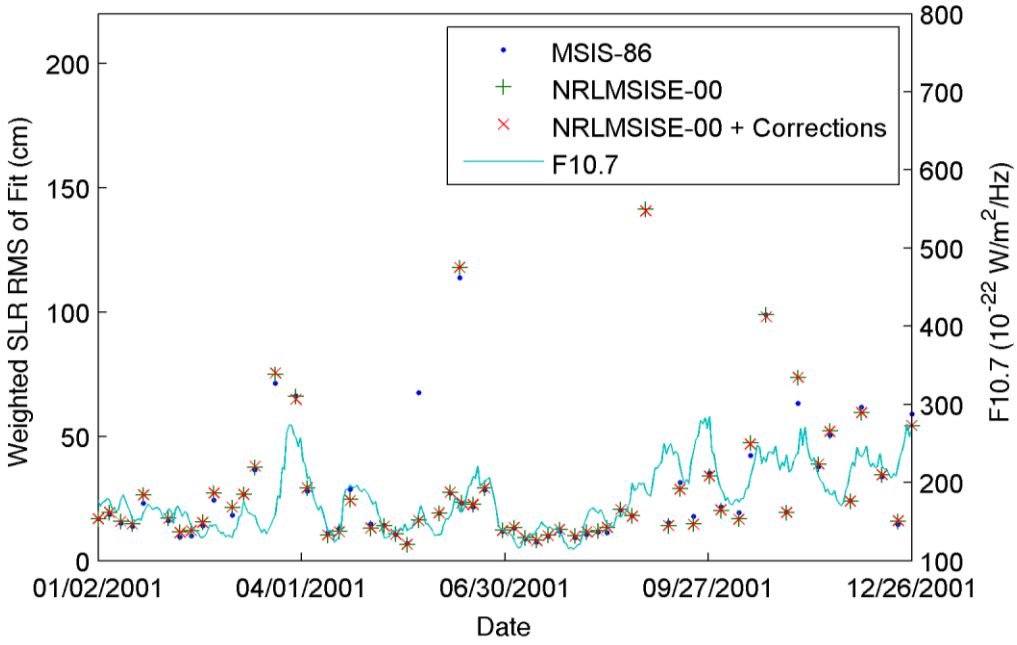

Figure 4.20 2001 GFO SLR RMS of Fit with F10.7.

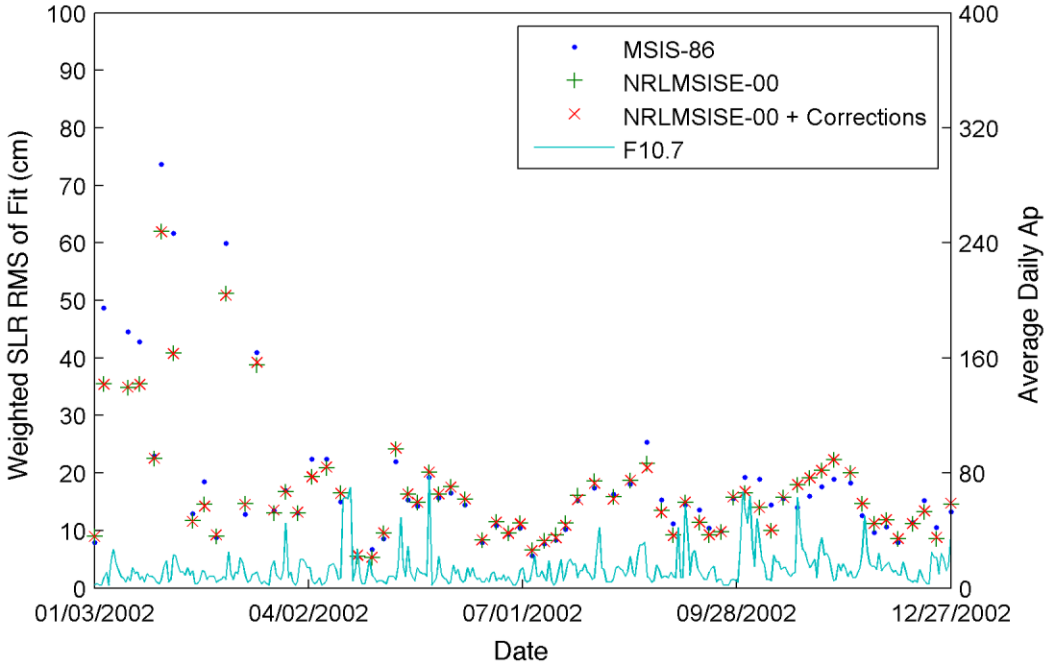

Figure 4.21 2002 GFO SLR RMS of Fit with Ap.

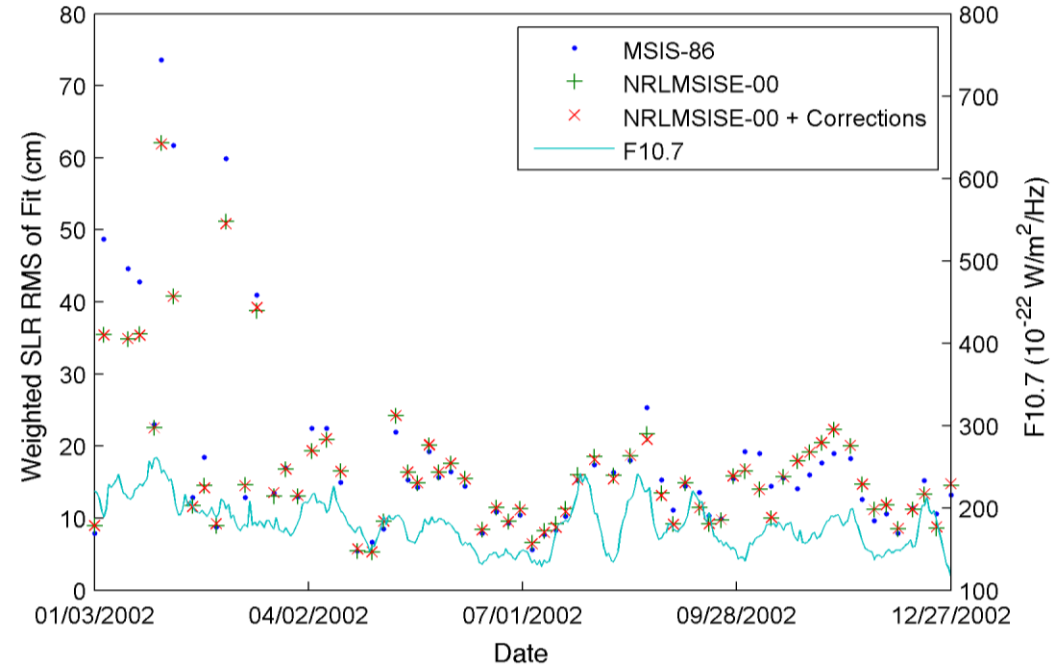

Figure 4.22 2002 GFO SLR RMS of Fit with F10.7.

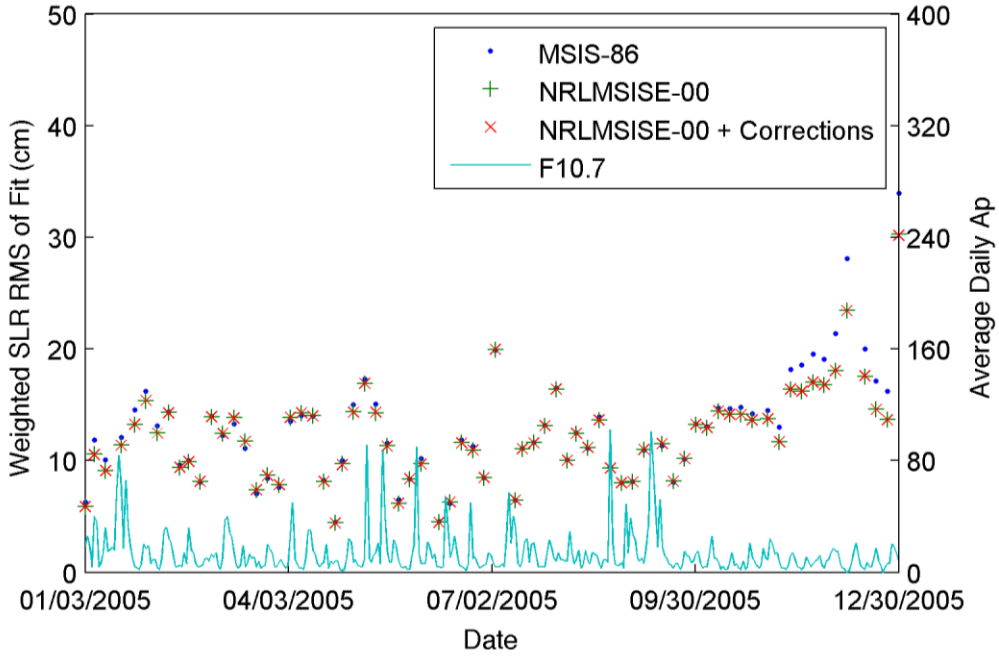

Figure 4.23 2005 GFO SLR RMS of Fit with Ap.

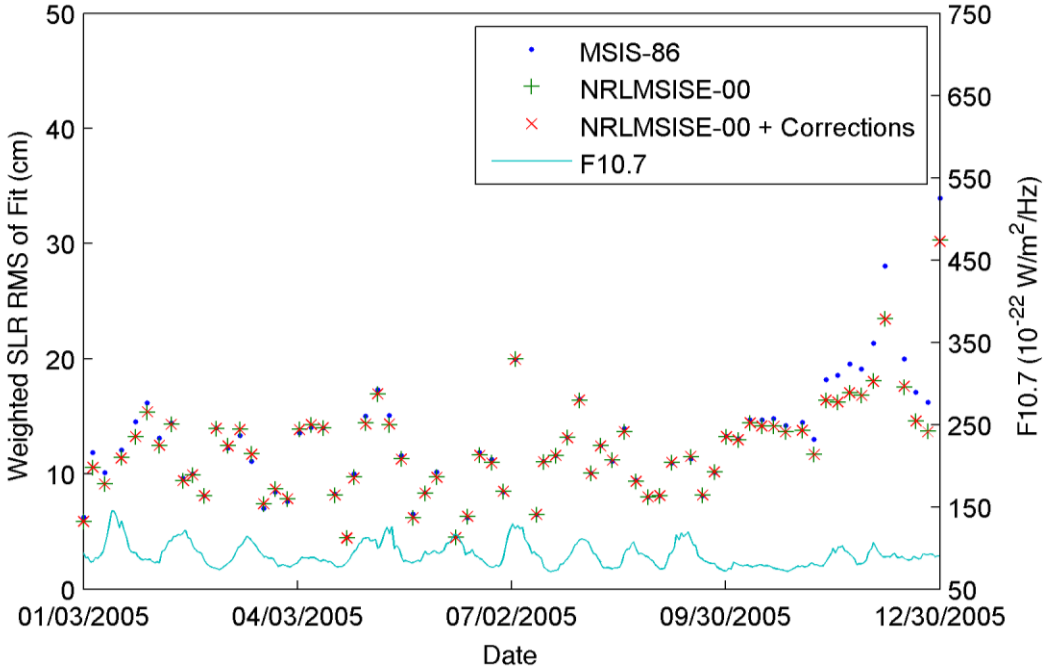

Figure 4.24 2005 GFO SLR RMS of Fit with F10.7.

Table 4.12 GFO Yearly Average of Daily SLR RMS of Fit (cm).

Year	MSIS-86	NRLMSISE-00	NRLMSISE-00 + DCA
2000	17.307	18.683	18.732
2001	29.180	28.614	28.559
2002	18.099	17.058	17.015
2005	12.779	12.217	12.213

Yearly averages for the SLR RMS of fits were taken for each GEODYN version and displayed in Table 4.12. The 2001 plots of Figure 4.19 and Figure 4.20 show most RMS values for all atmospheric models coincide with the exception of one outlier for MSIS-86 in May. This outlier is likely the source causing the MSIS-86 yearly average in Table 4.12 to perform worse. A number of high RMS values in early 2002 that improve with the new density models, seen in Figure 4.21 and Figure 4.22 are likely the cause of the 2002 average showing an improvement with the new routines. The 2005 SLR RMS values show the most consistent improvements with the new routines of all the years.

The SLR RMS values were again binned by both solar and geomagnetic activity in order to show performance at various activity levels. Table 4.13 and Figure 4.25 show a consistent trend for the new density models to achieve lower RMS values at higher activity levels. When binned in this manor, the new routines actually outperformed the MSIS-86 model in all solar activity levels. The changes were very marginal in each case, with no improvements greater than a few millimeters. Figure 4.25 is promising though because the new density models show consistent

improvement for most cases in high solar activity. These results are not thrown off by outliers.

Table 4.13 GFO SLR RMS of Fit Average Arranged by Solar Activity (cm).

Solar Activity	MSIS-86	NRLMSISE-00	NRLMSISE-00 + DCA
Low Solar Activity (F10.7 < 75)	11.661	11.552	11.553
Moderate Solar Activity (75 < F10.7 < 150)	12.289	12.184	12.174
Elevated Solar Activity (150 < F10.7 < 190)	20.450	20.023	20.057
High Solar Activity (F10.7 > 190)	28.614	28.580	28.503

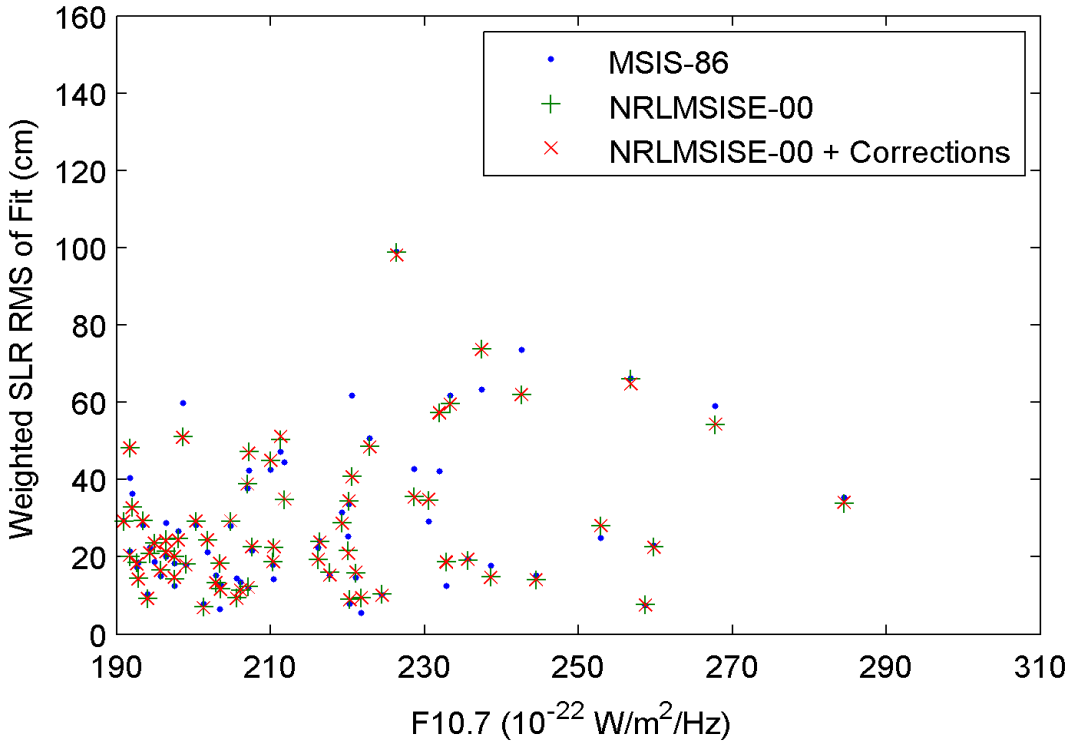

Figure 4.25 GFO SLR RMS of Fit vs. High F10.7.

Table 4.14 GFO SLR RMS of Fit Average Arranged by Geomagnetic Activity (cm).

Geomagnetic Activity	MSIS-86	NRLMSISE-00	NRLMSISE-00 + DCA
Quiet Ap (Ap <10)	18.189	17.651	17.628
Moderate Ap (10 < Ap < 50)	20.043	20.178	20.165
Active Ap (Ap > 50)	19.336	20.494	20.621

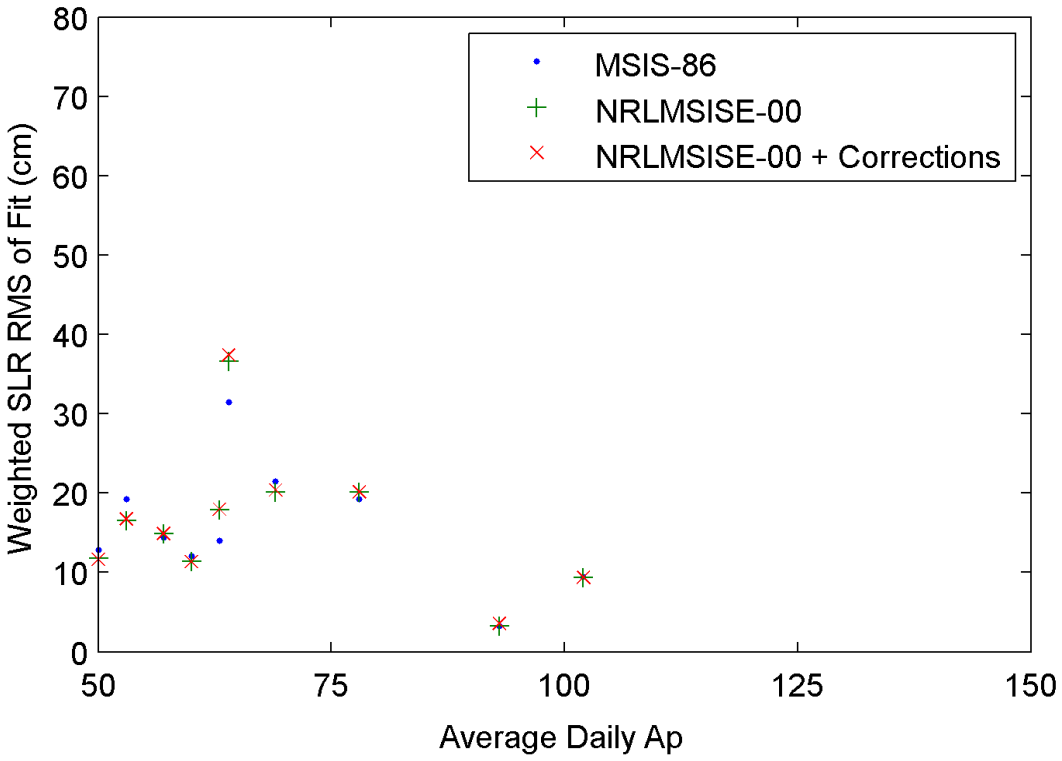

Figure 4.26 GFO SLR RMS of Fit vs. Active Ap.

The SLR RMS values binned into geomagnetic activity are displayed in Table 4.14 and Figure 4.26. These bins exhibited the opposite trend from the solar activity bins. Only ten days out of the four years run coincided with 'active' geomagnetic

conditions, which is not nearly large enough of a sample size to make any conclusions. The variations in the 'moderate' condition of these bins are slight, but at around 5mm the quiet condition is improved the most.

4.2.2 Altimeter Crossover RMS of Fit

The altimeter crossovers were obtained using the same method detailed in the previous section. The crossovers were extracted from each arc of data and displayed in Figure 4.27 through Figure 4.30. The yearly averages of the crossover RMS of fit were also taken and displayed in Table 4.15.

Table 4.15 GFO Yearly Average of Daily Altimeter Crossover RMS of Fit (cm).

Year	MSIS-86	NRLMSISE-00	NRLMSISE-00 + DCA
2000	19.23	20.88	20.93
2001	28.29	28.82	28.74
2002	22.13	21.13	20.99
2005	16.81	15.75	15.74

The MSIS-86 routine in the 2000 and 2001 sets of data seen in Figure 4.27 and Figure 4.28 show the smallest RMS values when compared to the new density routines. Figure 4.29 and Figure 4.30 show the opposite trend for the 2002 and 2005 data sets. These trends are further reinforced in Table 4.15. Again, this trend is the opposite of what was expected; the height of the solar maximum, 2000-2001 exhibited no improvement from the newer density models, where the relatively lower solar activity years were improved. This phenomenon will be further analyzed by binning the RMS values by solar activity.

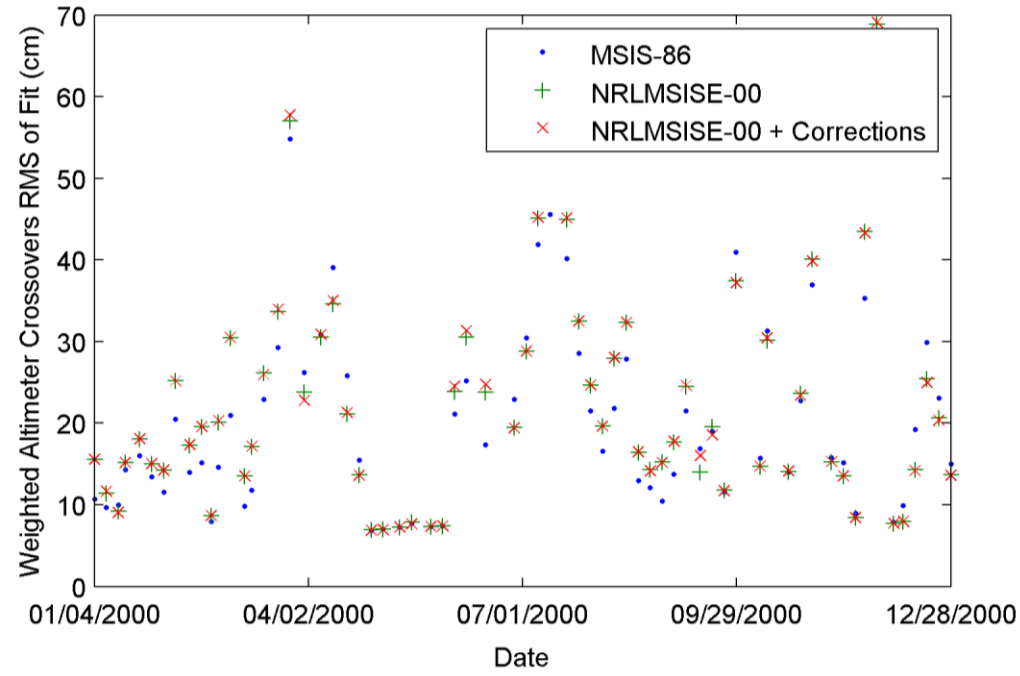

Figure 4.27 2000 GFO Altimeter Crossover RMS of Fit.

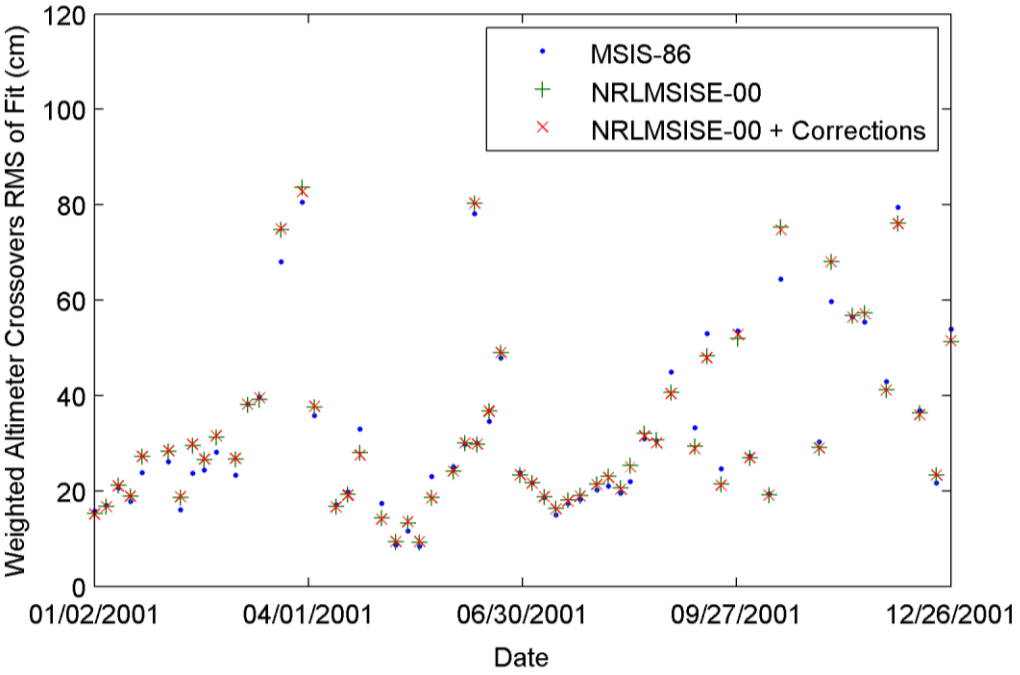

Figure 4.28 2001 GFO Altimeter Crossover RMS of Fit.

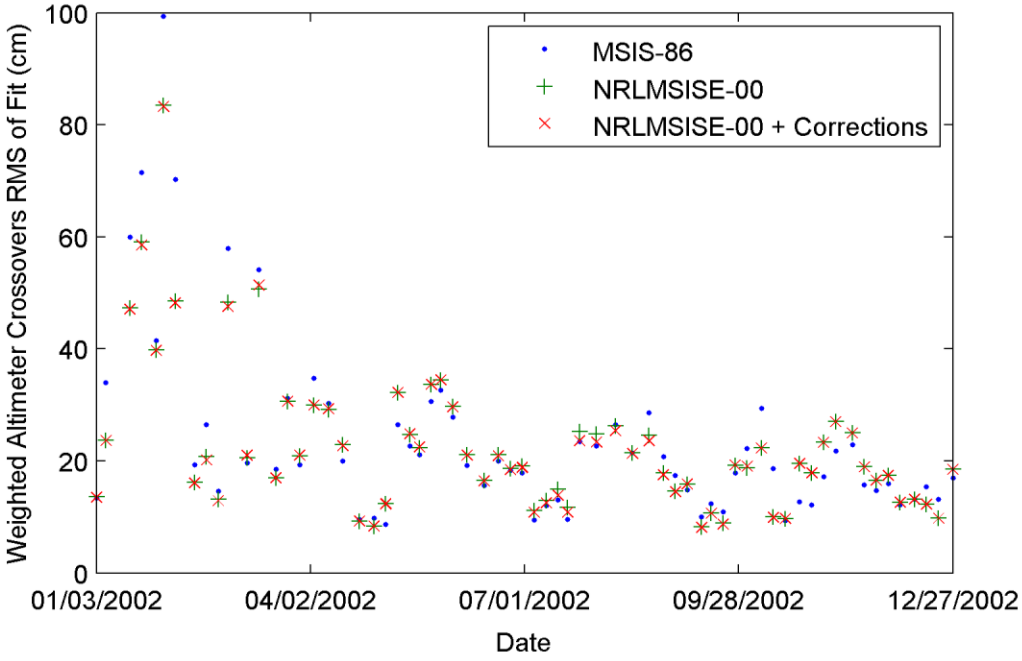

Figure 4.29 2002 GFO Altimeter Crossover RMS of Fit.

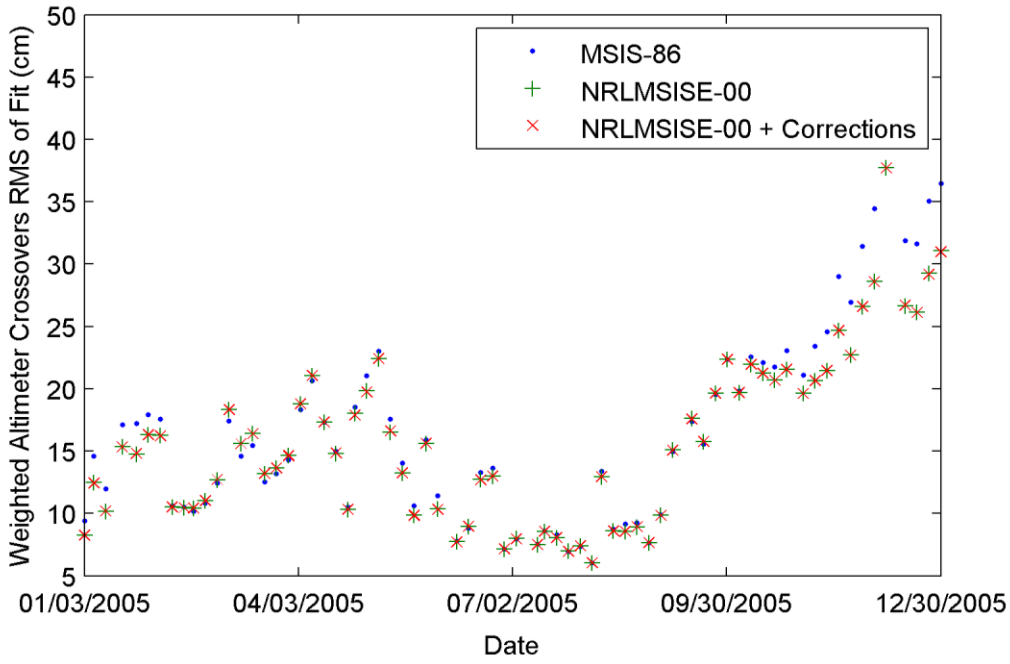

Figure 4.30 2005 GFO Altimeter Crossover RMS of Fit.

Table 4.16 GFO Altimeter Crossovers Average Arranged by Solar Activity (cm).

Solar Activity Level	MSIS-86	NRLMSISE-00	NRLMSISE-00 + DCA
Low Solar Activity (F10.7 < 75)	14.47	14.09	14.08
Moderate Solar Activity (75 < F10.7 < 150)	16.91	16.66	16.64
Elevated Solar Activity (150 < F10.7 < 190)	21.92	22.42	22.45
High Solar Activity (F10.7 > 190)	36.02	35.94	35.74

After binning the altimeter crossover RMS values into solar activity levels in Table 4.16, the NRLMSISE-00 with DCA corrections were found to have the best performance in all levels except 'elevated'. The corrections showed the most improvement over the NRLMSISE-00 routine by itself in 'high' solar activity.

The crossover RMS values were binned by geomagnetic activity in Table 4.17, but did not show improvement for the new routines except in the 'quiet' condition.

Table 4.17 GFO Altimeter Crossovers Average Arranged by Geomagnetic Activity (cm).

Geomagnetic Activity	MSIS-86	NRLMSISE-00	NRLMSISE-00 + DCA
Quiet Ap (Ap < 10)	23.05	22.73	22.68
Moderate Ap (10 < Ap < 50)	23.68	24.04	23.98
Active Ap (Ap > 50)	21.94	23.41	23.49

4.2.3 Orbit Overlaps

The orbit overlaps were computed using the procedure described in the previous section. The RMS of the components of position for the four years of arcs studied were averaged and are listed in Table 4.18 for the along-track, cross-track, and radial directions for each version of GEODYN. Since any improvement in the atmospheric drag modeling would be in the along-track direction, each of the along-track rows have been highlighted in yellow. The best case for each year in the along-track direction is colored orange. The NRLMSISE-00 routine with the corrections performed the best for 2002 and 2005, while MSIS-86 performed the best for 2000 and 2001. Yearly averages of the total position output from the orbit overlap routine are also tabulated in Table 4.18. The NRLMSISE-00 based routines are best for the 2002 and 2005 data sets, and the MSIS-86 is best in 2000 and 2001.

Table 4.18 GFO Yearly Average of RMS of Orbit Overlap Position Components (cm).

Density Routine	Direction	Year			
		2000	2001	2002	2005
MSIS-86	Along-track	105.5	161.8	132.5	92.0
	Cross-track	45.5	56.4	45.5	47.5
	Radial	31.3	58.9	37.9	31.7
	Total	124.8	185.1	153.0	113.9
NRLMSISE-00	Along-track	115.7	166.0	123.1	85.4
	Cross-track	47.7	57.5	46.1	47.5
	Radial	35.8	60.0	36.4	29.6
	Total	135.5	189.4	143.6	107.3
NRLMSISE-00 + DCA	Along-track	115.9	165.3	122.3	85.4
	Cross-track	47.8	57.6	46.2	47.5
	Radial	35.7	59.9	36.0	29.5
	Total	135.8	188.8	142.7	107.3

4.2.4 Drag Coefficient Analysis

In order to investigate what is happening behind the scenes in the computation of each arc, the GEODYN program was modified to output the estimated drag coefficient values. The drag coefficients are specified via the 'DRAG' input cards to be estimated every 8 hours. The drag coefficient values are essentially a scale factor to balance the two sides of the drag acceleration equation (Eqn. **(1.1)**), so any inconsistencies in the parameters in the drag equation will appear in this term. The drag coefficient values have been obtained from GEODYN for the four years of setups available. For each year, two plots were created and appear as Figure 4.31 through Figure 4.38. The first plot of each year is the drag coefficient value for each version of GEODYN. The second plot of each year is the drag coefficient difference from the original version of GEODYN which uses MSIS-86. This allows for a comparison of the relative influence of the density models.

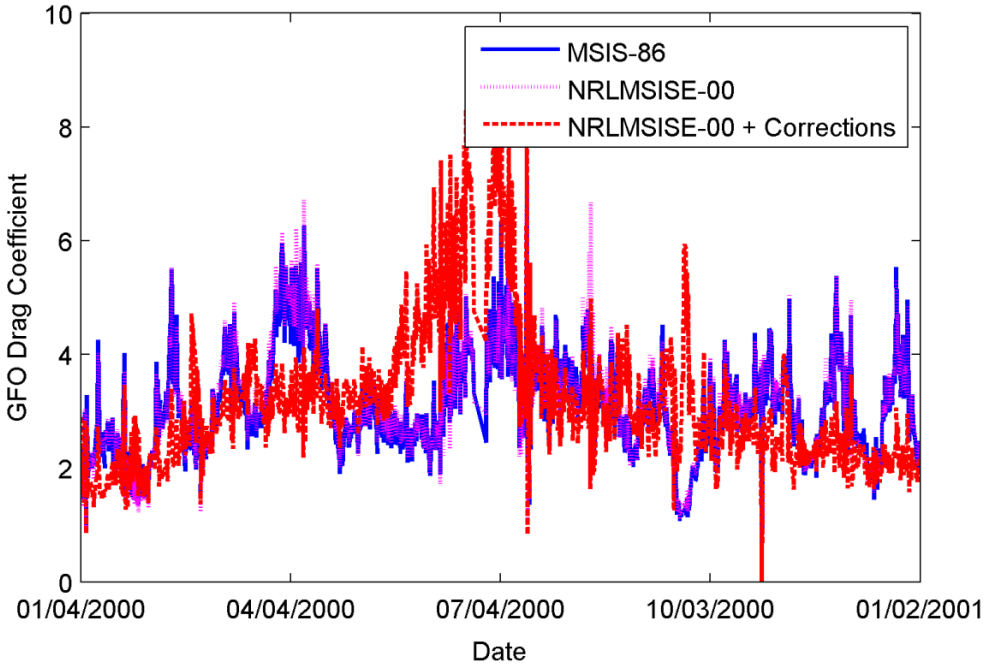

Figure 4.31 2000 GFO Drag Coefficient.

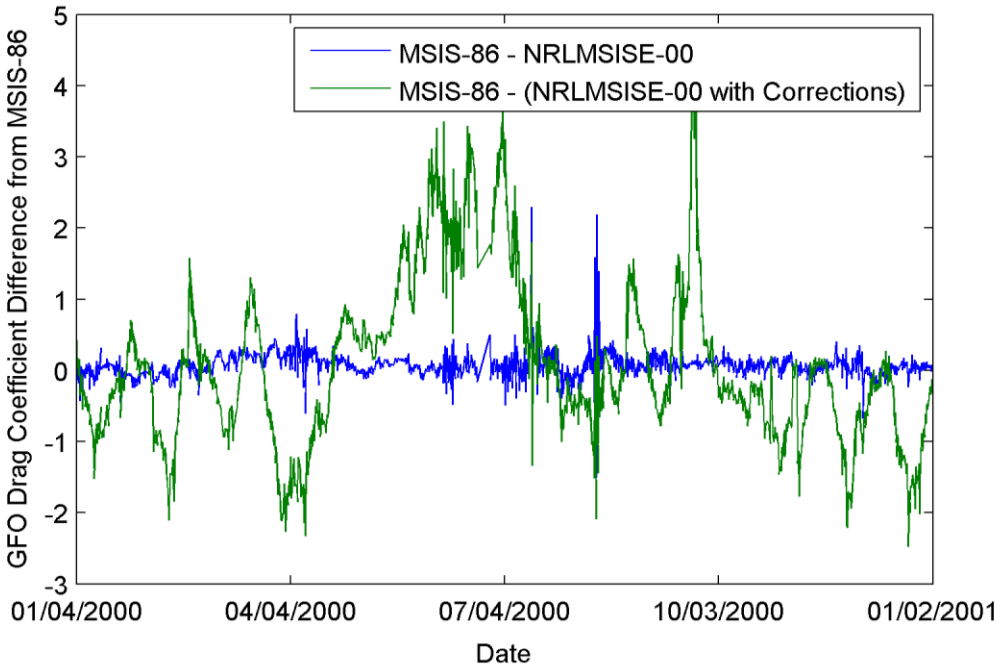

Figure 4.32 2000 GFO Drag Coefficient Differences.

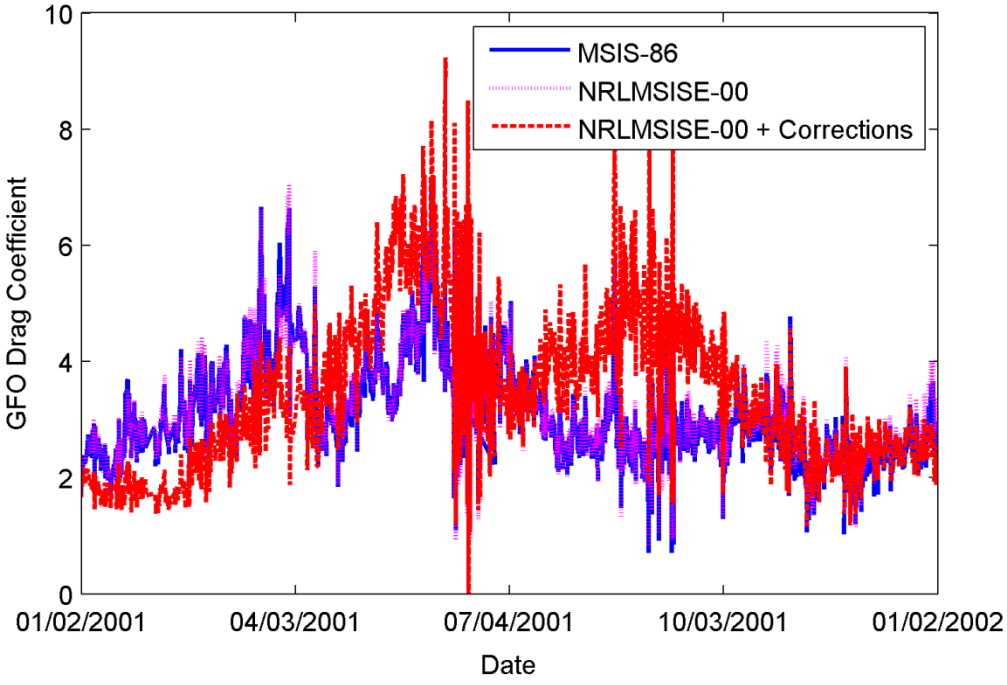

Figure 4.33 2001 GFO Drag Coefficient.

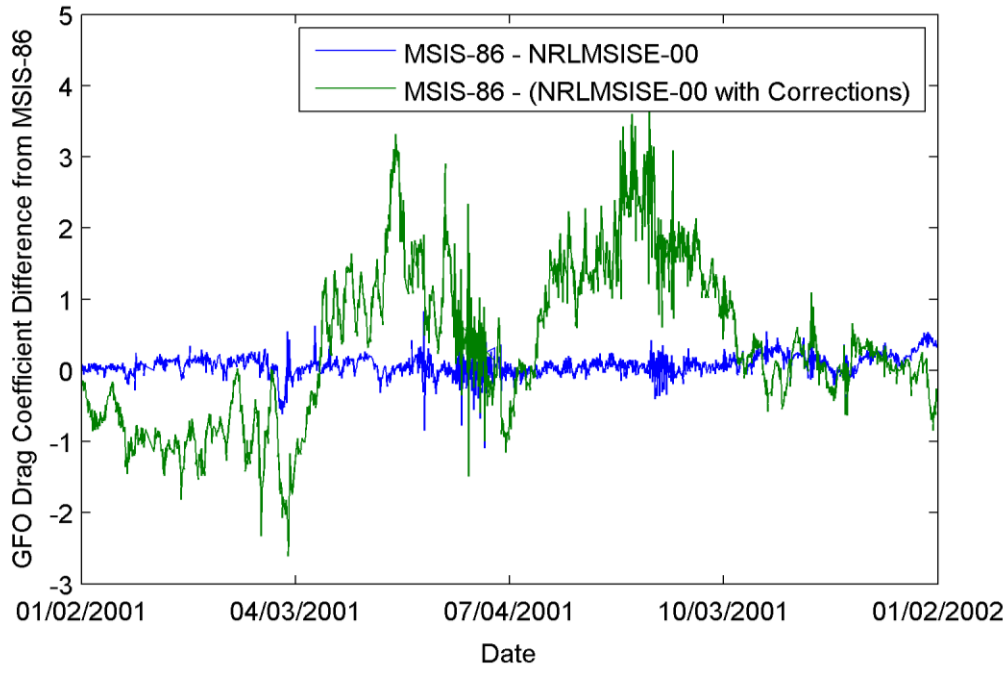

Figure 4.34 2001 GFO Drag Coefficient Differences.

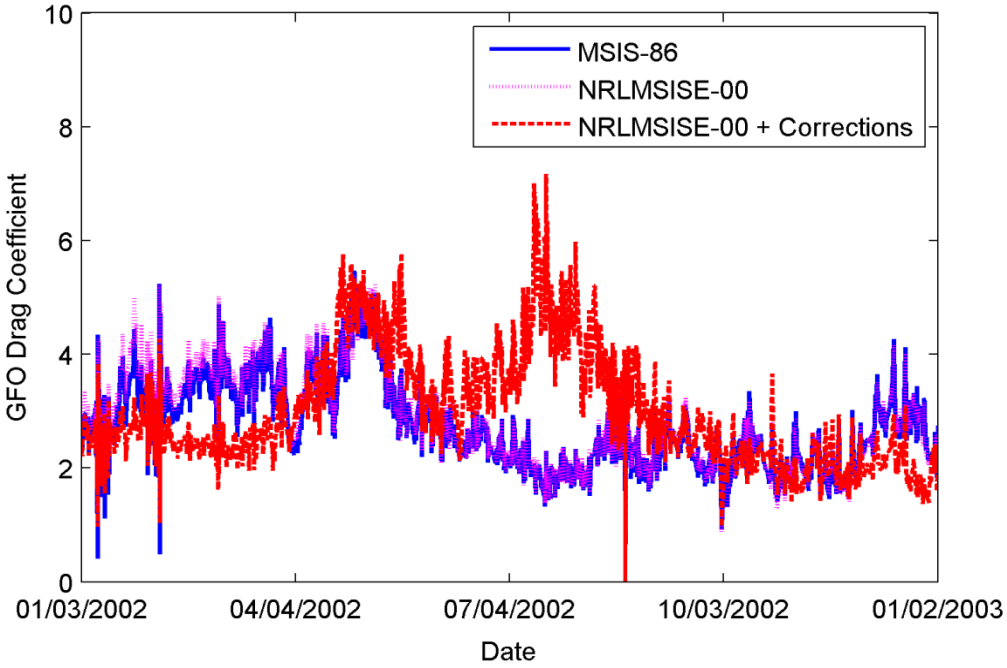

Figure 4.35 2002 GFO Drag Coefficient.

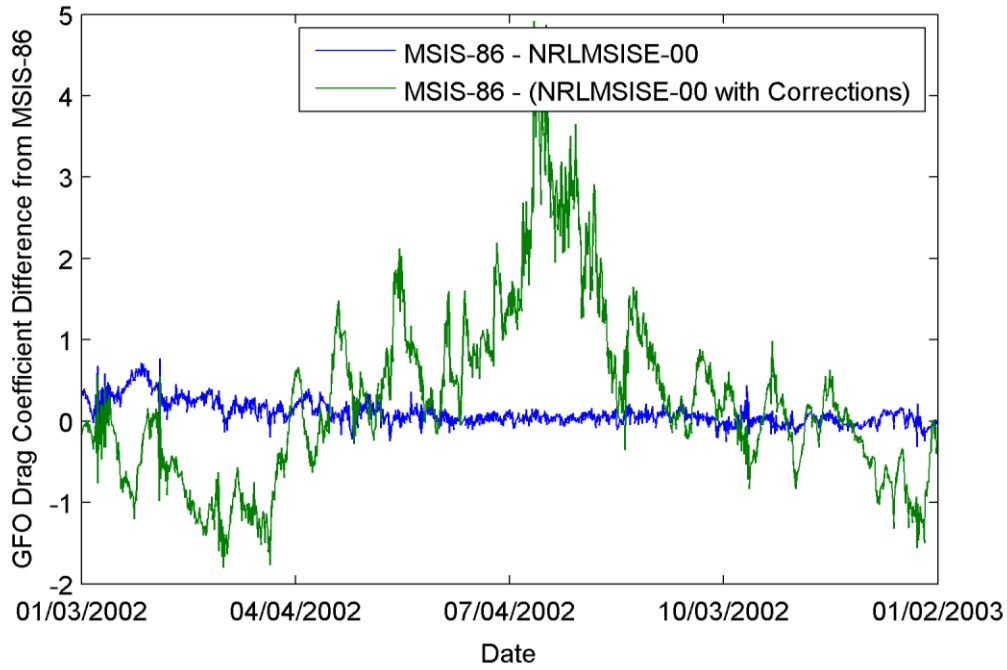

Figure 4.36 2002 GFO Drag Coefficient Differences.

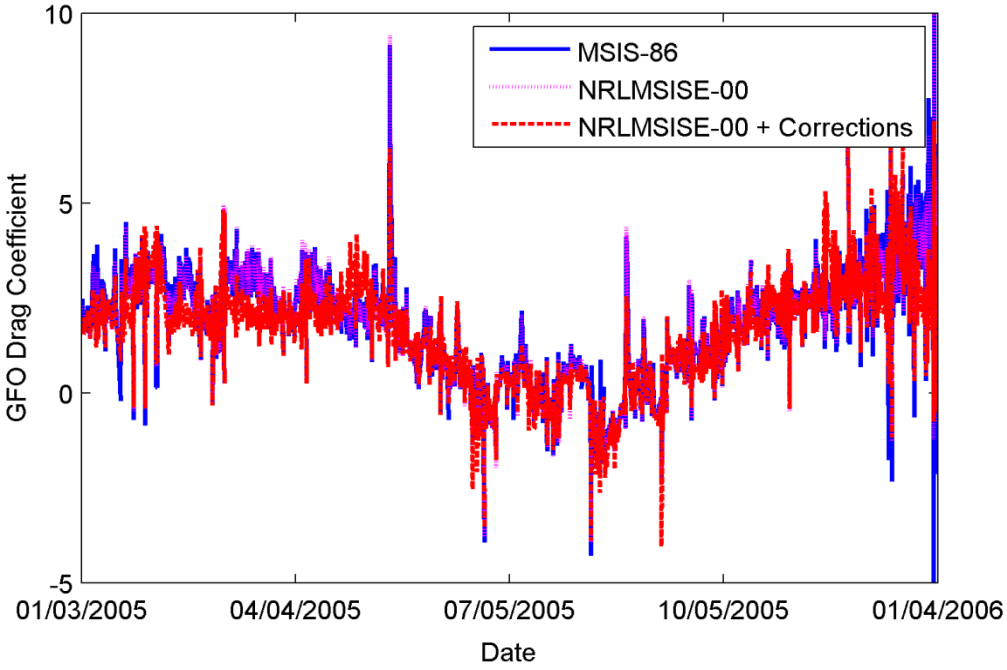

Figure 4.37 2005 GFO Drag Coefficient.

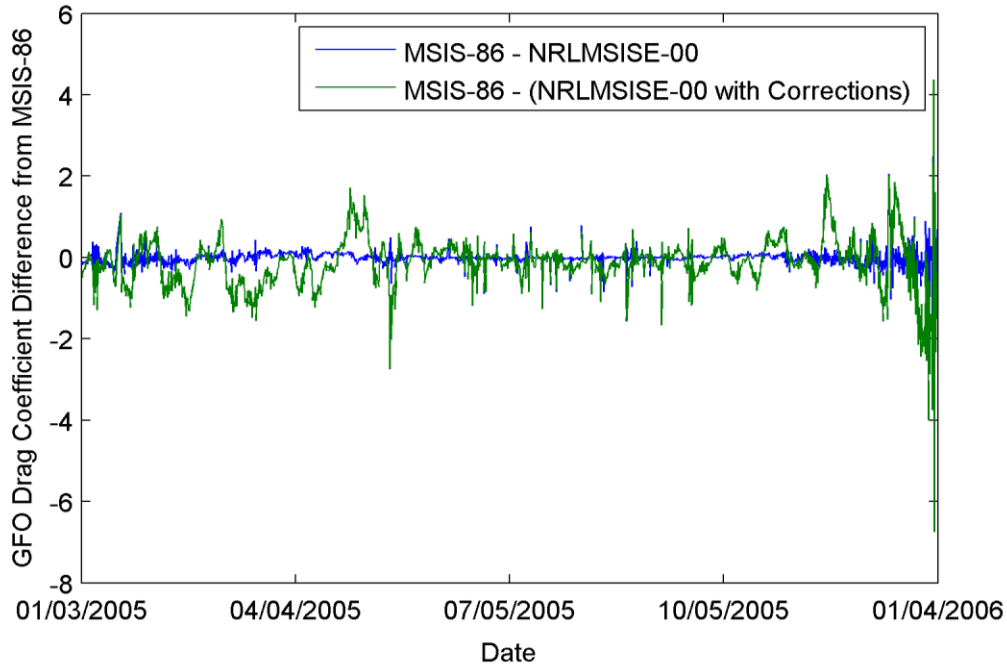

Figure 4.38 2005 GFO Drag Coefficient Differences.

The results of these plots were surprising. The DCA corrections produced drag coefficient values which are significantly different from either the MSIS-86 or the NRLMSISE-00 density routines. A common value for a satellite drag coefficient used for rough approximation is 2.2, but due to the geometry of GFO, this value may likely be greater. The values seen in these plots are vastly different than the commonly accepted approximation, mostly likely because of the absorption of errors in other parameters by the drag coefficient values, especially density. The difference between the C_D values obtained by the DCA correction routine and the MSIS-86 routine is staggering. The differences are +/- 4 for the years close to solar max and still surprisingly large in 2005. The yearly averages of the drag coefficient values are shown in Table 4.19.

Table 4.19 GFO Yearly Average of Drag Coefficient

Year	MSIS-86	NRLMSISE-00	NRLMSISE-00 + DCA
2000	3.0469	3.1121	3.1203
2001	3.1231	3.1895	3.4866
2002	2.7230	2.8171	2.9960
2005	1.7426	1.7328	1.5947

4.3 Summary of Results

Four years of GFO data have been processed using three different versions of GEODYN with empirical accelerations estimated every time step. For most metrics of comparison, the results presented using this setup all fell within close proximity to each other. The NRLMSISE-00 model appeared to present a slight improvement in modeling atmospheric drag in periods of higher solar activity. This is evident in the

analysis of the predicted empirical accelerations. When the along-track accelerations were binned by solar activity, the ‘high’ activity bin showed the most improvement using the NRLMSISE-00 model and also the new model and DCA corrections. The SLR RMS values showed that the periods of high solar and geomagnetic activity are better modeled by the NRLMSISE-00 routine, but the improvement shown here was very slight (less than one millimeter). The performance of the new routines with altimeter crossovers was not improved at all, but the orbit overlaps were improved for several years by the NRLMSISE-00 routine.

After achieving negligible improvement with the upgraded density models, the GFO setups were modified to not estimate the OPR empirical accelerations. This provides a better insight into the performance of the density routines by removing the possibility that some of the improvements in density modeling were absorbed in the estimated once per revolution accelerations. After re-running these cases with the new setups, the same metrics of comparison were evaluated with an additional drag coefficient study.

When evaluating the SLR RMS of fit values, the cases run with empirical accelerations do not correlate well with the cases run without empirical accelerations. The MSIS-86 version was best in 2000 and 2002 in the runs with empirical accelerations, but for the runs without OPR accelerations, MSIS-86 was better in 2000 and 2001. This lack of correlation is further evidenced by examining the SLR RMS bins of solar and geomagnetic activity. The MSIS-86 is superior with empirical accelerations in low and moderate solar activity, but was not the best in any solar

activity bins with the empirical acceleration estimation removed. The new density routines did exhibit better performance in SLR RMS values for each setup type in both elevated and high solar activity levels. The geomagnetic activity did not show any commonality between the setup types. Each bin had different performance depending on activity type.

The altimeter crossover values showed a similar trend when averaged by year, with the earlier years favoring MSIS-86, and the later years favoring the DCA corrections. When binned into solar and geomagnetic activity levels, the correlation stops. The high solar activity favors the DCA corrections for the runs with empirical accelerations, and MSIS-86 in the runs without.

The orbit overlaps produced similar results for both setup types with the exception of 2000. For runs without empirical accelerations estimated, 2000 was improved with the NRLMSISE-00 routine, but for the runs without, MSIS-86 was preferred. This trend is also the opposite of expected because of the lack of the expected performance increase from the yearly averages closer to solar maximum (2000-2001).

The drag coefficient analysis of the runs without empirical accelerations showed that the DCA corrections produced C_D values which did not correlate with either of the two other routines. The application of corrections that are not suitable for GFO's altitude increasing density error is likely the cause of the large differences. The mechanism that is changing C_D is probably from the inability for the DCA

routine to properly model density, so the C_D term has to absorb that error in the drag equation.

A general trend was found for the NRLMSISE-00 and corrections to improve the atmospheric drag force modeling in 2002 and 2005 in most metrics of comparison for both setup conditions. MSIS-86 outperformed the NRLMSISE-00 based GEODYN versions fairly consistently in the year 2001. The year 2000 was rather split, with some comparison methods favoring MSIS-86, and some methods favoring the newer models. The NRLMSISE-00 based versions of GEODYN generally showed a better response in periods of high solar activity, but overall did not exhibit superior performance in the years averaged near the peak of the most recent solar maximum (2000-2001).

Table 4.20 GFO Performance Summary.

	Empirical Accelerations Estimated			No Empirical Accelerations		
	SLR	**Cross-over**	**Orbit Overlaps**	**SLR**	**Cross-over**	**Orbit Overlaps**
2000	M86	M86	NRL00	M86	M86	M86
2001	NRL00	M86	M86	DCA/ NRL00	M86	M86
2002	M86	M86	NRL00	DCA/ NRL00	DCA/ NRL00	DCA/ NRL00
2005	NRL00	NRL00	No Change	DCA/ NRL00	DCA/ NRL00	NRL00 /DCA
Low Solar Activity	M86	M86		NRL00 /DCA	DCA/ NRL00	
Moderate Solar Activity	M86	M86		DCA/ NRL00	DCA/ NRL00	
Elevated Solar Activity	NRL00	M86		NRL00 /DCA	M86	
High Solar Activity	NRL00	M86		DCA/ NRL00	DCA/ NRL00	
Quiet Geomagnetic Activity	M86	M86		DCA/ NRL00	DCA/ NRL00	
Moderate Geomagnetic Activity	NRL00	M86		M86	M86	
Active Geomagnetic Activity	NRL00	DCA		M86	M86	

Table 4.20 has been created to summarize which models performed best under what conditions. The Cross-over column represents the altimeter crossover study performed. ‘M86’ represents the MSIS-86 version of GEODYN, ‘NRL00’ represents the NRLMSISE-00 version, and ‘DCA’ represents the GEODYN version with DCA corrections implemented to the NRLMSISE-00 model. The cases where both the DCA corrections and the NRLMSISE-00 model performed better than the MSIS-86

are indicated by both values in one cell. The version that performed best in these cases is listed first. So in the 2001 analysis of SLR for no empirical accelerations, the DCA corrections performed slightly better than the NRLMSISE-00 routine, but both performed better than the MSIS-86 routine.

Obviously any improvement in the runs with OPR empirical accelerations estimated will mean more than an improvement with the estimations removed since this will directly impact the accuracy of the altimeter measurements. So when looking at just these results, the performance of the new routines had a mixed response and did not produce any significant improvements. There were some cases where the new routines performed better, but most improvements were relatively small and were not consistent enough to warrant a permanent upgrade of GEODYN.

5 ADDITIONAL SATELLITES PROCESSED WITH GEODYN

In order to further evaluate the performance of the new atmospheric density models applied to GEODYN, three additional satellites were processed; Stella, Starlette, and GFZ-1. The spherical Stella and Starlette satellites are identical in construction; they consist of a large mass in a small form factor. The main difference lies in their orbit. Stella is in a near circular, ~800 km retrograde orbit and Starlette is in an elliptical orbit of 49.8 degree inclination at an altitude ranging from 800 km to 1100 km. These satellites have been designed to have a consistent and precisely known cross-sectional area in order to measure the long term effects of the residual atmosphere and radiation pressures. The orbit of GFZ-1 was much lower than the Stella and Starlette satellites. Launched from an altitude of around 400 km, the satellite reentered the atmosphere in 1999 after four years in orbit. Also being spherical, this satellite provides better feedback since it is at a lower altitude, and thus the effect due to atmospheric drag is increased. Processing these satellites will provide additional insight into the performance of the density routines because of their constant cross-sectional area and mass.

Each of these three satellites have been processed with empirical accelerations removed since the main focus of this investigation is not necessarily to improve their orbits, but to evaluate the performance of the new density models incorporated into GEODYN.

5.1 Stella

Stella provides a slightly different profile from Starlette in that it progresses through the entire atmosphere of the Earth due to its near-polar retrograde orbit. Stella is in a near-circular orbit at a slightly lower altitude, so the effects due to atmospheric drag will be larger than Starlette. However, both Stella and Starlette are at a higher altitude than the altitude of 600 km which the DCA corrections were designed for, so results from the DCA corrections are not expected to be improvements.

Stella was processed using GEODYN setups provided by NASA GSFC. The OPR empirical accelerations were removed prior to running the arcs to see the true effect of the updated atmospheric models. The arcs run were from 2000-2004 in order to see the effect throughout the most recent waning of solar maximum. Performance of the Stella satellite was evaluated using the same metrics of comparison described in the previous chapter and covers the SLR RMS values, orbit overlaps and drag coefficient analysis.

5.1.1 SLR RMS of Fit

To evaluate how well the predicted orbits fit to the SLR observations, the SLR RMS of fit is again taken. The results are presented in a similar fashion to the previous examples, with the SLR RMS values being first plotted against both Ap and F10.7, then averages taken in yearly and binned conditions. The plots for each the five years processed appear as Figure 5.1 through Figure 5.9. The yearly averages for each year are tabulated as Table 5.1.

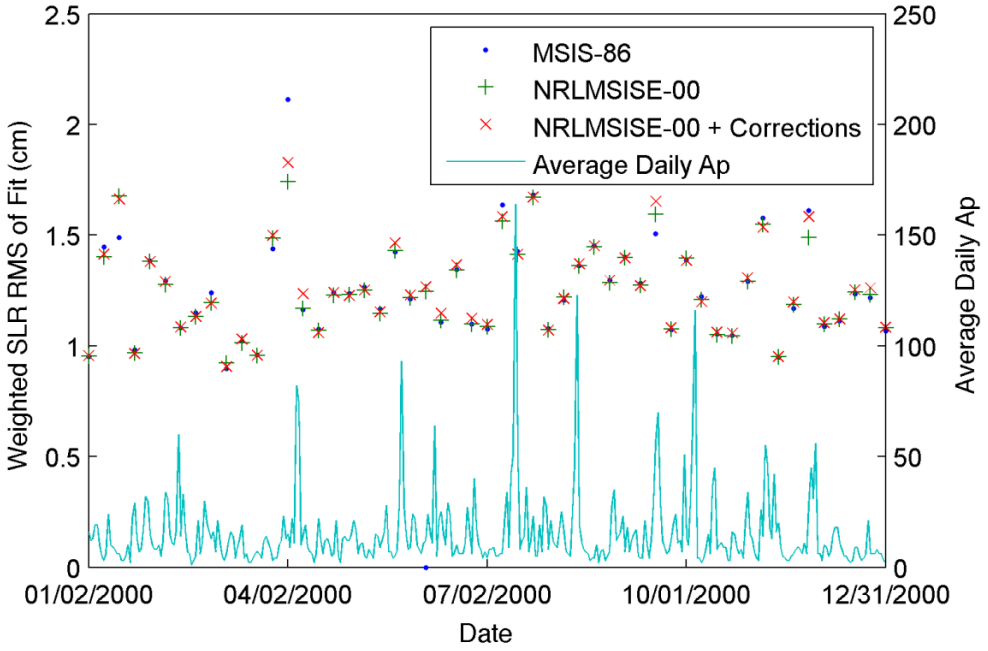

Figure 5.1 2000 Stella SLR RMS of Fit with Ap.

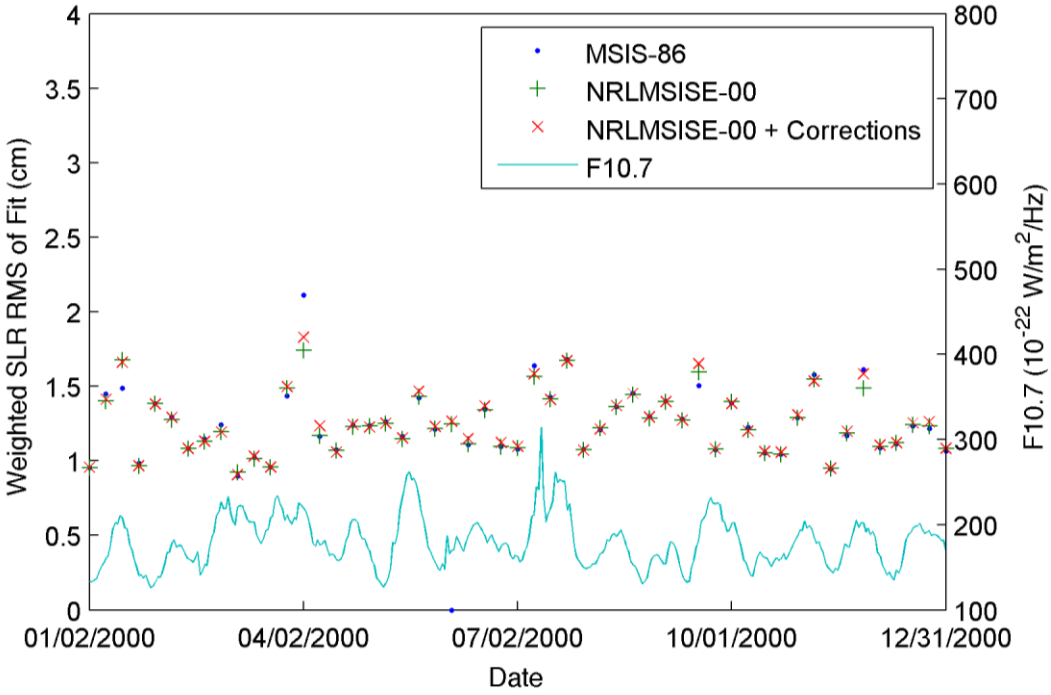

Figure 5.2 2000 Stella SLR RMS of Fit with F10.7.

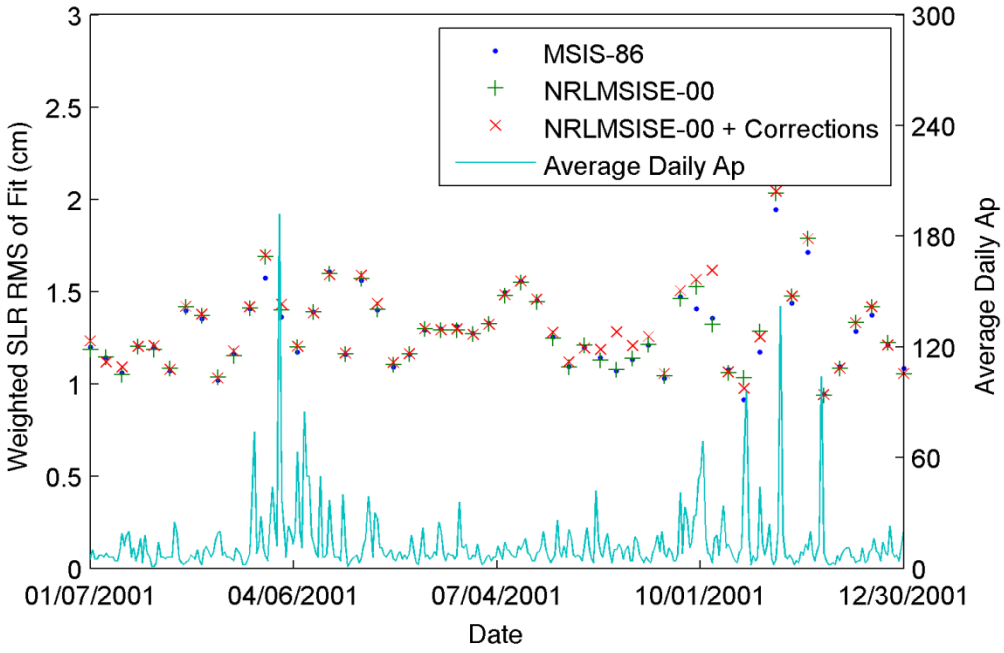

Figure 5.3 2001 Stella SLR RMS of Fit with Ap.

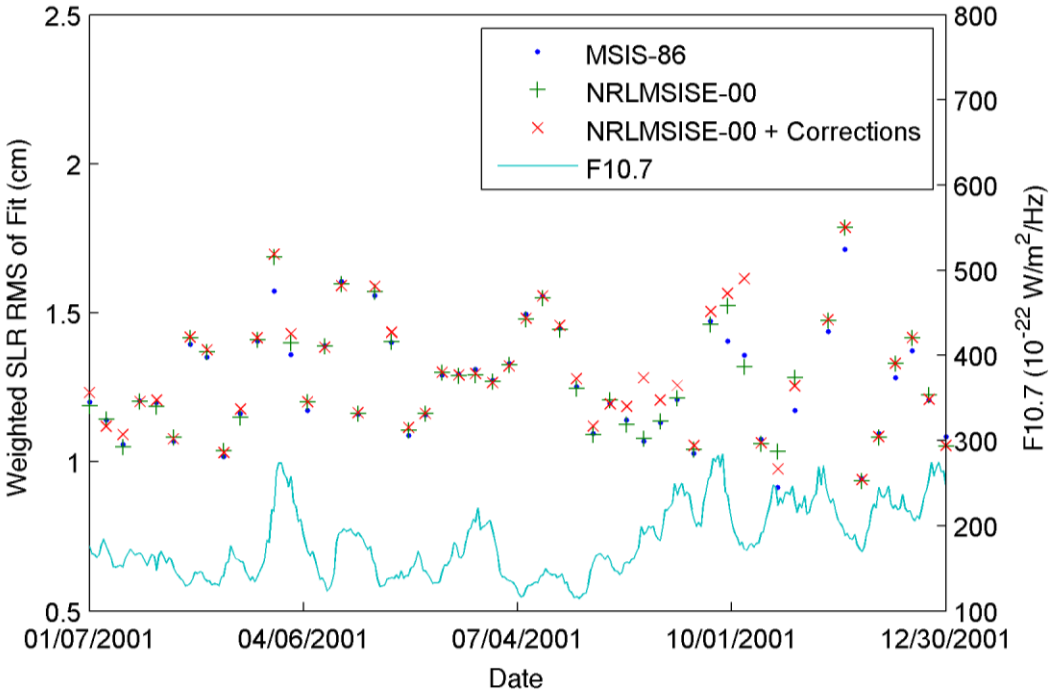

Figure 5.4 2001 Stella SLR RMS of Fit with F10.7.

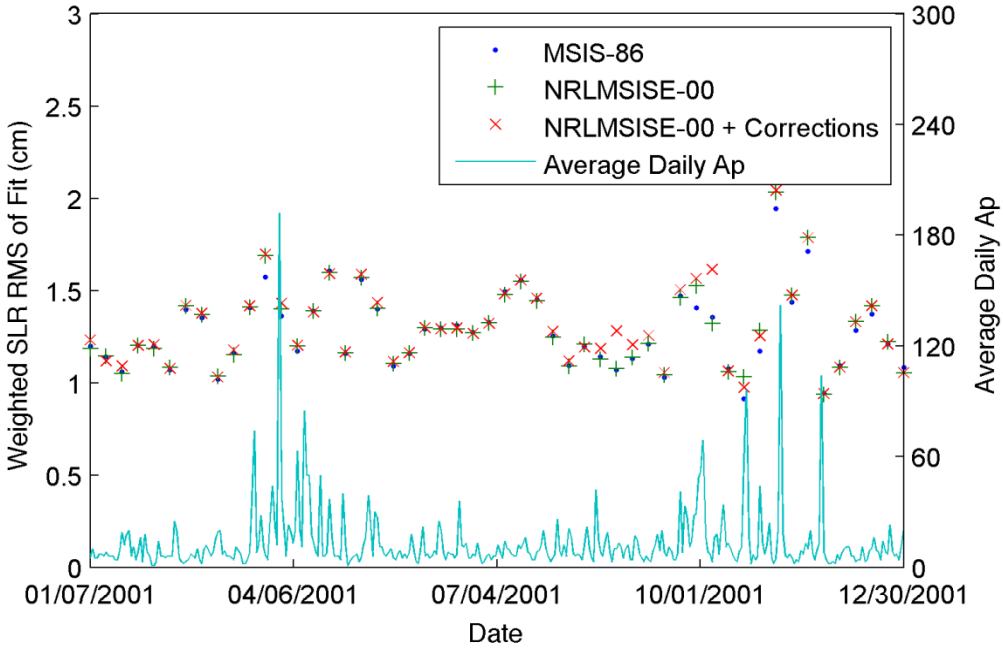

Figure 5.5 2002 Stella SLR RMS of Fit with Ap.

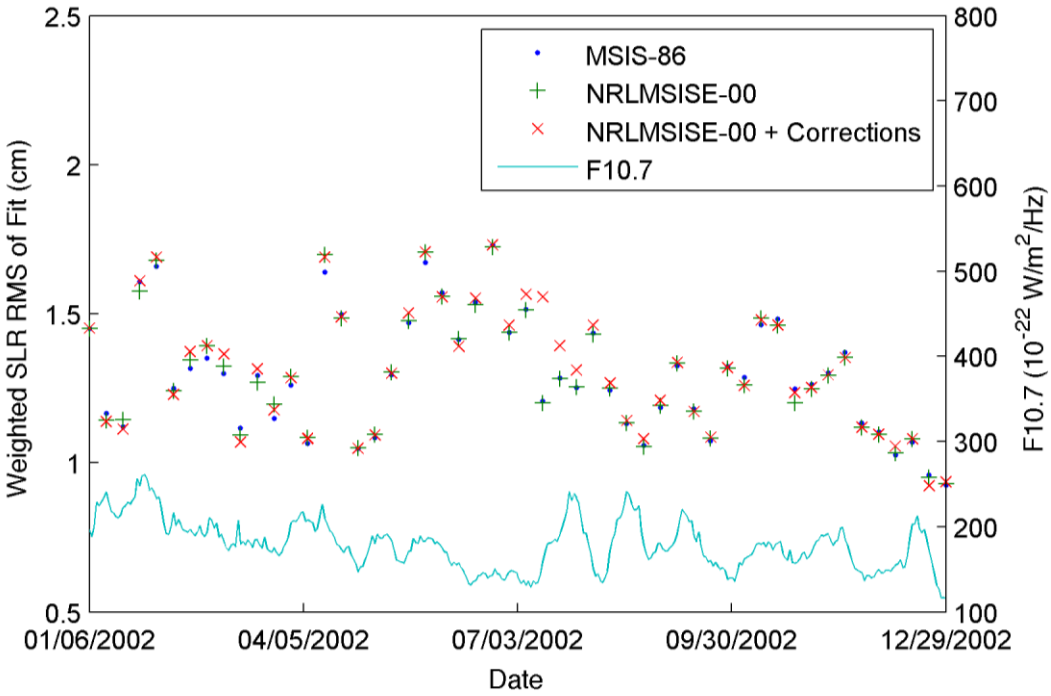

Figure 5.6 2002 Stella SLR RMS of Fit with F10.7.

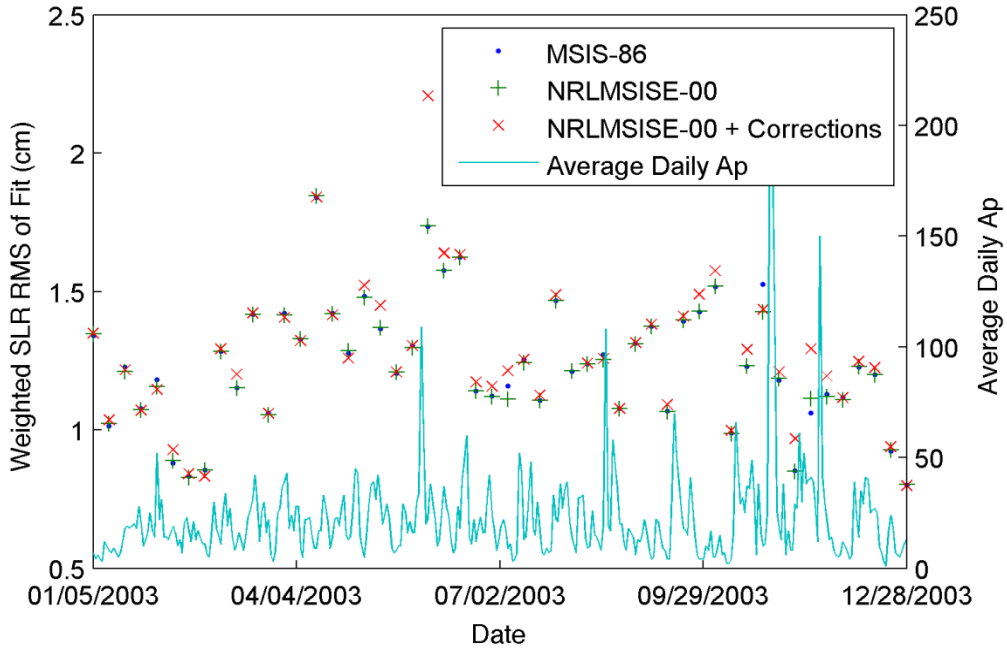

Figure 5.7 2003 Stella SLR RMS of Fit with Ap.

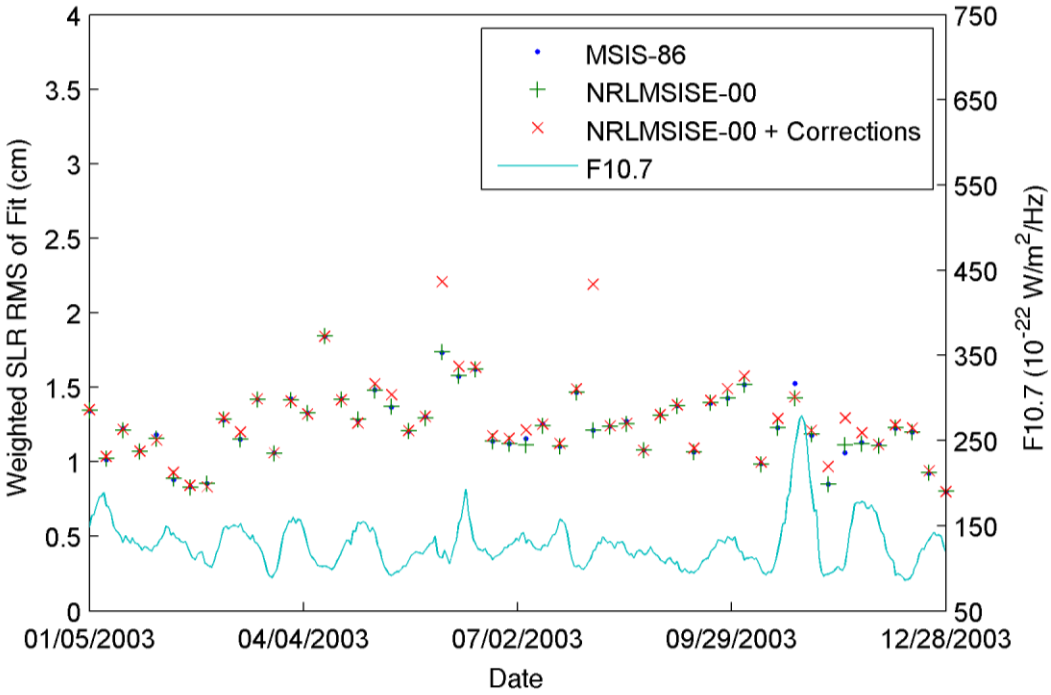

Figure 5.8 2003 Stella SLR RMS of Fit with F10.7.

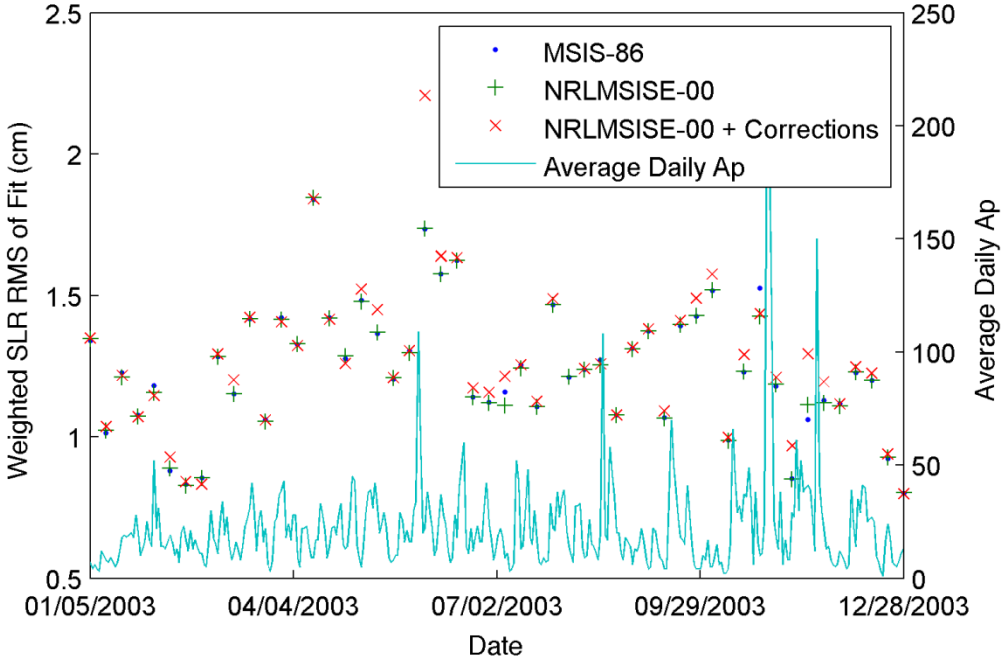

Figure 5.9 2004 Stella SLR RMS of Fit with Ap.

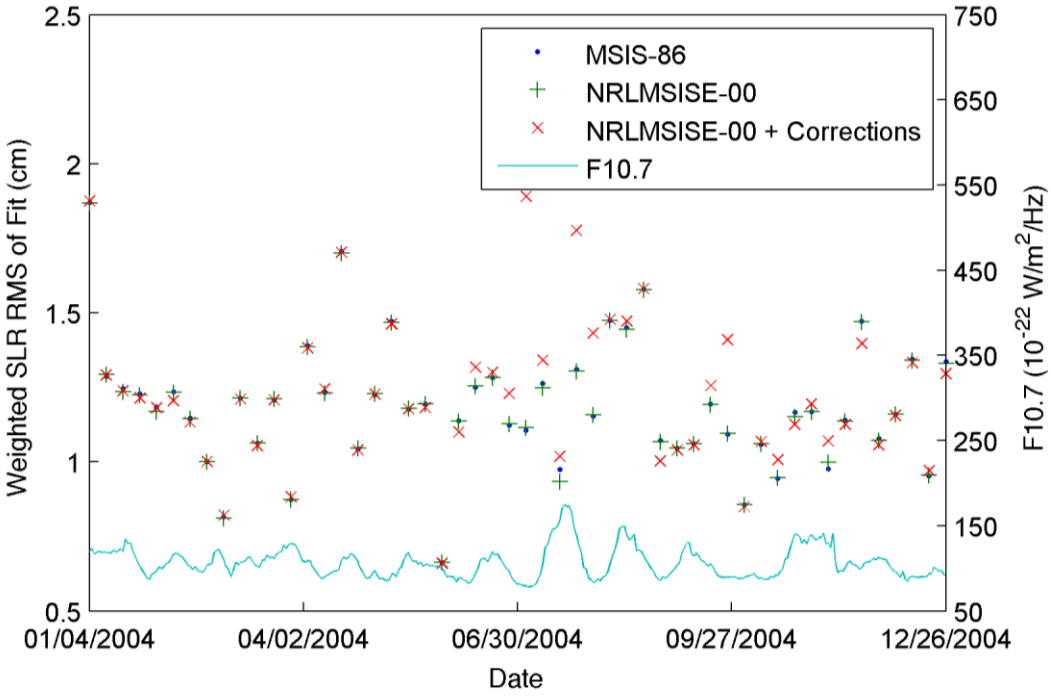

Figure 5.10 2004 Stella SLR RMS of Fit with F10.7.

Table 5.1 Stella Yearly Average of Daily SLR RMS of Fit (cm).

Year	MSIS-86	NRLMSISE-00	NRLMSISE-00 + DCA
2000	1.255	1.248	1.259
2001	1.275	1.289	1.307
2002	1.295	1.297	1.313
2003	1.236	1.233	1.284
2004	1.164	1.185	1.226

The RMS values came out very similar for each density model for most of the years processed. There were few improvements for individual arcs each year that would imply skewed results. The yearly averages listed in Table 5.1 also all came out very close to each other, with no improvements more than around one millimeter.

Table 5.2 Stella SLR RMS of Fit Average Arranged by Solar Activity (cm).

Solar Activity	MSIS-86	NRLMSISE-00	NRLMSISE-00 + DCA
Moderate Solar Activity (75 < F10.7 < 150)	1.215	1.223	1.260
Elevated Solar Activity (150 < F10.7 < 190)	1.240	1.240	1.265
High Solar Activity (F10.7 > 190)	1.320	1.326	1.335

The solar activity bins tabulated in Table 5.2 also show no large improvements, and no clear trend of improvements at any solar activity level. The 'low' solar activity bin is not listed because there were no days of low solar activity in the time period processed. The high solar activity binned values are depicted in Figure 5.11. No clear trend can be seen in the plotted data, and no outliers are found that would skew the results.

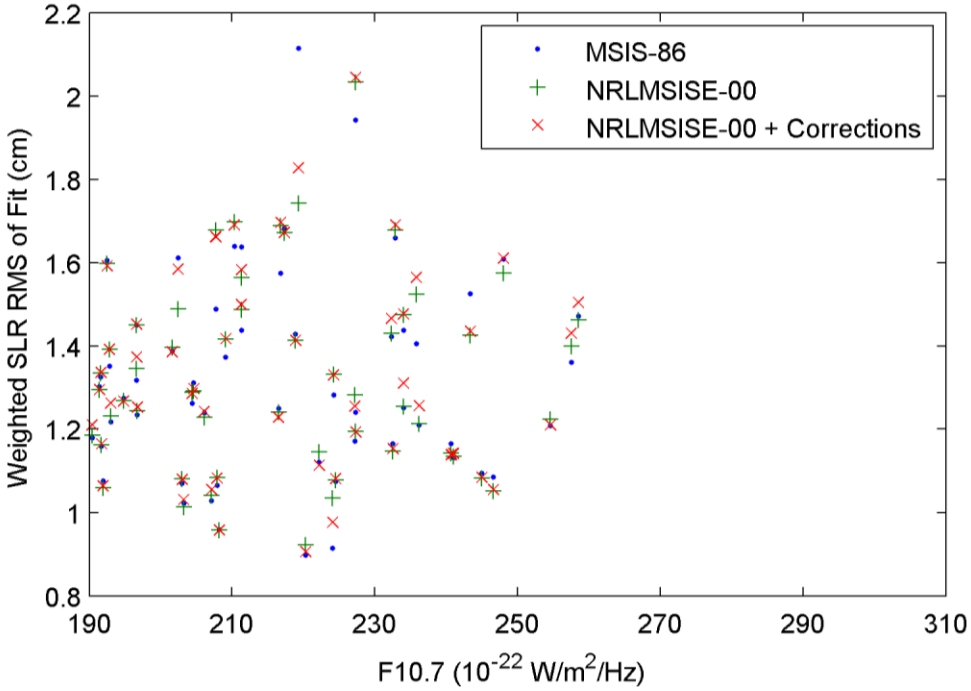

Figure 5.11 Stella SLR RMS of Fit vs. High F10.7.

The geomagnetic activity bins are shown in Table 5.3. In every bin, the MSIS-86 routine performs slightly better on average. These changes are also very slight. The quiet and moderate activity level bins are only around one millimeter from the NRLMSISE-00 routine, and there are only four cases where SLR residuals were available for active geomagnetic conditions, so trends from these days are not entirely trustworthy.

Table 5.3 Stella SLR RMS of Fit Average Arranged by Geomagnetic Activity (cm).

Geomagnetic Activity	MSIS-86	NRLMSISE-00	NRLMSISE-00 + DCA
Quiet Ap (Ap < 10)	1.264	1.267	1.295
Moderate Ap (10 < Ap < 50)	1.230	1.236	1.261
Active Ap (Ap > 50)	1.213	1.243	1.319

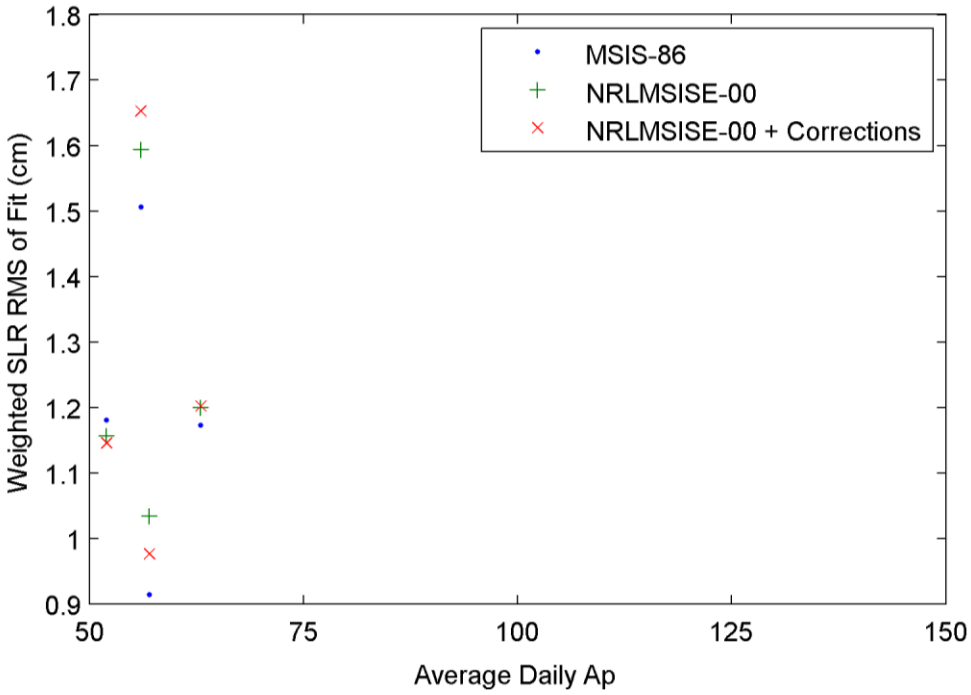

Figure 5.12 Stella SLR RMS of Fit vs. Active Ap.

The few cases of active geomagnetic activity are shown in Figure 5.12. This condition seems to favor the MSIS-86 routine for the four cases shown, but a definite conclusion cannot be made without more data in this condition. There are a limited number of RMS values in this condition because some active geomagnetic days did not coincide with days on which SLR residuals were available.

5.1.2 Orbit Overlaps

An orbit overlap study was also conducted for Stella using the same procedure described in the previous chapter. The results of the overlaps are displayed in Table 5.4 showing the position component overlap values and the total position overlaps.

Table 5.4 Stella Yearly Average of RMS of Orbit Overlap Position Components (cm).

Density Routine	Direction	Year				
		2000	2001	2002	2003	2004
MSIS-86	Along-track	49.21	20.69	14.03	13.48	14.66
	Cross-track	3.84	3.37	2.96	3.21	3.43
	Radial	3.06	2.43	1.62	1.74	1.42
	Total	50.53	22.15	15.08	14.61	16.10
NRLMSISE-00	Along-track	50.74	23.26	15.87	15.87	17.01
	Cross-track	3.88	3.39	2.98	3.18	3.63
	Radial	3.04	2.69	1.75	1.90	1.41
	Total	52.08	24.95	16.92	16.90	18.43
NRLMSISE-00 + DCA	Along-track	58.15	44.44	23.32	21.26	24.88
	Cross-track	3.95	3.46	2.97	3.39	3.70
	Radial	4.15	3.08	2.53	1.93	1.92
	Total	59.35	45.56	24.30	22.41	26.16

The orbit overlaps show a clear preference for the MSIS-86 density model. Each of the five years run have a considerable difference in the along-track direction between density routines. This difference in the along-track direction translates into differences in the total position of the same magnitude since the along-track direction dominates the overlap difference.

5.1.3 Drag Coefficient

The last comparison done was an evaluation of the drag coefficients estimated by GEODYN every 12 hours. The C_D values were extracted by modifying the GEODYN source code to output the coefficients to a file and the results are depicted in Figure 5.13 through Figure 5.20. The first plot of each year is the drag coefficient for each year. The second plot is the difference of either the NRLMSISE-00 routine or DCA correction routine from the MSIS-86 version of GEODYN. The nominal value of C_D for Stella and Starlette is 2.52 obtained from Reference 79 using a gas-surface interaction analysis. Since the C_D in GEODYN represents a scaling factor to balance the drag equation, the drag coefficient value is expected to be around 2.52, but will vary based on the quality of the atmospheric drag model and errors in C_D theory. The drag coefficient appears to be very close to this value for each year, although displays considerable variability.

The same behavior exhibited for the GFO satellite in the DCA routine is seen in the C_D plots for Stella. The new NRLMSISE-00 density model produces drag coefficient values similar to MSIS-86, but the NRLMSISE-00 model with the DCA corrections deviates considerably from either of the other two routines.

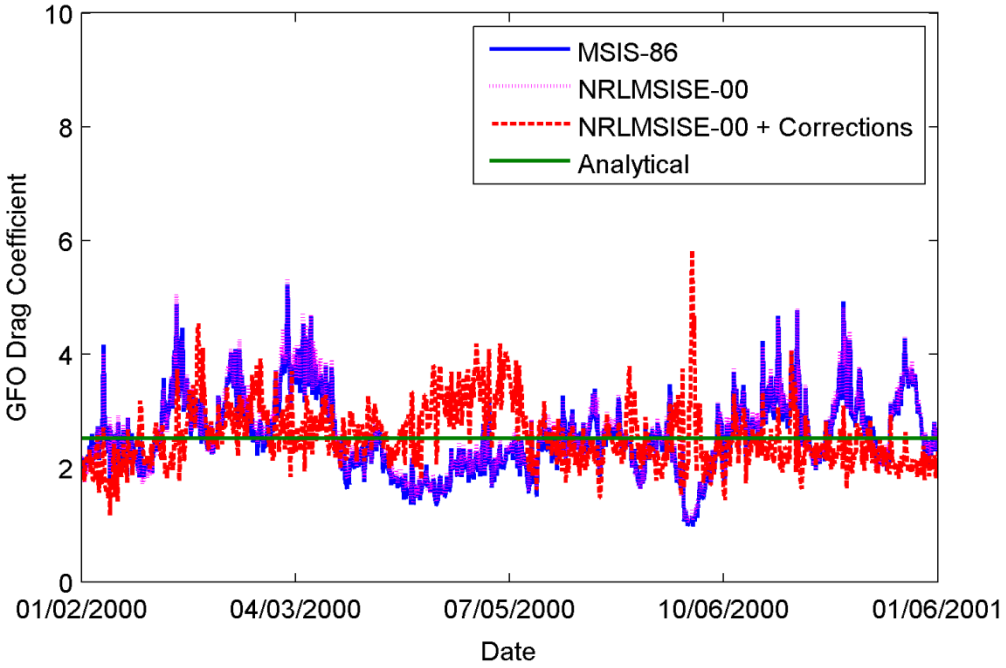

Figure 5.13 2000 Stella Drag Coefficient.

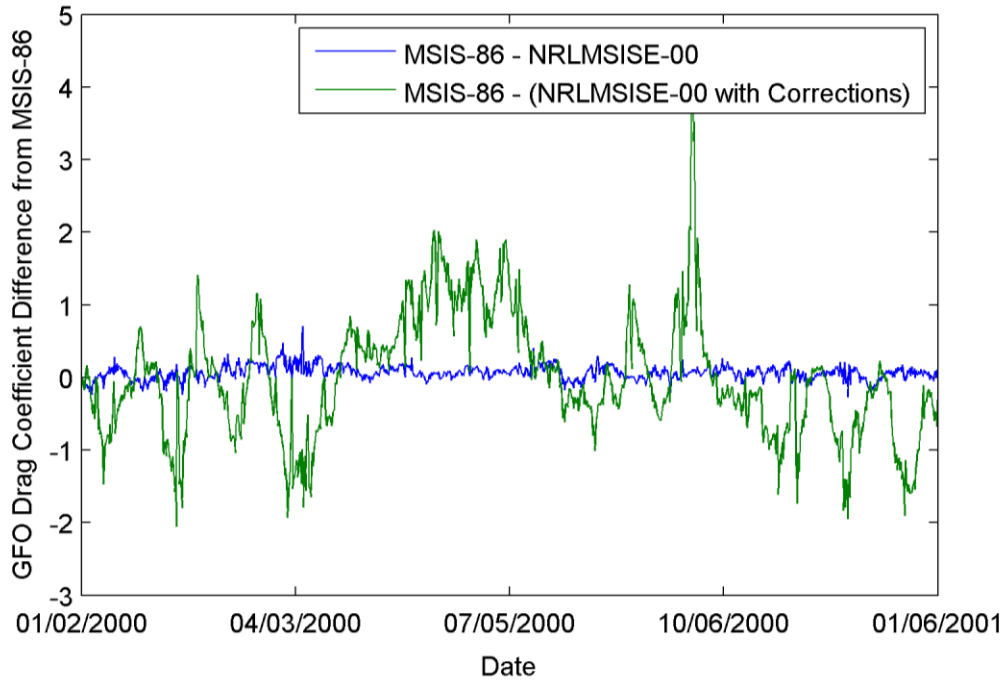

Figure 5.14 2000 Stella Drag Coefficient Differences.

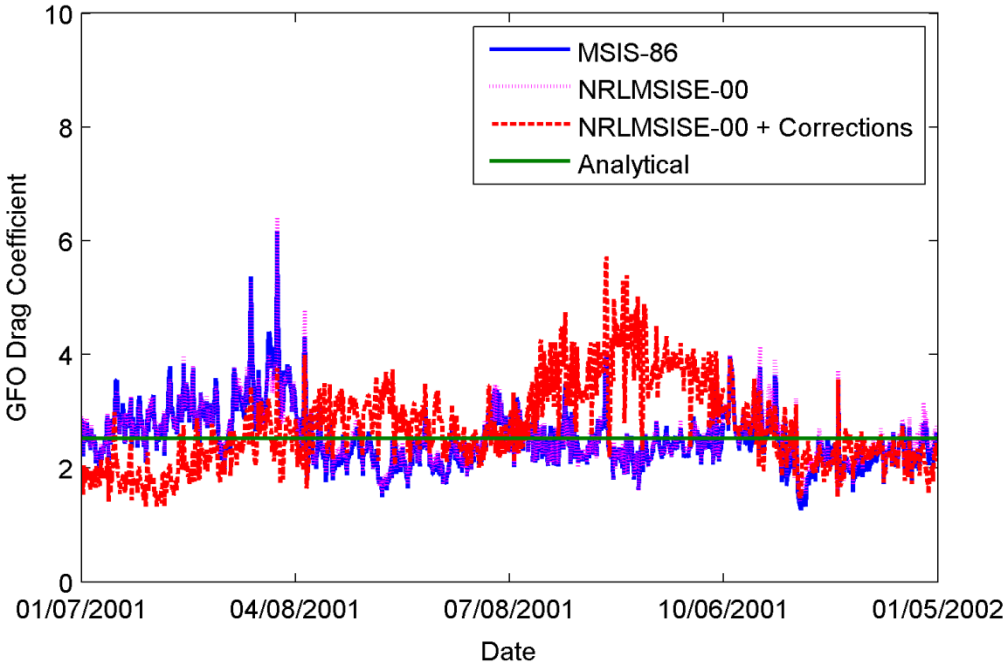

Figure 5.15 2001 Stella Drag Coefficient.

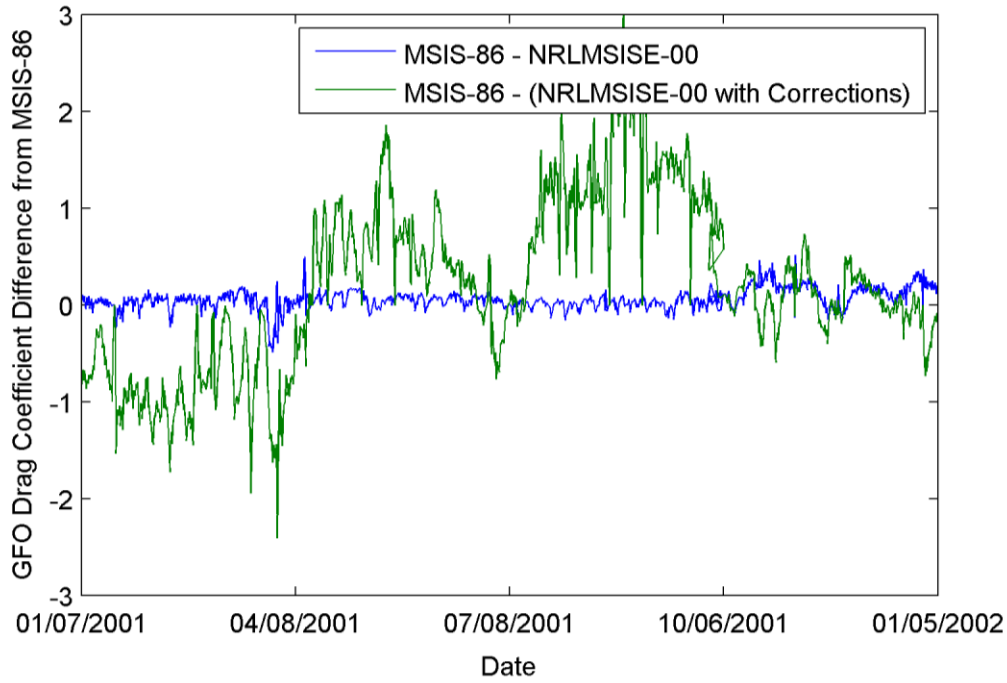

Figure 5.16 2001 Stella Drag Coefficient Differences.

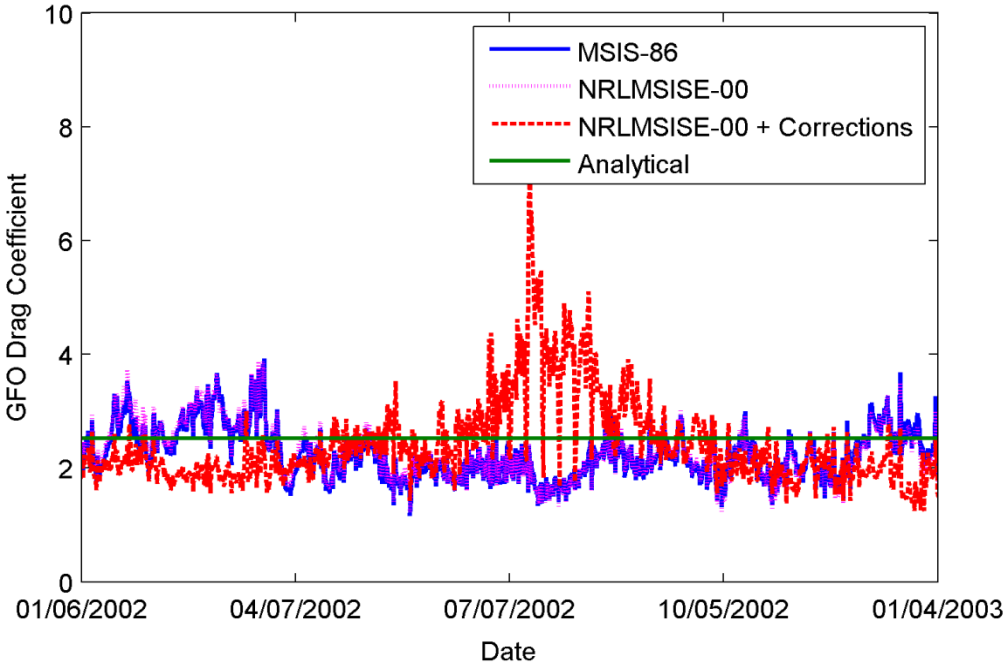

Figure 5.17 2002 Stella Drag Coefficient.

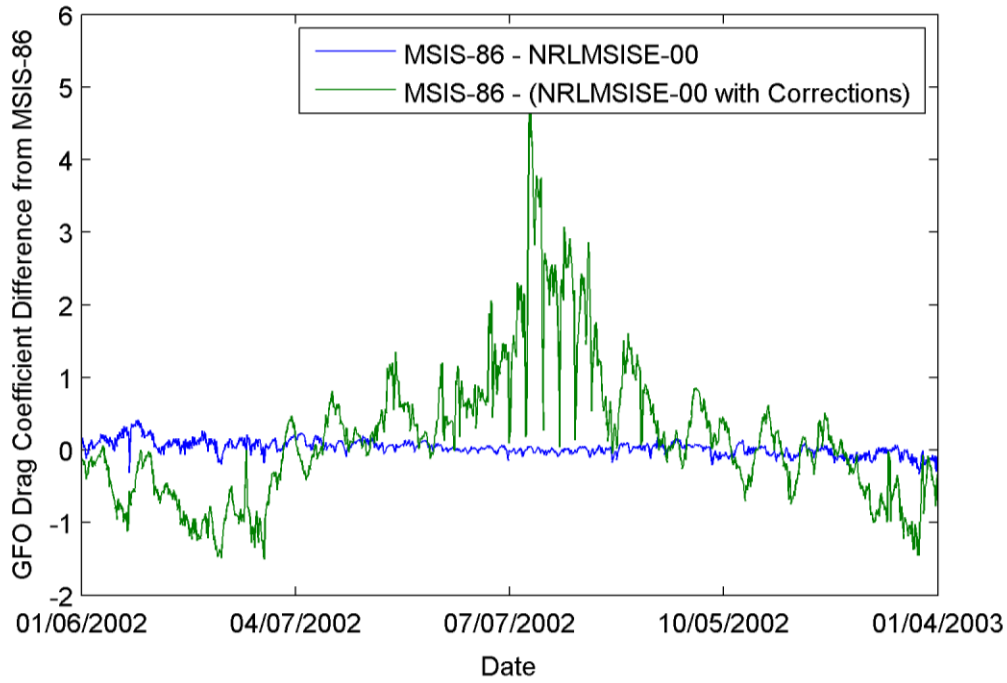

Figure 5.18 2002 Stella Drag Coefficient Differences.

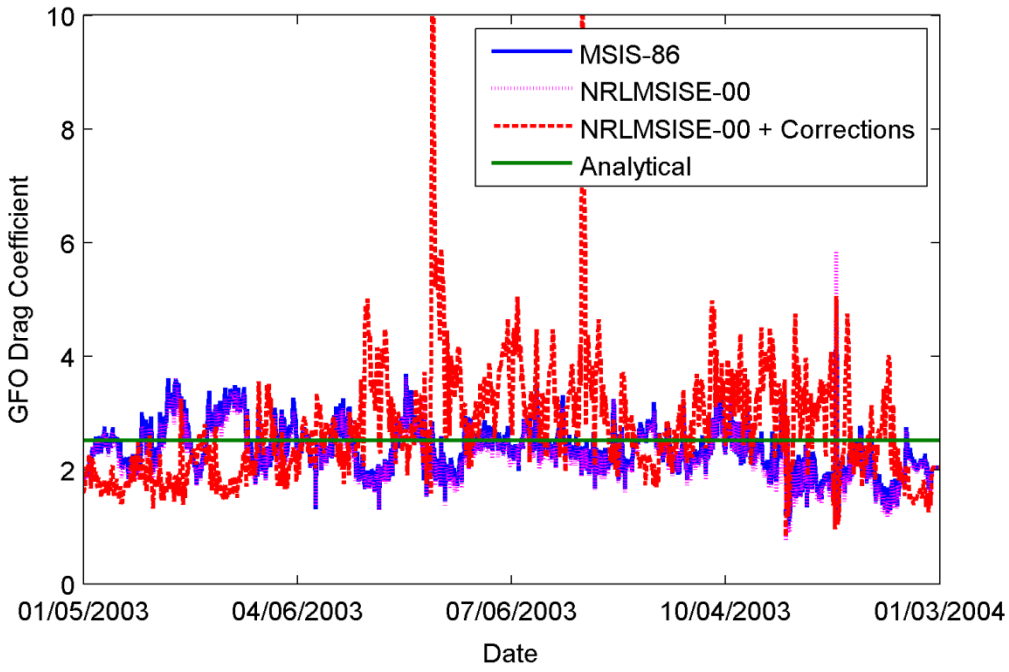

Figure 5.19 2003 Stella Drag Coefficient.

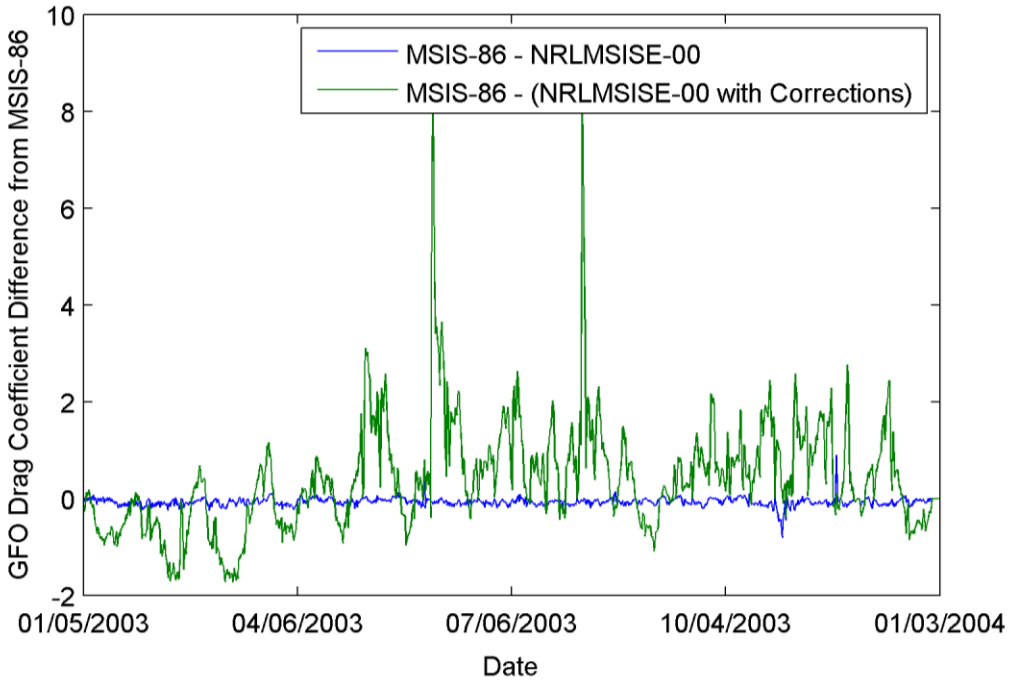

Figure 5.20 2003 Stella Drag Coefficient Differences.

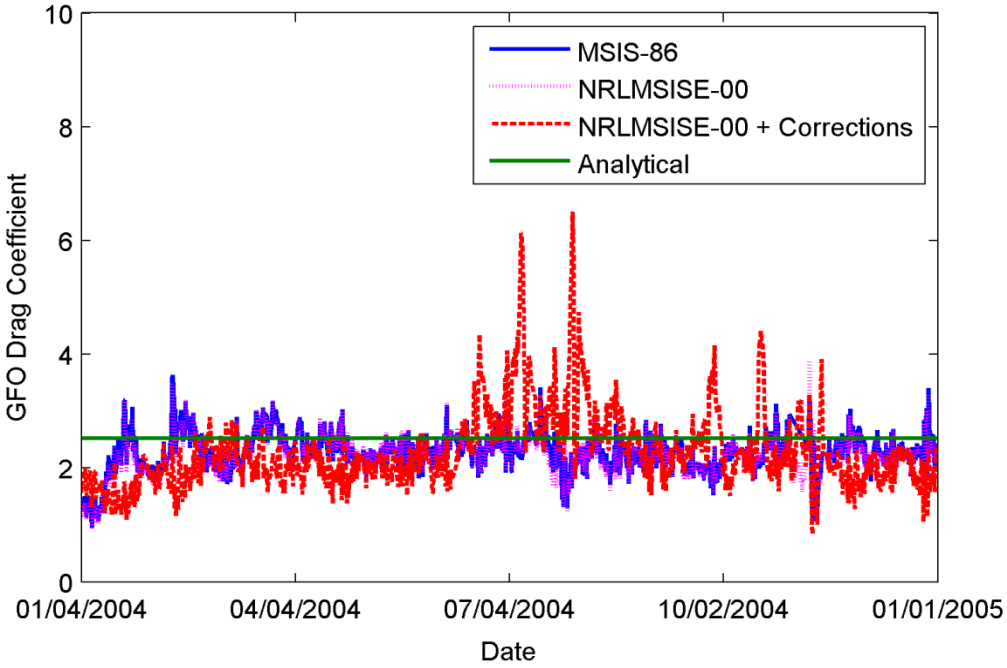

Figure 5.21 2004 GFO Drag Coefficient.

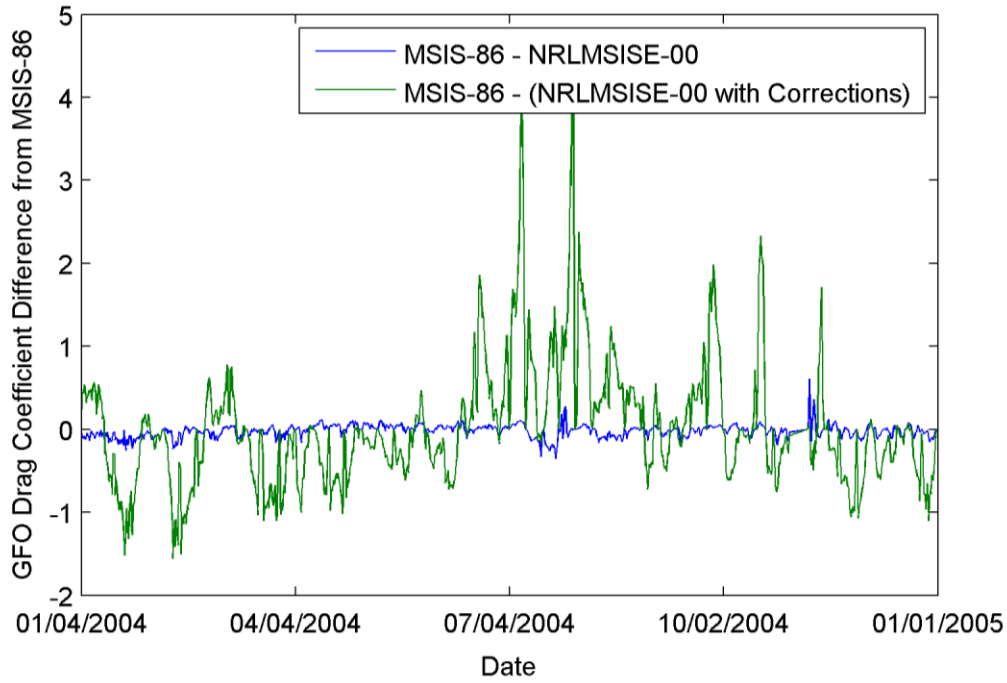

Figure 5.22 2004 Stella Drag Coefficient Differences.

5.2 Starlette

The Starlette satellite has a slightly more elliptical orbit than Stella and its 49.8 degree inclination does not allow the satellite to experience as much as the Earth's atmosphere latitudinally. The satellite will also not be exposed to as much atmosphere as Stella due to its elliptical orbit ranging from 800 km at perigee and 1100 km at apogee. Starlette is also above the range for the DCA corrections, so results from this routine are not expected to show significant improvement for DCA.

Five years of Starlette setups were obtained from NASA GSFC ranging from 2000-2004. These setups were modified to remove the estimation of empirical accelerations and run using each of the three GEODYN versions mentioned previously. The performance of the routines at processing Starlette was evaluated using the same metrics of comparison used in the previous section.

5.2.1 SLR RMS of Fit

The results from processing Starlette using the three versions of GEODYN are compared by evaluating the relative strength of the GEODYN versions at matching the estimated orbit to the SLR observations. The RMS of fit for the SLR measurements is a good indicator of the accuracy of the force modeling on the spacecraft. Similarly to the previous section, the SLR RMS of fits were obtained from the GEODYN output summary file and plotted along both Ap and F10.7 through time. These plots are displayed in Figure 5.23 through Figure 5.32. The first plot of each series is with Ap, the second is with F10.7.

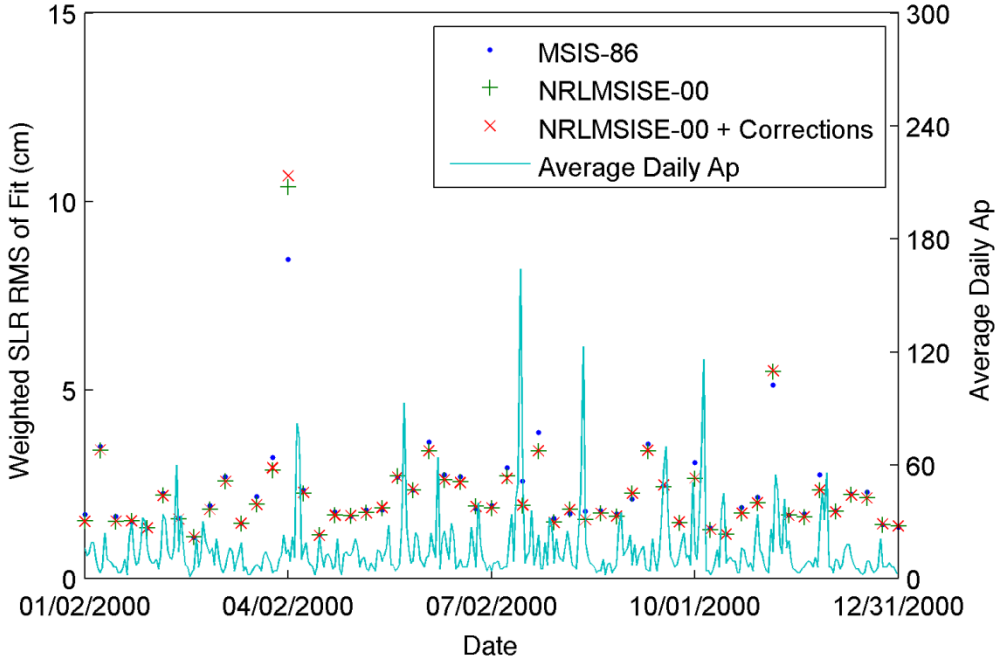

Figure 5.23 2000 Starlette SLR RMS of Fit with Ap.

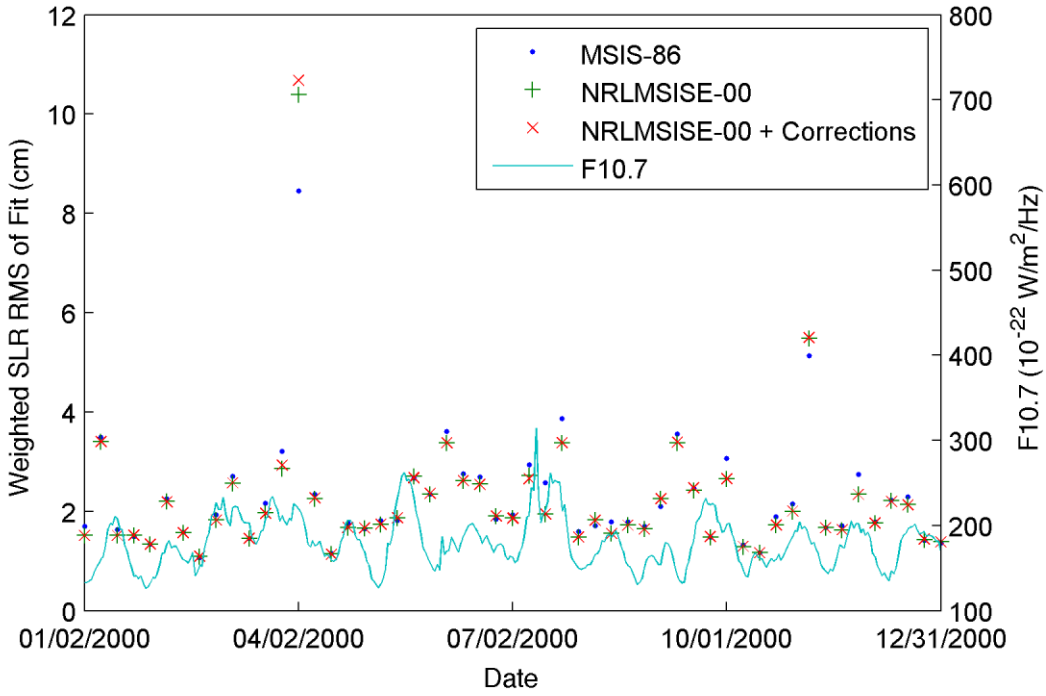

Figure 5.24 2000 Starlette SLR RMS of Fit with F10.7.

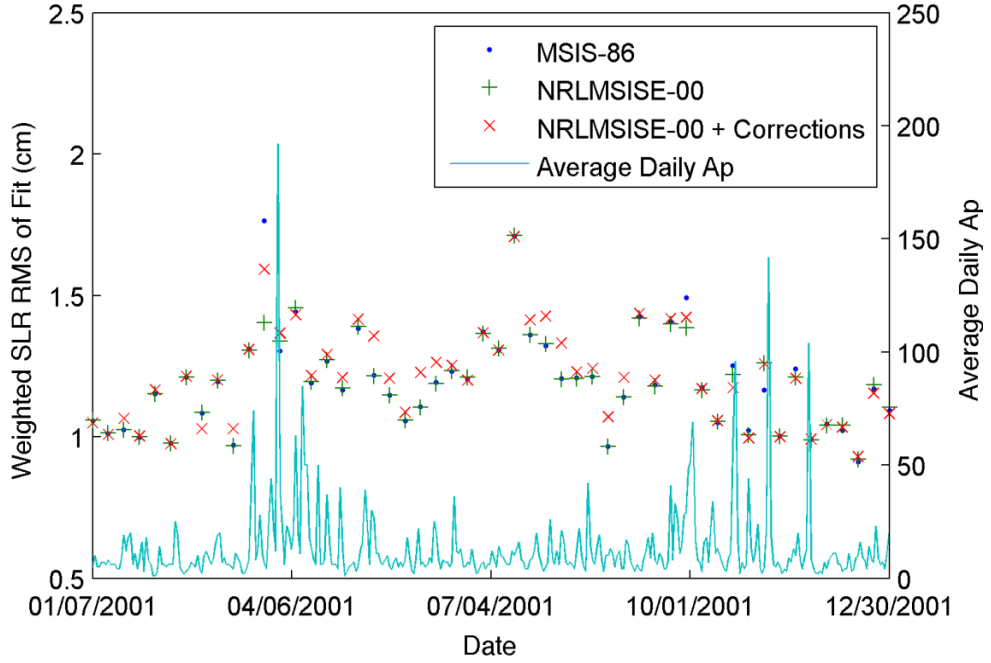

Figure 5.25 2001 Starlette SLR RMS of Fit with Ap.

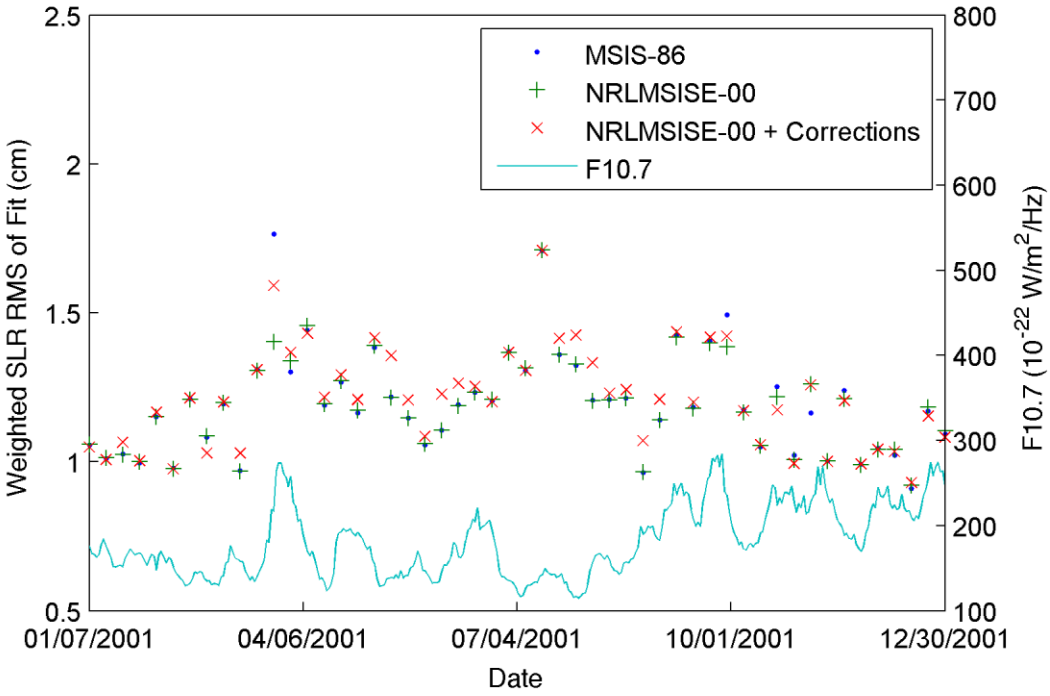

Figure 5.26 2001 Starlette SLR RMS of Fit with F10.7.

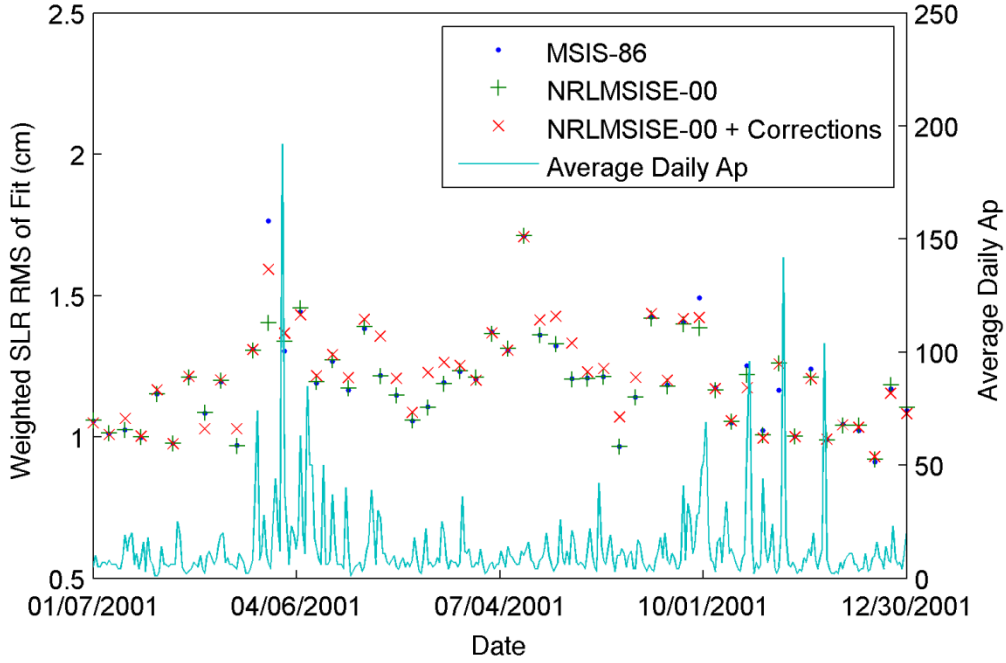

Figure 5.27 2002 Starlette SLR RMS of Fit with Ap.

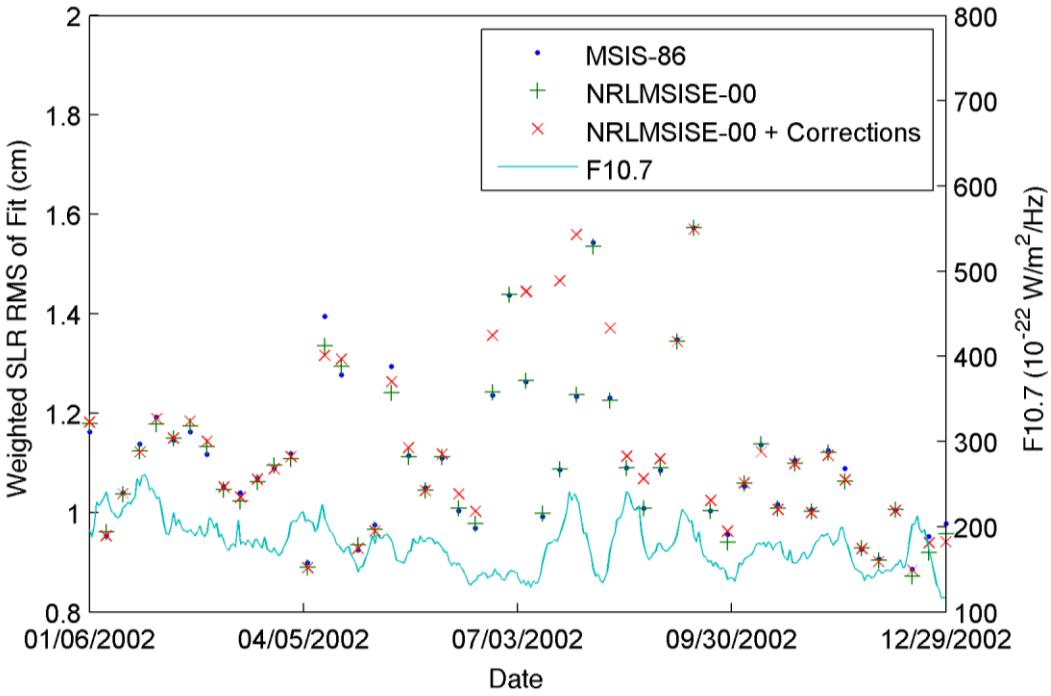

Figure 5.28 2002 Starlette SLR RMS of Fit with F10.7.

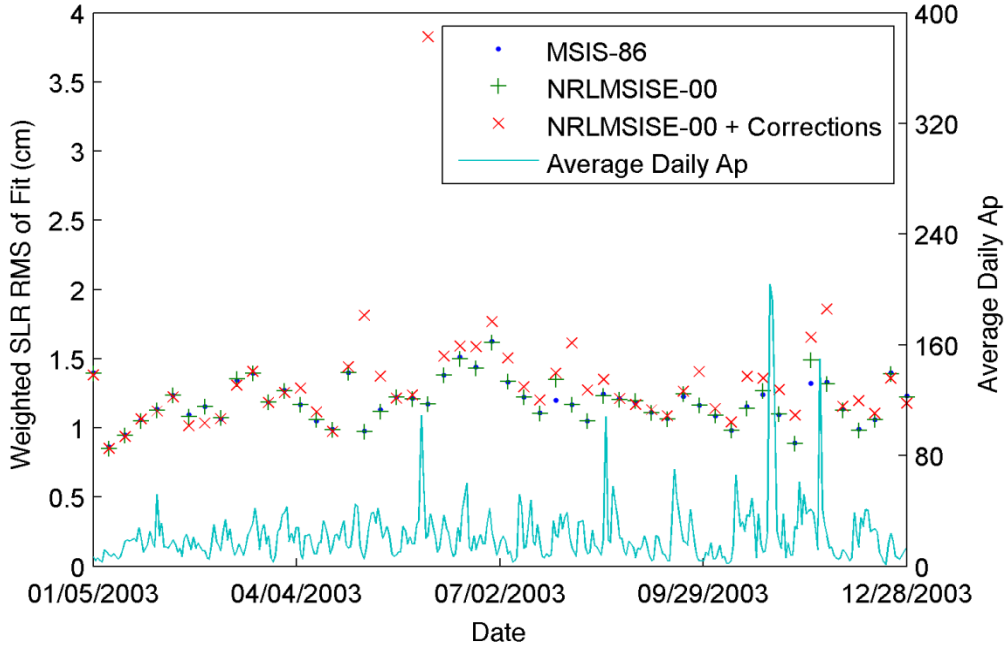

Figure 5.29 2003 Starlette SLR RMS of Fit with Ap.

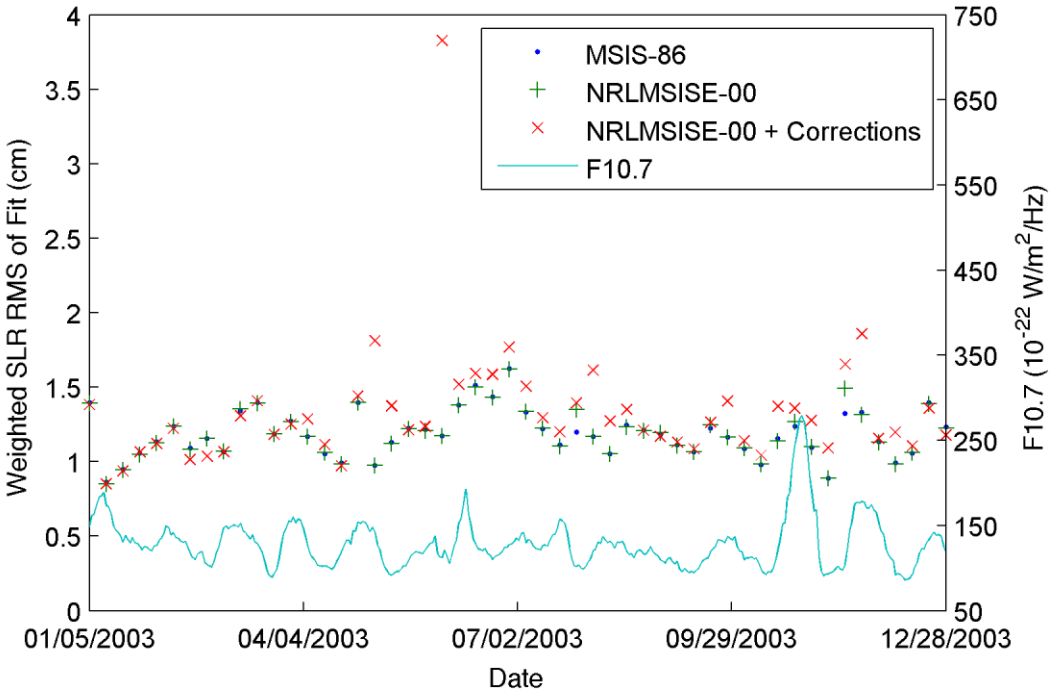

Figure 5.30 2003 Starlette SLR RMS of Fit with F10.7.

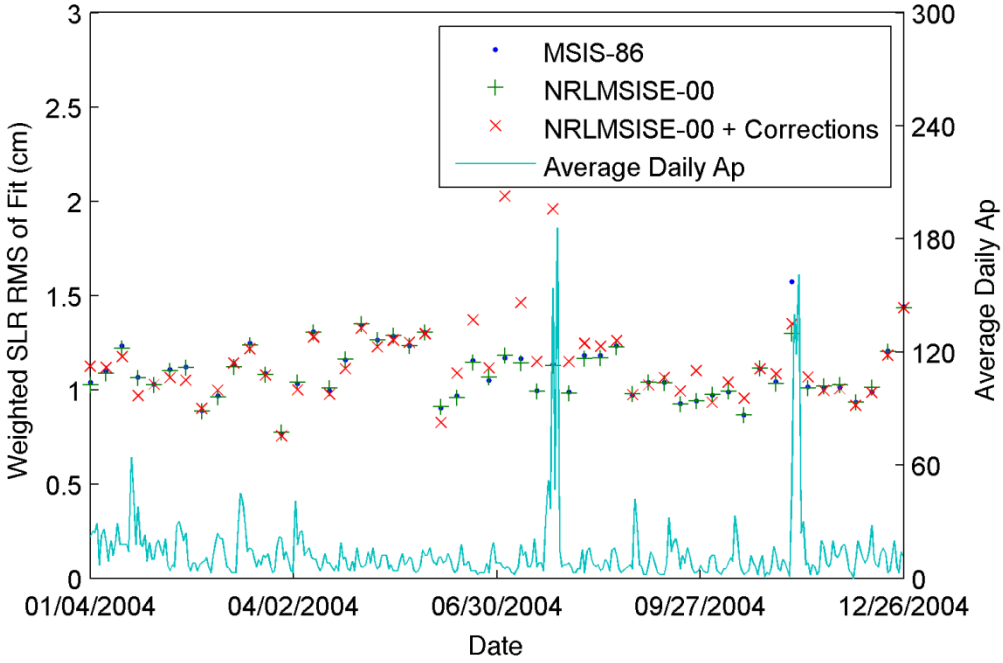

Figure 5.31 2004 Starlette SLR RMS of Fit with Ap.

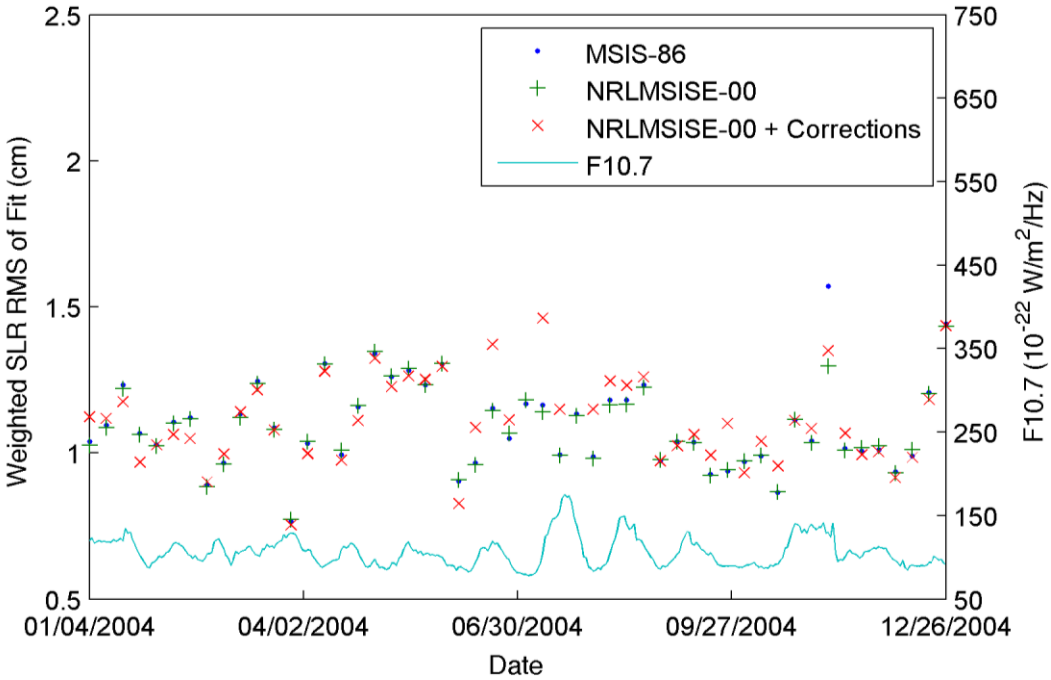

Figure 5.32 2004 Starlette SLR RMS of Fit with F10.7.

Table 5.5 Starlette Yearly Average of Daily SLR RMS of Fit (cm).

Year	MSIS-86	NRLMSISE-00	NRLMSISE-00 + DCA
2000	2.271	2.219	2.226
2001	1.195	1.188	1.212
2002	1.107	1.103	1.156
2003	1.185	1.190	1.333
2004	1.094	1.087	1.143

The SLR RMS values for Starlette came out very similar to Stella. Apart from one data point possibly skewing the results in 2000 (Figure 5.23 and Figure 5.24), the results for each year were very close for MSIS-86 and NRLMSISE-00. This is further reinforced when the yearly averages are computed and displayed in Table 5.5. The NRLMSISE-00 routine seems to perform marginally better most of the time, but all of the changes are on the order of less than one millimeter.

Table 5.6 Starlette SLR RMS of Fit Average Arranged by Solar Activity (cm).

Solar Activity	MSIS-86	NRLMSISE-00	NRLMSISE-00 + DCA
Moderate Solar Activity (75 < F10.7 < 150)	1.194	1.188	1.269
Elevated Solar Activity (150 < F10.7 < 190)	1.461	1.448	1.489
High Solar Activity (F10.7 > 190)	1.655	1.626	1.647

Table 5.6 shows the RMS values binned by solar activity levels. The NRLMSISE-00 routine performs slightly better than the MSIS-86 routine in all activity levels, but the changes are all less than one millimeter. There are only three activity levels because there were no days of low activity in the cases run. Figure 5.33 is a plot of the SLR

RMS value versus solar activity level at high solar activity. Apart from one outlier which slightly skews the results, the newer NRLMSISE-00 routine performs consistently either better or the same as the MSIS-86 routine except for one large difference seen in the top portion of Figure 5.33.

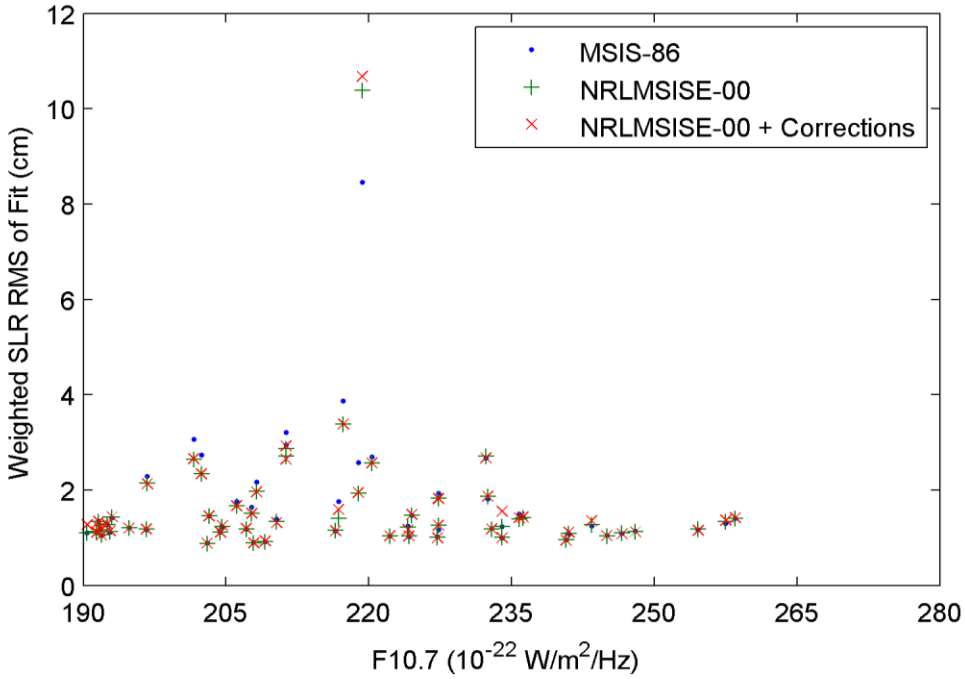

Figure 5.33 Starlette SLR RMS of Fit vs. High F10.7.

Table 5.7 Starlette SLR RMS of Fit Average Arranged by Geomagnetic Activity (cm).

Geomagnetic Activity	MSIS-86	NRLMSISE-00	NRLMSISE-00 + DCA
Quiet Ap (Ap < 10)	1.315	1.299	1.347
Moderate Ap (10 < Ap < 50)	1.410	1.407	1.466
Active Ap (Ap > 50)	1.654	1.512	1.636

The results have also been binned into the three geomagnetic activity levels mentioned previously. The NRLMSISE-00 routine performs slightly better for all geomagnetic conditions, but again, these changes are very slight; less than one millimeter. Figure 5.34 shows a plot of the four active geomagnetic SLR RMS values. Since there are only four SLR residuals available during active conditions, more cases in this condition must be run in order to draw any firm conclusions.

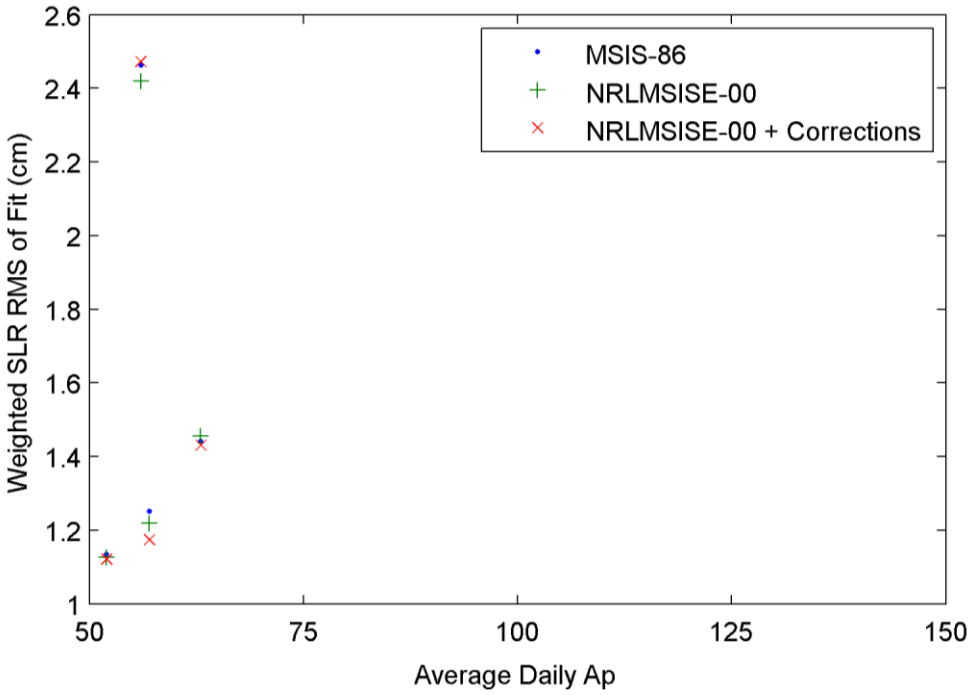

Figure 5.34 Starlette SLR RMS of Fit vs. Active Ap.

5.2.2 Orbit Overlaps

The orbit overlaps between adjacent arcs were also studied for Starlette. The orbit overlaps were obtained from the GEODYN output files and averaged by year to

compare the relative accuracies. Table 5.8 shows the yearly averages of the position components and the total position yearly averages.

Table 5.8 Starlette Yearly Average of RMS of Orbit Overlap Position Components (cm).

Density Routine	Direction	Year				
		2000	2001	2002	2003	2004
MSIS-86	Along-track	39.91	9.61	11.28	9.35	9.61
	Cross-track	3.22	2.96	3.01	2.80	2.64
	Radial	3.37	1.71	1.31	1.39	1.85
	Total	41.56	11.13	12.37	10.75	10.68
NRLMSISE-00	Along-track	38.84	10.34	11.05	9.60	9.36
	Cross-track	3.48	2.97	3.01	2.80	2.63
	Radial	3.84	1.77	1.28	1.38	1.83
	Total	40.24	11.86	12.15	10.97	10.46
NRLMSISE-00 + DCA	Along-track	40.25	15.31	14.74	15.75	13.44
	Cross-track	3.52	3.04	3.08	3.03	2.77
	Radial	3.91	2.07	2.19	1.77	1.81
	Total	42.10	16.68	15.83	16.84	14.50

The orbit overlaps for the MSIS-86 and NRLMSISE-00 runs were very close. The routine with the DCA corrections was consistently higher than either of the two other routines. The most accurate routine was split between NRLMSISE-00 and MSIS-86, with neither of them being more accurate than the other by more than a few millimeters.

5.2.3 Drag Coefficient

An analysis of the drag coefficients estimated every 12 hours by GEODYN was also performed on Starlette. The drag coefficients were extracted from GEODYN and are displayed in Figure 5.35 through Figure 5.44. The first plot of each year is the

drag coefficient for each year. The second plot is the difference of either the NRLMSISE-00 routine or DCA correction routine from the MSIS-86 version of GEODYN. As mentioned in the previous section, the nominal value for an aluminum sphere of the Stella and Starlette satellite's size and shape has a nominal value for CD of 2.52 according to a gas-surface interaction study performed in Reference 79. Since the C_D in GEODYN represents a scaling factor to balance the drag equation, the drag coefficient value is expected to be around 2.52, but will vary based on the quality of the atmospheric drag model and errors in C_D theory. The drag coefficient appears to be very close to this value for each year, although it displays considerable variability.

The MSIS-86 and NRLMSISE-00 routines have very similar drag coefficients, but the same variability from the other two models is seen in the NRLMSISE-00 routine with the DCA corrections for each of the years processed. This can be seen in the second plot in each year and is likely a result of a misrepresentation of the density on the satellite.

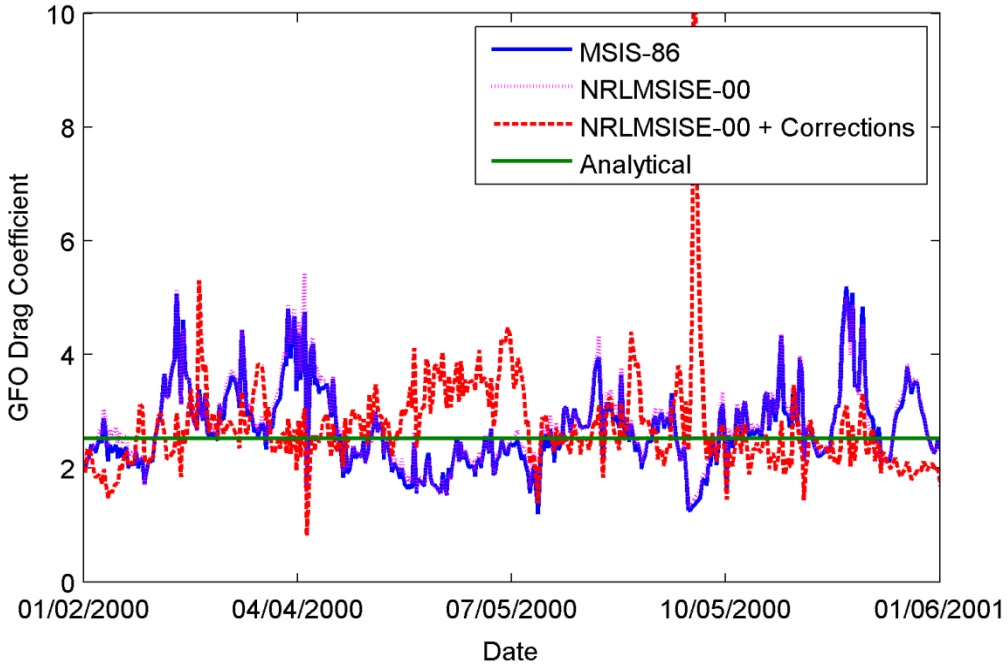

Figure 5.35 2000 Starlette Drag Coefficient.

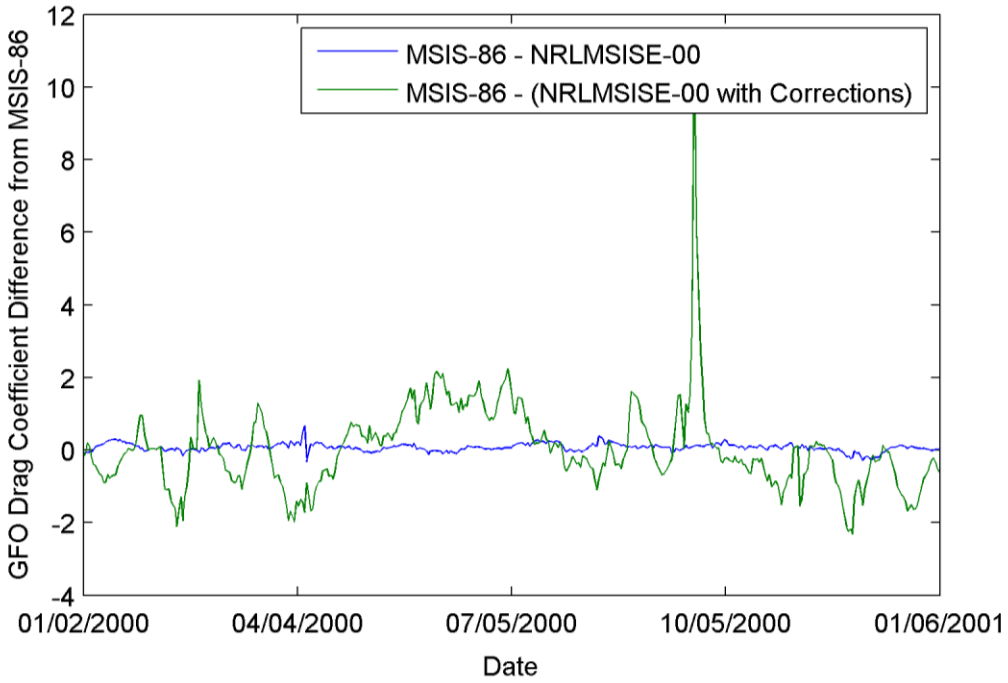

Figure 5.36 2000 Starlette Drag Coefficient Differences.

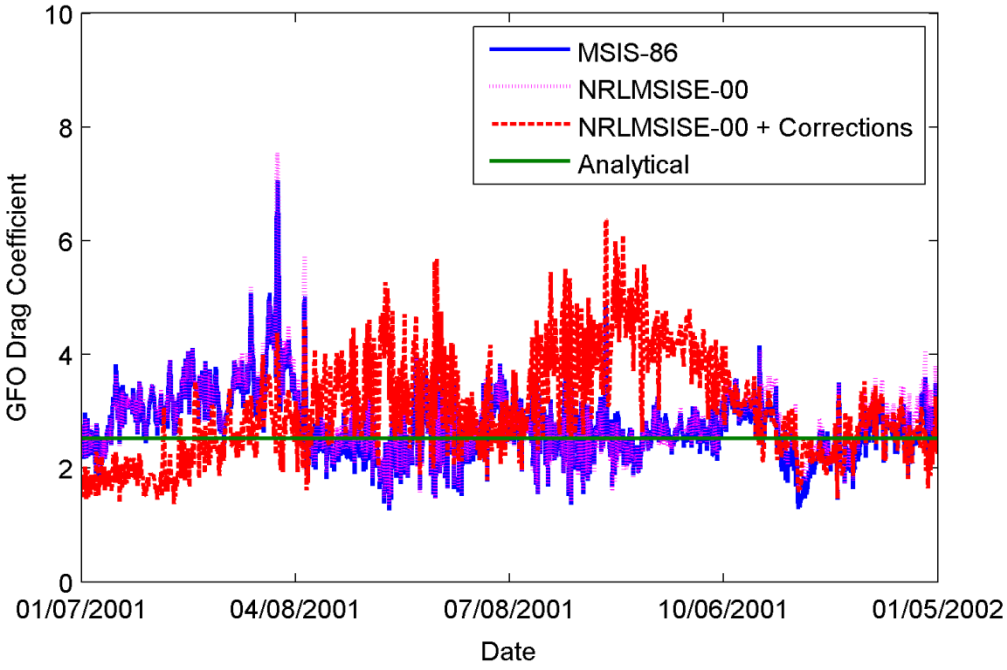

Figure 5.37 2001 Starlette Drag Coefficient.

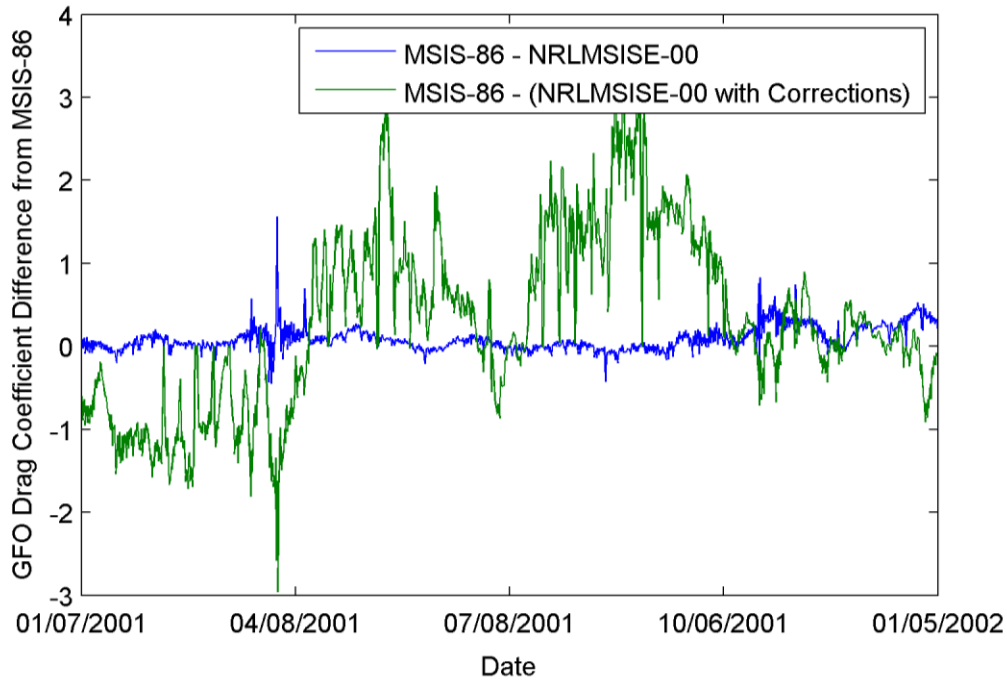

Figure 5.38 2001 Starlette Drag Coefficient Differences.

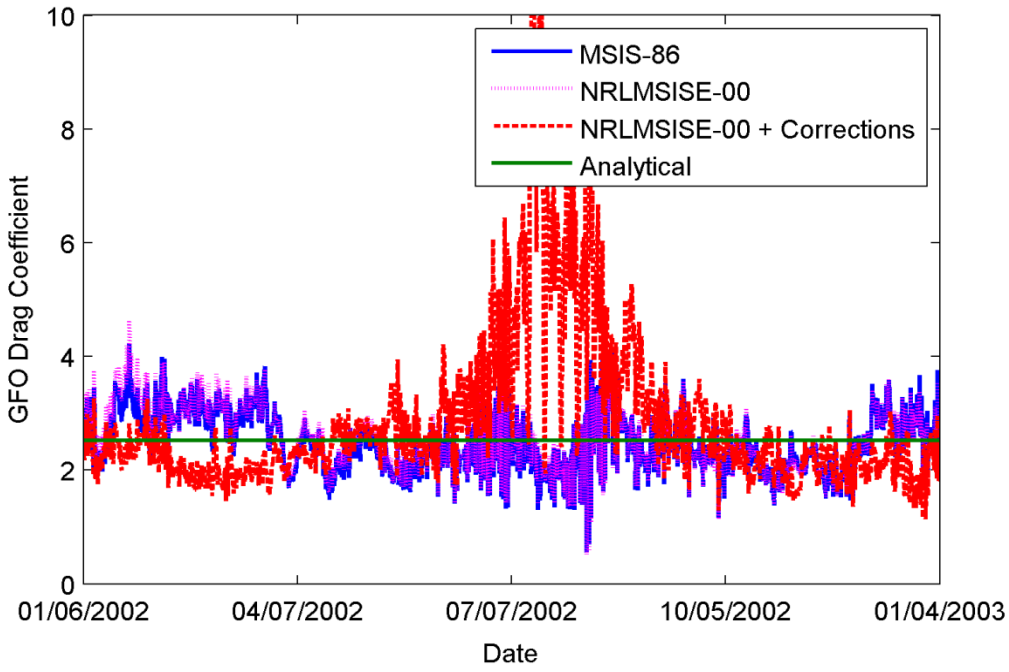

Figure 5.39 2002 Starlette Drag Coefficient.

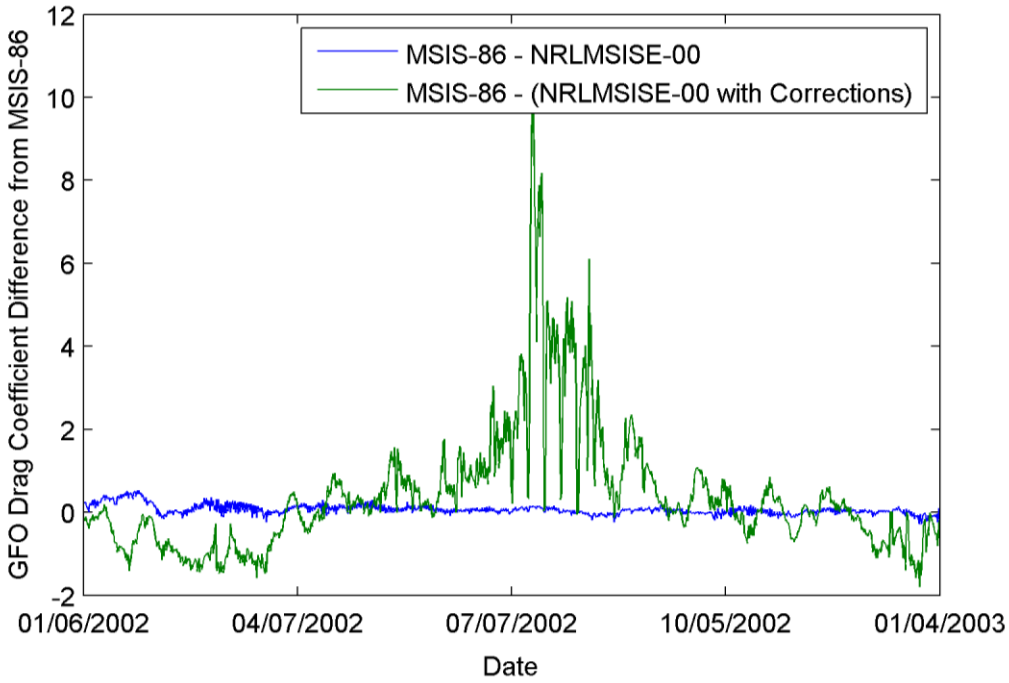

Figure 5.40 2002 Starlette Drag Coefficient Differences.

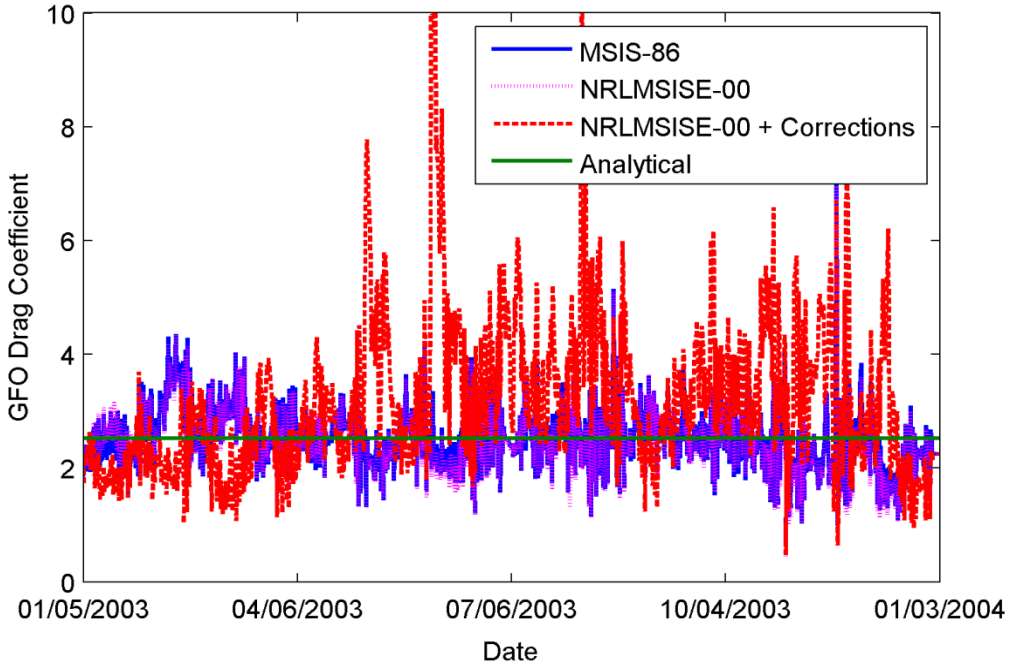

Figure 5.41 2003 Starlette Drag Coefficient.

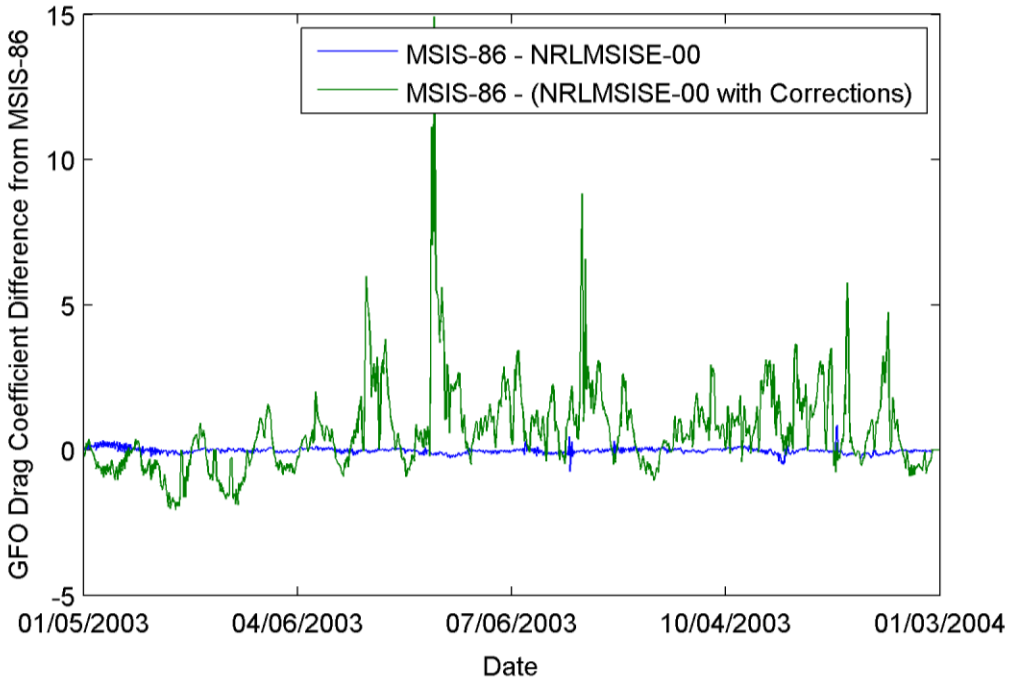

Figure 5.42 2003 Starlette Drag Coefficient Differences.

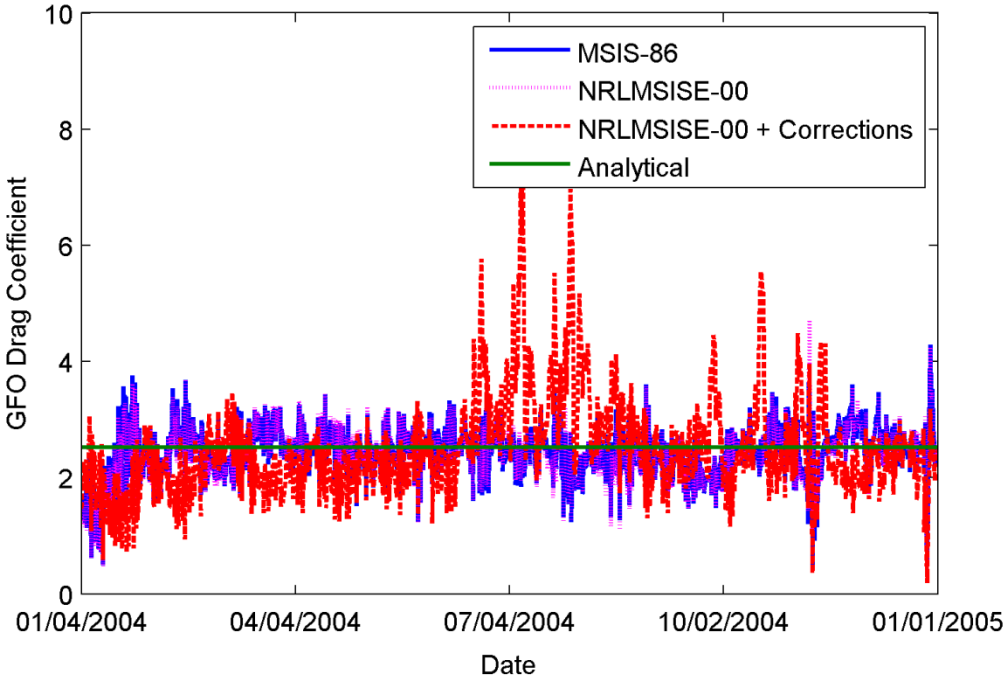

Figure 5.43 2004 GFO Drag Coefficient.

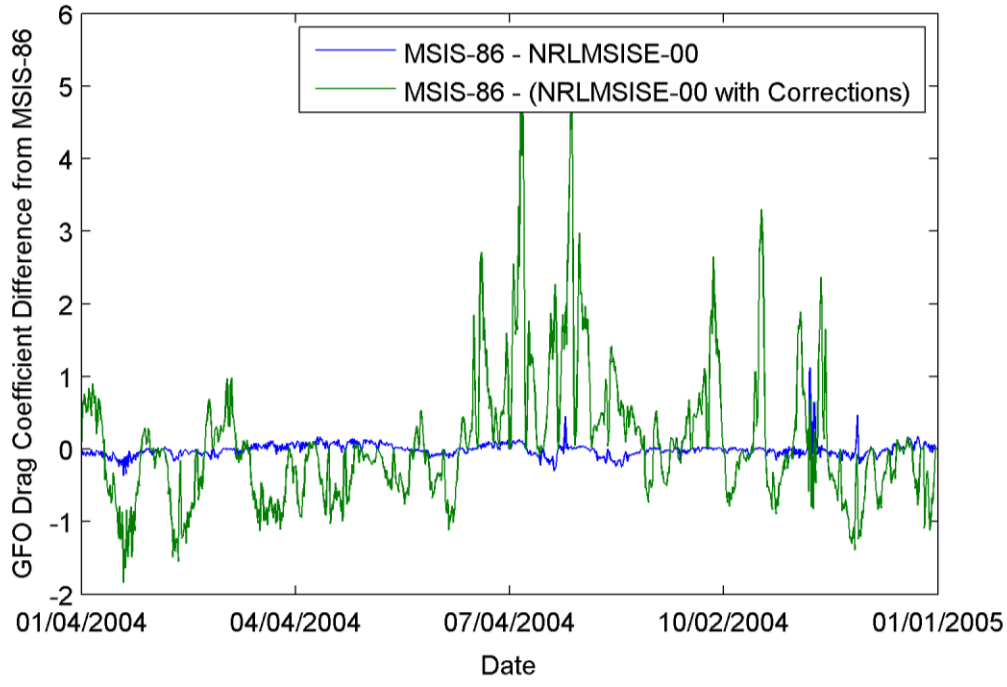

Figure 5.44 2004 Starlette Drag Coefficient Differences.

The drag coefficients for Stella and Starlette were averaged by year and formed into ballistic coefficient values using the constant mass and area given in Chapter 1. These ballistic coefficients are listed in Table 5.9 and Table 5.10 with the yearly ballistic coefficients found using C_D theory and the TLE method described in Chapter 3. Clearly the TLE derived ballistic coefficients are substantially different from both theoretical and GEODYN processed values. The MSIS-86 routine seems to perform the closest to theoretical values in each year processed for both Starlette and Stella.

Table 5.9 Starlette Yearly Average of Ballistic Coefficient Techniques.

Year	GEODYN			Theory	TLE
	MSIS-86	NRLMSISE-00	NRLMSISE-00 + DCA		
2000	0.002565036	0.0026341	0.002587146	0.0023916	
2001	0.002618692	0.002701731	0.002897831	0.0023916	0.1101215
2002	0.002368891	0.002429037	0.002735043	0.0023916	0.1153363
2003	0.002399892	0.002377578	0.003029937	0.0023916	0.1909776
2004	0.002311927	0.002298258	0.002370007	0.0023916	0.2461247

Table 5.10 Stella Yearly Average of Ballistic Coefficient Techniques.

Year	GEODYN			Theory	TLE
	MSIS-86	NRLMSISE-00	NRLMSISE-00 + DCA		
2000	0.002444395	0.00250441	0.002425182	0.0023916	
2001	0.002396077	0.002450268	0.002594879	0.0023916	0.0083539
2002	0.002141424	0.002168545	0.002315403	0.0023916	0.0080232
2003	0.00224712	0.002176542	0.00261669	0.0023916	0.0208017
2004	0.002166314	0.002138559	0.002173916	0.0023916	0.0506063

5.3 GFZ-1

The GFZ-1 satellite was deployed from the MIR space station on April 19, 1995. Due to its lower launch altitude of 398 km, the satellite's orbit decayed over the course of four years until it burned up in the atmosphere in June of 1999. Setups obtained from NASA GSFC were modified to remove the estimation of empirical accelerations and processed using the three versions of GEODYN. Due to complications predicting and tracking a satellite at such a low altitude, the number of arcs which converged to reasonable values was considerably less than the number of arcs supplied. The lower a satellite is, the more difficult the satellite is to track because variations in the atmosphere. These variations cause difficulties predicting the orbit of the spacecraft. The predicted orbit is used to get a fix on the satellite while tracking, so the lower the altitude, the more complications arise in prediction. When this is coupled with the shorter arcs due to the lower altitude, even more problems arise. If any version of GEODYN did not converge to a reasonable value, the results from the other routines were removed in order to properly compare the results.

The only method of comparison that can be performed on GFZ-1 is an analysis of the SLR RMS values. This is due to the scarcity of the arcs that converged upon reasonable results. Since there were so few of these arcs, the data could also not be binned into solar and geomagnetic activity levels. For this reason, the yearly averages are the only way of comparing the performance of the routines. Corrections to NRLMSISE-00 using the DCA technique were not available for these years, so the results from that routine and the NRLMSISE-00 routine were exactly the same.

The SLR RMS of fit values that were obtained were extracted from the GEODYN output files and plotted as Figure 5.45 through Figure 5.50. The values are much larger than the values from any of the other satellites run. This is because of the low altitude that GFZ-1 orbits. The lower altitude means that the variations from the atmosphere become more pronounced. When this is coupled with the problems already mentioned in tracking the satellite, the orbits become much more difficult to estimate when supplied with only one measurement source with limited tracking data. From the few arcs that have been processed, the MSIS-86 routine has been found to have lower SLR RMS values rather consistently.

Unfortunately determining whether or not arcs have converged to reasonable values becomes more difficult for this satellite with the limited SLR coverage. SLR RMS of fit values of 2 meters are unreasonable to produce precise orbits, but are likely a result of not estimating the empirical accelerations each integration step. The large RMS values are not necessarily unwanted since the main objective is to perform a comparison, not to derive precise orbits. Letting the empirical accelerations go unestimated means the other force models represent the forces on the spacecraft without interference. Allowing the empirical accelerations to be estimated would provide more precise orbits, but would not necessarily provide as meaningful results because of possible complications of the empirical accelerations absorbing some of the forces due to drag on the spacecraft.

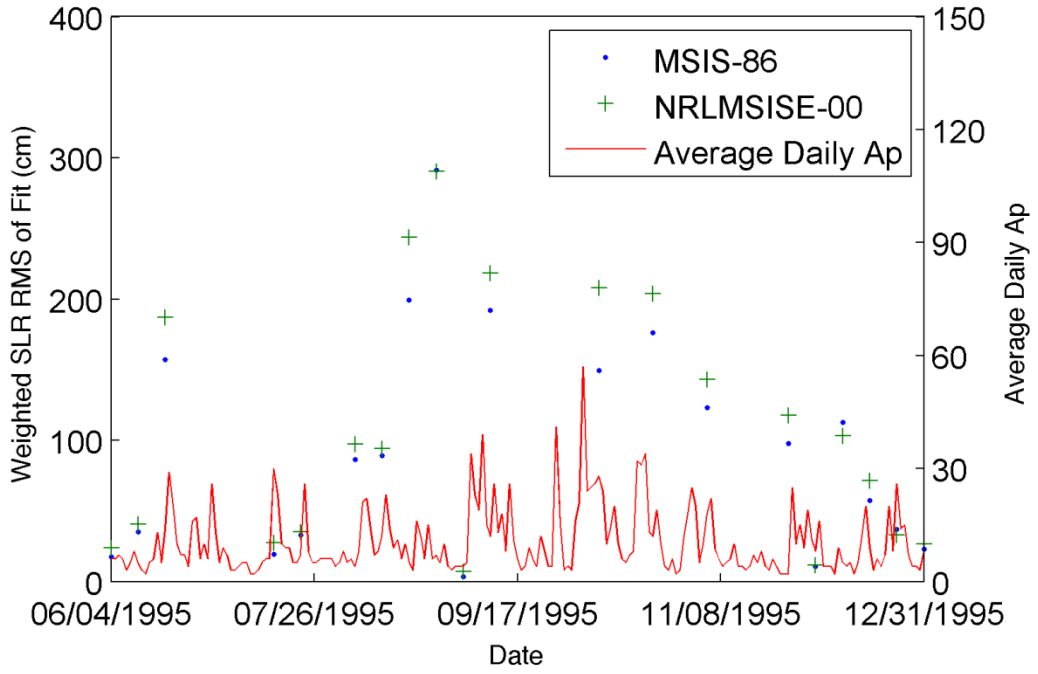

Figure 5.45 1995 GFZ-1 SLR RMS of Fit with Ap.

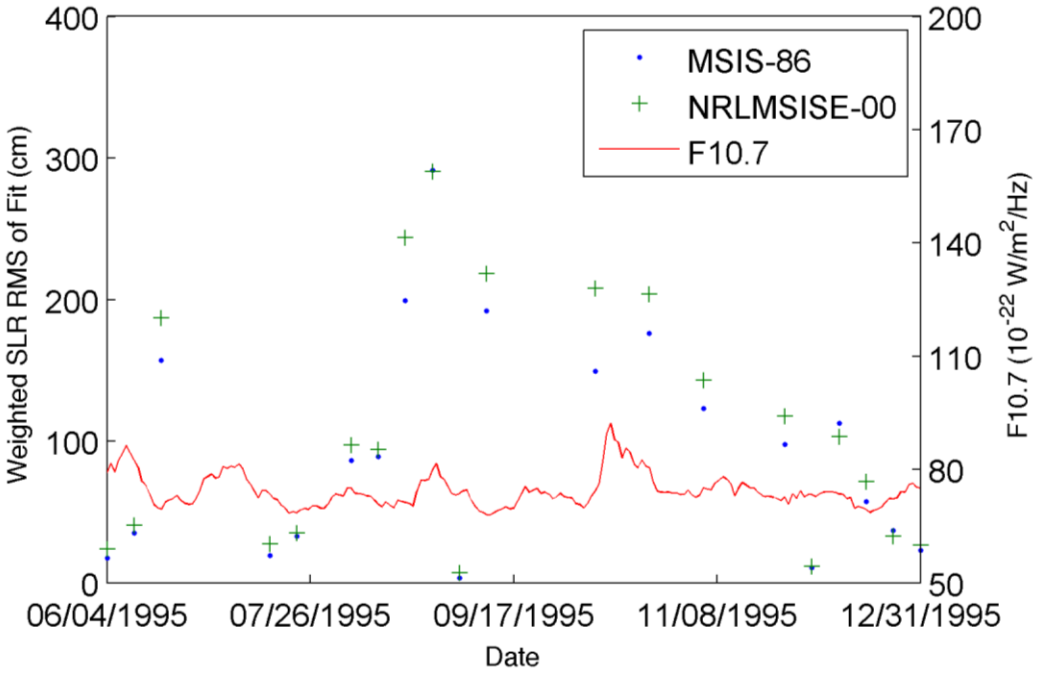

Figure 5.46 1995 GFZ-1 SLR RMS of Fit with F10.7.

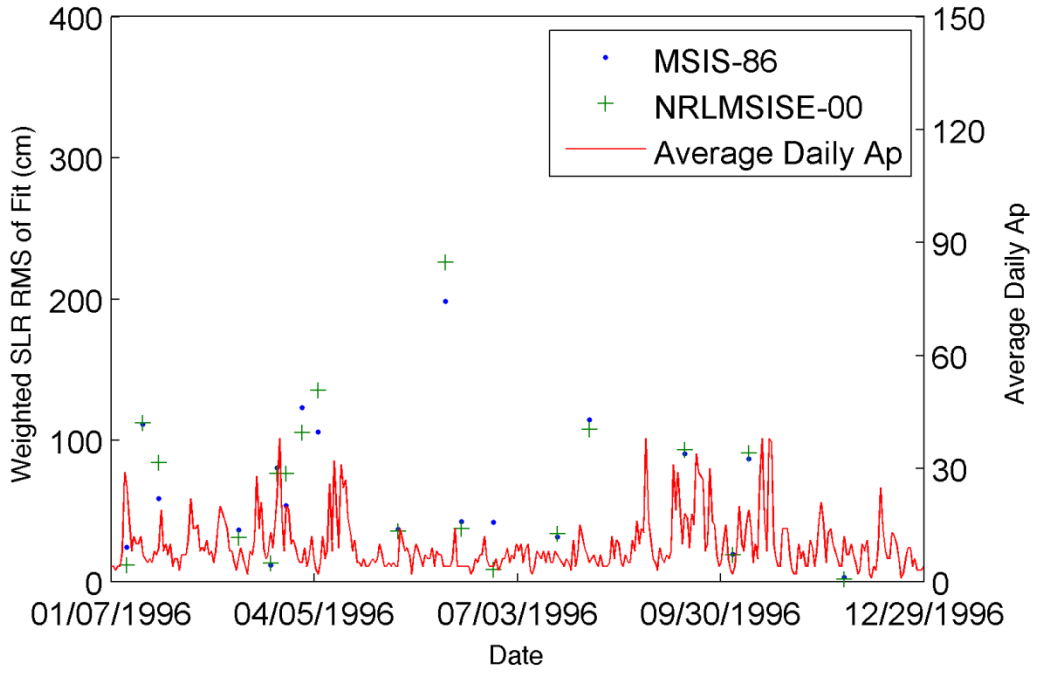

Figure 5.47 1996 GFZ-1 SLR RMS of Fit with Ap.

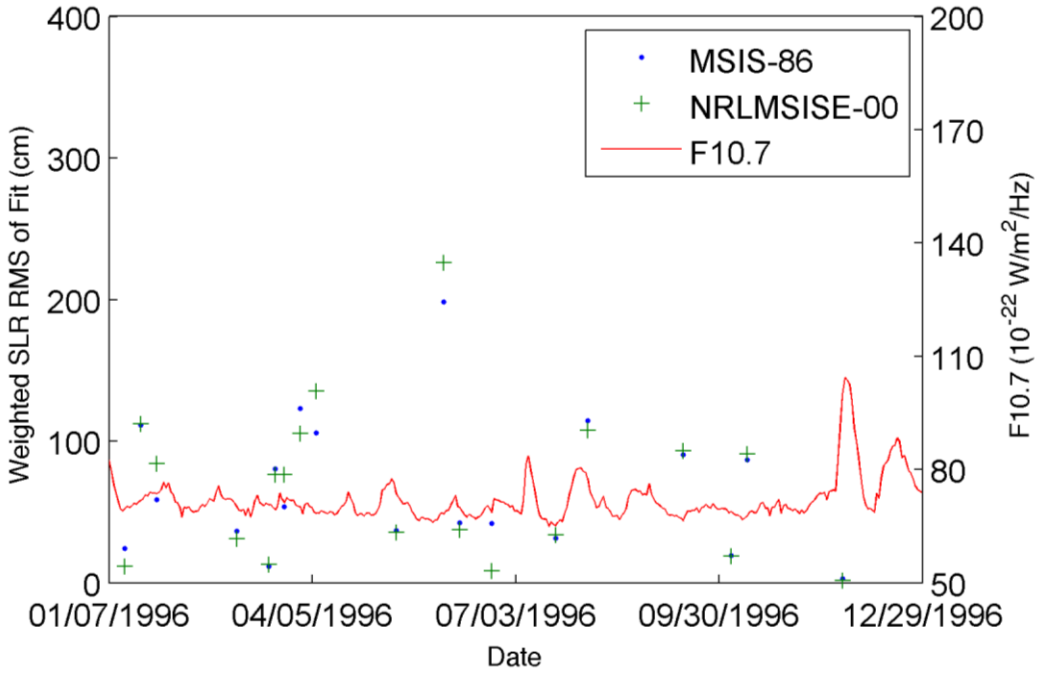

Figure 5.48 1996 GFZ-1 SLR RMS of Fit with F10.7.

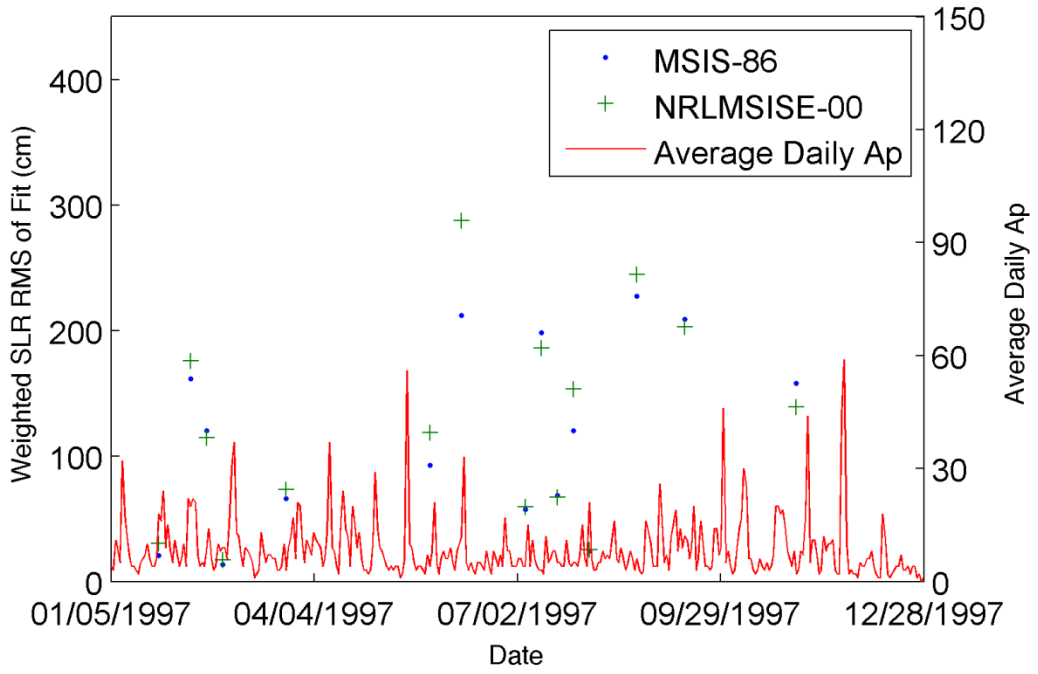

Figure 5.49 1997 GFZ-1 SLR RMS of Fit with Ap.

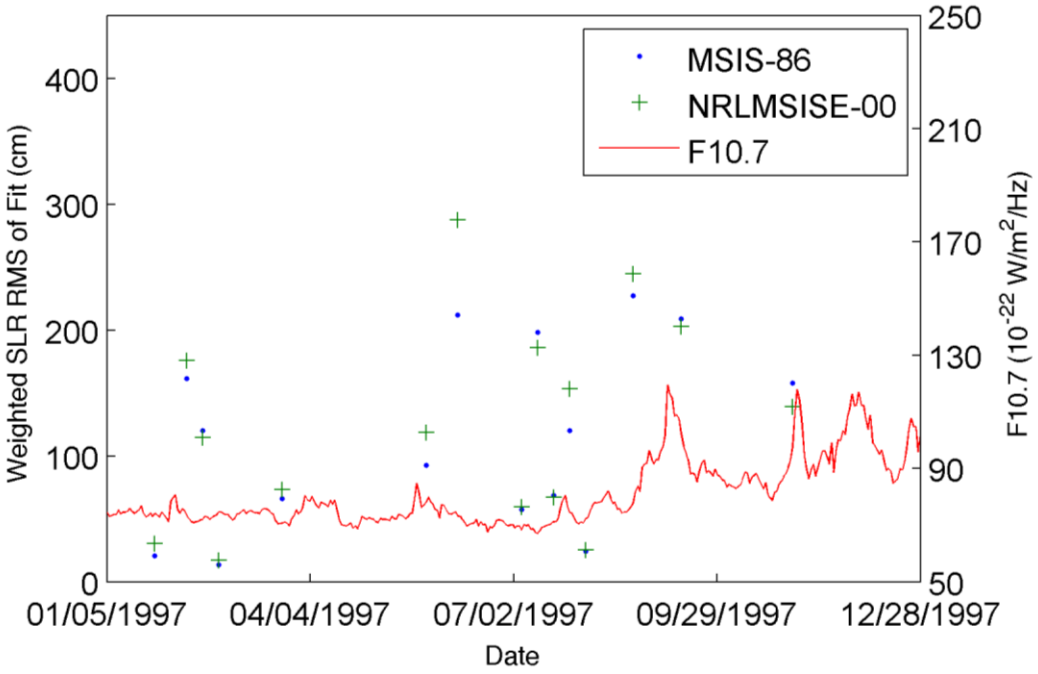

Figure 5.50 1997 GFZ-1 SLR RMS of Fit with F10.7.

Table 5.11 GFZ Yearly Average of Daily SLR RMS of Fit (cm).

Density Routine	1995	1996	1997
MSIS-86	95.5	69.2	110.4
NRLMSISE-00	109.1	72.5	120.0

Table 5.11 shows the SLR RMS of fit values averaged by year. The MSIS-86 routine performs consistently better for the three years of data analyzed. This is only further reinforced when looking at the SLR RMS plots.

5.4 Summary of Results

The three satellites analyzed in this section produced results consistent with the processing of GFO. The Stella and Starlette satellites returned SLR RMS values which showed a marginal improvement with the NRLMSISE-00 routine. These satellites also reinforced the fact that the DCA corrections are not designed for these altitudes. The drag coefficient study of the Starlette and Stella satellites showed nearly exactly the same trend. The drag coefficients estimated in the DCA correction version of GEODYN were vastly different than the other two versions. This reinforces the results found from GFO and is likely due to the mismodeling of the atmospheric density. If the density is mismodeled, the drag coefficient has to incorporate the error in order to balance the drag equation.

Many of the arcs provided by NASA GSFC did not converge using GEODYN with or without empirical accelerations estimated. Variations in the atmosphere become more apparent at lower altitudes. These variations cause difficulties tracking

satellites because of a challenge in predicting the orbit. When this is coupled with the very short amount of time for each pass, limited tracking data is usually the result. The arcs that could be processed suggested that the MSIS-86 routine was better at modeling the variations in the atmosphere at the lower altitude of GFZ-1. Doing drag studies with GFZ-1 has come under question due to its inconsistent surface. Bowman [Ref. 80] suggests that GFZ-1 is not suitable for a drag coefficient study because the corner reflectors for SLR observations are recessed into the sphere. According to Bowman, this causes the drag coefficient to have an effective shape of a cylinder flying with its main axis in the along-track direction.

6 SUMMARY, CONCLUSIONS, AND FUTURE WORK

6.1 Summary

Modeling forces on a spacecraft as accurately as possible is crucial to producing precise estimates and/or predictions of a satellite's orbit. Advances in conservative force modeling have reduced errors due to geopotential sources considerably in the past several years. These advancements have now switched the dominant error source for some satellites to the non-conservative forces such as solar radiation pressure, Earth albedo, Earth IR, and atmospheric drag. In periods of high solar activity, the variability of atmospheric drag causes the error due to drag modeling to become one of the highest of all non-conservative forces. For this reason, increasing the accuracy and fidelity of atmospheric density models is crucial in order to further increase the accuracy of orbit determination during these times.

Some satellites carry accelerometers on board to measure the accelerations imparted to the spacecraft. These accelerations can be converted to atmospheric drag by modeling all of the forces on the spacecraft to the highest degree possible and considering the remainder to be atmospheric drag. However, complications exist when converting the acceleration due to drag into atmospheric density because of difficulties predicting the interaction between the atmosphere and the spacecraft. At satellite altitudes, the atmosphere consists of free floating particles, and can no longer be considered a continuum fluid. This means that typical approaches to estimating the drag force must be modified. Approaching drag estimation for satellites requires as

much knowledge as possible of the atmosphere any given spacecraft is traveling through. This includes the density of the neutral particles, charged particles, the constituents of the atmosphere and precise knowledge of the spacecraft's position, geometry and attitude. These effects are increased with lower satellite mass, higher satellite area, and lower orbit. This interaction influences the coefficient of drag which is the factor balancing the acceleration due to drag and the density in the drag equation.

One objective of this research was to investigate a method of determining ballistic coefficient values from two line element sets (TLE). The ballistic coefficient is defined as the ratio C_DA/m which appears in the drag equation. This is actually the inverse of the traditional formulation of the ballistic coefficient. TLEs are based on radar and optical observations and are thus not nearly as accurate as other tracking methods. Using two line element sets is advantageous because of the multitude of satellites cataloged over the last several decades. Ballistic coefficients provided using this method can be determined quickly without significant resources since TLEs are widely available. The BCs generated from this research can be used to find rough approximations of fixed drag coefficient values.

Creating corrections to existing density models has become a popular way of capturing more accuracy in atmospheric models. Corrections to the NRLMSISE-00 empirical model of the atmosphere have been generated using the dynamic calibration of the atmosphere technique. This research tests the performance of the NRLMSISE-00 empirical density model and the corrections to that model using the GEODYN

precision orbit determination and parameter estimation program. Any improvements using these new density routines will provide a direct benefit to orbit estimation which has the potential to improve science data. This research also has the potential to improve prediction and determination for lower accuracy orbits which would improve catalog maintenance.

The new density routines were first tested on the GEOSAT Follow-on (GFO) satellite altimeter. Due to a failure of GPS receivers just after deployment, maintaining the accuracy of this satellite has been a challenge. By utilizing SLR and DORIS observations and a state-of-the-art geopotential model, orbit error in the radial direction for GFO was reduced considerably. The upgraded density models have the potential to improve the precise orbits for GFO during the most recent solar maximum by better modeling the atmospheric drag forces on the spacecraft. Three versions of GEODYN were analyzed; an original version of GEODYN with the MSIS-86 density routine, a version with the NRLMSISE-00 model, and a version with the NRLMSISE-00 density model with DCA corrections.

First, the years of 2000-2002 and 2005 were run for the GFO satellite with the three versions of GEODYN while estimating empirical accelerations once per revolution. The OPR accelerations soak up force modeling errors, leading to a more accurate estimation of the orbit. GFO was then run with the GEODYN versions again without estimating the empirical accelerations. In each case, the SLR and altimeter crossover residuals, and orbit overlaps were used as metrics of comparison. The results were also binned by solar and geomagnetic activity levels to determine any

correlation. For the runs with empirical accelerations estimated, the actual values estimated for the empirical accelerations were plotted and binned to determine any change between density models. For the runs without empirical accelerations estimated, the drag coefficient estimated every eight hours by GEODYN was extracted and compared for each version of GEODYN.

To investigate the performance of the routines further, three more satellites were analyzed using the three different versions of GEODYN without empirical accelerations estimated; Stella, Starlette, and GFZ-1. The Stella and Starlette satellites were evaluated from 2000-2004 using the same metrics of comparison as GFO. The GFZ satellite was short-lived; only three years of data was available for processing because of difficulties with SLR measurements; 1995-1997. The GFZ-1 satellite could not be evaluated for orbit overlaps or for binned values because of the sparse tracking data.

6.2 Conclusions

6.2.1 Ballistic Coefficient Generation Technique

After analyzing the results of the ballistic coefficient generation technique utilized in this research, the following conclusions can be made:

1. The performance of the ballistic coefficient generation routine is reasonable for lower LEO satellites in the 2001-2004 period.

2. Satellites with perigee altitudes below 500 km achieved an 8.2% error on average where the satellites with perigee altitudes around 800 km had errors significantly over 100%.
3. The poor performance at higher altitudes is mostly due to drag becoming less significant and partly a result of the HASDM density routine not being suitable for altitudes above 600 km. There may also be an issue with observability or accuracy due to the densities being so much lower at higher altitudes.
4. The BCs of the CHAMP satellite have tended to decrease going into the 2008 solar minimum. This could either be a result of a change in the constituency of the atmosphere, or a result of the HASDM model overestimating the density.

The results of this ballistic coefficient study were reasonable based on the quality of the data used. Since TLEs are not nearly as accurate as other tracking methods, differences of 8.2% from analytical methods for satellites below 500 km is promising for this routine. The trend for the CHAMP satellite to have decreasing BC values into the 2008 solar minimum is difficult to analyze because of the waning of solar activity coinciding with the decrease in the satellite's altitude.

6.2.2 GFO Processing with Empirical Accelerations Estimated

For the GFO satellite processed using the three versions of GEODYN described above, the following conclusions can be made:

1. The analysis of empirical accelerations indicated a marginal improvement in the along-track direction for the new density routines in 2000 and 2001. These are periods of higher solar activity so not surprisingly, when the data was binned into solar activity levels, the newer routines performed slightly better at the highest solar activity level.
2. When binned into geomagnetic activity levels, the new routines performed better at the less active geomagnetic conditions.
3. No one routine was found to be consistently superior over the others in any of the averages done using empirical accelerations.
4. In the residual study performed with SLR RMS values, the averaging produced mixed results. No improvement or worsening of more than around one millimeter were found, but slight improvements using the new density routines were found for elevated and high solar activity and moderate and active geomagnetic conditions.
5. The altimeter crossovers contradicted the SLR RMS averages slightly. The averaging done with these indicated a preference for MSIS-86 in virtually all cases except active geomagnetic conditions.
6. The orbit overlaps showed some improvement for the new density routines in three of the four years run. These improvements were on the order of centimeters in most cases.

Processing with empirical accelerations estimated produced rather inconsistent and marginal results. For the most part, all routines returned similar

results. The SLR RMS analysis indicated a slight improvement for some conditions with the new density routines. This is the most significant conclusion because the SLR analysis is the best metric of comparison that can be performed due to the high accuracy of the SLR tracking data. The mixed results indicated the need for further investigation into the performance by removing the estimation of OPR empirical accelerations.

6.2.3 GFO Processing without Empirical Accelerations Estimated

After analyzing the results of the GFO satellite processed using the three versions of GEODYN without the empirical accelerations estimated, the following conclusions can be made:

1. The new density routines improved SLR RMS values for every year run except 2000. The SLR RMS values were much higher due to the removal of the estimated empirical accelerations, so the improvements were much larger.
2. When the SLR RMS values were binned by solar activity, each bin showed a preference for the new routines.
3. The SLR RMS values binned by geomagnetic activity indicated the new routine only showed improvement in the quiet activity level.
4. The 2002 and 2005 yearly averaged altimeter crossovers were improved by the new density routines, but the 2000-2001 averages were not.

However, when binned by solar activity levels, every bin except the elevated level was improved by the new routines.

5. The geomagnetic activity bins for altimeter crossovers showed that the new routine only improved quiet conditions.
6. The orbit overlaps indicated the same trend as the SLR RMS values when looking at the yearly averages in the along-track direction. The 2000-2001 years had a clear preference for the MSIS-86 routine, while the 2002 and 2005 years were improved by the new routines.
7. One of the most significant findings of this research was the way GEODYN estimated the drag coefficient using each of the density routines. The MSIS-86 and NRLMSISE-00 routines produced very similar drag coefficients when extracted from GEODYN, but the NRLMSISE-00 version with the corrections did not correlate with the other two routines.

The most important finding from this section are in the plots of the drag coefficient. The fact that the NRLMSISE-00 routine with the DCA corrections produced in most cases very similar results, but estimated the drag coefficient so differently is very surprising. This indicates the drag coefficient was absorbing significant error in modeling the drag force on the spacecraft while processing.

6.2.4 Conclusions from Additional Satellites Processed

1. The Stella satellite indicated little improvement from the new density routines through SLR residuals. The NRLMSISE-00 routine was

marginally better than the MSIS-86 routine for 2000 and 2003, but the only solar or geomagnetic activity level bin that was improved was an elevated solar condition. These changes were very slight, in all cases they were less than one millimeter.

2. The orbit overlaps for Stella were not improved at all by the new density models.
3. The drag coefficient analysis for Stella suggested the same behavior when analyzing the DCA correction routine. The C_D values for the DCA routine did not correlate well at all with the other two routines.
4. Starlette indicated more improvement from the MSIS-86 routine when examining the SLR RMS values. The NRLMSISE-00 routine was found to be an improvement for every year averaged except for 2003 and for every binned average of both solar and geomagnetic activity. Again, these changes were very slight, with each being on the order of one millimeter.
5. The orbit overlaps for Starlette produced mixed results; 2000, 2002, and 2004 were all improved by the new NRLMSISE-00 model, while 2001 and 2003 were not.
6. The drag coefficient for Starlette exhibited the same behavior as the other satellites processed. The drag coefficient estimated using the DCA correction routine produced C_D values which did not correlate with the other two routines processed.

7. The GFZ-1 satellite had a limited amount of useable arcs, so the only comparison that could be performed was a yearly averaging of the SLR RMS values. The MSIS-86 routine was found to be superior in each of the three years.

Since Stella is in a near-circular, retrograde orbit of 98.6 degrees, the results are more significant than that of Starlette. Stella remains in the atmosphere longer than Starlette because of its circular orbit compared to the elliptical orbit of Starlette, and covers more latitude due to its inclination. Stella did not show promising improvements using any method of comparison, so this carries more weight than the improvements made by Starlette.

The findings of the drag coefficient analysis reinforce what was found in the GFO study. The drag coefficient for the DCA routine suggests there are problems using this routine to derive precise orbits reliably at these altitudes. This is likely a result of the corrections not being suitable for altitudes above 600 km.

6.3 Future Work

6.3.1 Ballistic Coefficient Processing Technique

In the future, the ballistic coefficient routine should be incorporated with multiple density models directly. This would allow for an even quicker process. Currently, the program relies on external processing to determine the HASDM density, but if this were to be incorporated into the routine along with other density

models, the program would be more robust. Since the routine has potential to be very quick and easy, the run time for the current version of the program should be reduced so that large numbers of satellites can be processed quickly. The results of this study should be compared with other software such as GEODYN for further validation. After the above are done and the results are validated, a ballistic coefficient database should be generated and distributed.

Another future venture for the ballistic coefficient processing technique would be to investigate a possible change in atmospheric composition during the most recent solar minimum. This coincides with the possibility that the HASDM density model could be overestimating density during the most recent solar minimum.

The drag coefficient values estimated by GEODYN could be compared to the ballistic coefficient values obtained using the TLE processing method to determine the correlation between the two techniques. Since the GEODYN values are more precise, the drag coefficient values from GEODYN could be used as another verification technique.

6.3.2 Investigation into Density Model Upgrades

In order to find out the true benefit of the DCA corrections, corrections will need to be generated that are valid up to 800 km or higher. Since the original corrections have already been incorporated into GEODYN, updating to a new density correction model should just be a matter of replacing the original coefficients with the updated versions once they are known. The new set of corrections should show

significant improvement on the routines presented here since the coefficients generated will be calculated directly from space objects affected in the same time span and in the same regime.

The potential for the current DCA corrections to NRLMSISE-00 to improve drag modeling could be verified by examining satellites at altitudes and time frames the corrections are valid for, such as the ANDE satellites.

The peculiar behavior exhibited in the drag coefficient analysis of each satellite must be investigated further to find the true source of the lack of correlation between the DCA corrections and the NRLMSISE-00 routine itself. This could be accomplished by fixing the drag coefficient throughout the computation of each arc and analyzing the results. When the new corrections are incorporated, a detailed analysis must be performed to ensure the same phenomenon does not occur.

A detailed comparison study using multiple orbit determination packages should be performed to further verify results obtained using this analysis. This will help to completely verify the validity of the density modeling improvements seen in this work. If the improvements are seen to be significant, the updated density models will be used to further enhance altimeter data for the GEOSAT Follow-on spacecraft by incorporating them into a future release of GEODYN.

REFERENCES

1. J. M. Picone, A. E. Hedin, D. P. Drob, and A. C. Aikin, "NRLMSISE-00 empirical model of the atmosphere: Statistical comparisons and scientific issues," *Journal of Geophysical Research*, 107 (A12), 1468, doi: 10.1029/2002JA009430, 2002.
2. M. F. Storz, B. R. Bowman, Major J. I. Branson, S. J. Casali, and W. K. Tobiska, "High Accuracy Satellite Drag Model (HASDM)," *Advances in Space Research*, Vol. 36, Issue 12, 2005, pp. 2497-2505.
3. D. A. Vallado, *Fundamentals of Astrodynamics and Applications*, Microcosm Press, El Segundo, CA, 3rd Edition, 2007, Chap. 8, App. B.
4. Y. P. Gorochov, and A. I. Nazarenko "Methodical Points in Building Models of the Fluctuations of the Atmosphere Parameters." *Astronomicheskii Sovet Akademii Nauk SSSR*, Vol. 80, 1982. Translated to English by K. Galabova (MIT), February 2004. The English translation is available from P. Cefola (cefola@mit.edu).
5. M. P. Wilkins, C. A. Sabol, P. J. Cefola, and K. T. Alfriend, "Discourse on corrections to the NRLMSISE-00 Atmospheric Density Model," *Proceedings of the 7th US / Russian Space Surveillance Workshop*, Naval Postgraduate School, Monterey, CA, 29 October – 2 November 2007, pp. 273-293.
6. B. D. Tapley, B. E. Schutz, G. H. Born, *Statistical Orbit Determination*, Elsevier Academic Press, Burlington, MA, 2004, Chap. 1, App. B.
7. F. G. Lemoine, S. C. Kenyon, J. K. Factor, R. G. Trimmer, N. K. Pavlis, D. S. Chinn, C. M. Cox, S. M. Klosko, S. B. Luthcke, M. H. Torrence, Y. M. Wang, R. G. Williamson, E. C. Pavlis, R. H. Rapp, and T. R. Olson, "The Development of the Joint NASA GSFC and National Imagery and Mapping Agency (NIMA) Geopotential Model EGM96," NASA TP/-1998-206861, NASA Goddard Space Flight Center, July 1998.
8. B. Tapley, S. Bettadpur, M. Watkins, C. Reigber "The Gravity Recovery and Climate Experiment: Mission Overview and Early Results," *Geophysical Research Letters*, Vol. 31, L09607, doi:10.1029/2004GL019920, 2004.
9. B. Tapley, J. Ries, S. Bettadpur, D. Chambers, M. Cheng, F. Condi, B. Gunter, Z. Kang, P. Nagel, R. Pastor, T. Pekker, S. Poole, and F. Wang, "GGM02 - An Improved Earth Gravity Field Model from GRACE," *Journal of Geodesy*, Volume 79, Issue 8, pp.467-478
10. C. Reigber, P. Schwintzer, R. Stubenvoll, R. Schmidt, F. Flechtner, U. Meyer, R. König, H. Neumayer, C. Förste, F. Barthelmes, S. Zhu, G. Balmino, R. Biancale, J.-M. Lemoine, H. Meixner, and J. C. Raimondo, "A high resolution global gravity field model combining CHAMP and GRACE

satellite mission and surface data: EIGEN-CG01C," Scientific Technical Report, GFZ Potsdam, in print, 2006.
11. C. M. Cox, F. G. Lemoine, "Precise Orbit Determination of the Low Altitude Spacecraft TRMM, GFZ-1, and EP/EUVE Using Improved Drag Models," *Spaceflight Mechanics 1999*, Vol. 102 of *Advances in the Astronautical Sciences*, 1999, AAS 99-189, pp. 1277-1296.
12. A. C. Tribble, *The Space Environment: Implications for Spacecraft Design*, Princeton University Press, Princeton, New Jersey, 2003.
13. J. K. Hargreaves, *The Solar-Terrestrial Environment*, Cambridge University Press, Cambridge, 1992.
14. M. Ziebart, S. Adhya, Ant Sibthrope, and P. Cross, "GPS Block IIR Non-Conservative Force Modeling: Computation and Implications," *Proceedings of ION GPS/GNSS 2003*, Portland, Oregon, USA, 2003.
15. S. Casotto, *Nominal Ocean Tide Models for TOPEX Precise Orbit Determination*, PhD Dissertation, University of Texas at Austin, 1989.
16. R. S. Nerem, B. H. Putney, J.A. Marshall, F. J. Lerch, E. C. Pavlis, S. M. Klosko, S. B. Luthcke, G. B. Patel, R. G. Williamson, and N. P. Zelensky, "Expected Orbit Determination Performance for the TOPEX/Poseidon Mission," *IEEE Transactions on Geoscience and Remote Sensing*, Vol. 31, No. 2, March 1993.
17. F. G. Lemoine, N. P Zelensky, S. B. Luthcke, D. D. Rowlands, D. S. Chinn, B. D. Beckley, and S. M. Klosko, "13 Years of TOPEX/Poseidon Precision Orbit Determination and the 10-fold Improvement in Expected Orbit Accuracy," *AIAA/AAS Astrodynamics Conference*, Keystone, Colorado, August 21-24, 2006, AIAA 2006-6672.
18. S. B. Luthcke, N.P. Zelensky, D. D. Rowlands, F.G. Lemoine, T.A. Williams, "The 1-Centimeter Orbit: Jason-1 Precision Orbit Determination Using GPS, SLR, DORIS, and Altimeter Data," *Marine Geodesy*, Vol. 26, p.p. 399-421, 2003.
19. C. A. McLaughlin, A. Hiatt, E. Fattig, T. Lechtenberg, "Ballistic Coefficient and Density Estimation," *AAS/AIAA Astrodynamics Specialist Conference*, Pittsburgh, PA, USA, Aug 9-13, 2009, AAS 09-439.
20. B. R. Bowman, "True Satellite Ballistic Coefficient Determination for HASDM," *AIAA/AAS Astrodynamics Specialist Conference*, Monterey, California, USA, Aug 5-8, 2002, AIAA 2002-4887.
21. C. Pardini, L. Anselmo, K. Moe, M. M. Moe, "Drag and Energy Accommodation Coefficients During Sunspot Maximum," *Advances in Space Research*, Vol. 45, No. 5, 2010, pp. 638-650.
22. G. E. Cook, "Satellite Drag Coefficients," *Planetary and Space Science*, Vol. 13, No. 10, 1965, pp. 929-946.

23. K. Moe, M. M. Moe and S. D. Wallace, "Improved Satellite Drag Coefficient Calculations from Orbital Measurements of Energy Accommodation," *Journal of Spacecraft and Rockets*, Vol. 35, No. 3, May-June 1998 pp. 266-272.
24. K. Moe, M. M. Moe and S. D. Wallace, "Drag Coefficients of Spheres in Free-Molecular Flow," *Advances in the Astronautical Sciences*, Vol. 93, No. 1, 1996, AAS 96-126 , pp. 391-406.
25. K. Moe and M. M. Moe, "Gas-surface interactions and satellite drag coefficients*," Planetary and Space Science*, Vol. 53, 2005, pp. 793-801.
26. E. M. Gaposchkin, "Calculation of Satellite Drag Coefficients," Technical Report 998, Lincoln Laboratory, MIT, Lexington, MA, USA, 18th July, 1994.
27. J. A. Storch, "Aerodynamic Disturbances on Spacecraft in Free-Molecular Flow," Aerospace Report 2003(3397)-1.
28. M. M. Moe, S. D. Wallace, and K. Moe, "Refinements in Determining Satellite Drag Coefficients: Method for Resolving Density Discrepancies," *Journal of Guidance, Control, and Dynamics*, Vol. 16, No. 3, pp. 441-445, May-June 1993.
29. P. C. E. Roberts, "Computational Modeling of Aerodynamic Disturbances of Spacecraft within a Concurrent Engineering Framework," PhD Thesis, Cranfield University, 2007.
30. D. Offermann, K. U. Grossmann, "Thermospheric Density and Composition as Determined by a Mass Spectrometer with Cryno Ion Source," *Journal of Geophysical Research*, Vol. 78, 1973, pp. 8296-8304.
31. T. Ondoh, K. Marubashi, *Science of Space Environment*, Ohmscha, Ltd. Japan, 2000, pp. 9-13.
32. E. K. Sutton, "Normalized Force Coefficients for Satellites with Elongated Shapes," *Journal of Spacecraft and Rockets*, v. 46, No. 1, 2009, pp. 112-116.
33. L. H. Sentman, "Free Molecule Flow Theory and its Application to the Determination of Aerodynamic Forces," Lockheed Missile and Space Co. Sunnyvale, Ca, TR LMSC-448514, AD 265-409, 1961.
34. R. A. Schamberg, "New Analytic Representation of Surface Interaction for Hyperthermal Free Molecular Flow," Rand Corporation, TR RM-2312, 1959.
35. L. G. Jacchia, *Revised Static Models for the Thermosphere and Exosphere with Empirical Temperature Profiles*, SAO Special Report No. 313, Cambridge, MA: Smithsonian Intuition Astrophysical Observatory, 1971.
36. A. E. Hedin, "MSIS-86 Thermospheric Model," *Journal of Geophysical Research*, Vol. 92, No A5, pp. 4649-4662, 1987.
37. A. E. Hedin, "Extension of the MSIS Thermosphere Model into the Middle and Lower Atmosphere," *Journal of Geophysical Research*, 96, pp. 1159-1172, 1991.

38. S. J. Casali, and W. N. Barker, "Dynamic Calibration Atmosphere (DCA) for the High Accuracy Satellite Drag Model (HASDM)" *AIAA/AAS Astrodynamics Specialist Conference*, Monterey, CA, Aug 5-8, 2002, AIAA 2002-488.
39. F. A. Marcos, M. J. Kendra, J. M. Griffin, J. N. Bass, D. R. Larson, and J. J. Liu, "Precision Low Earth Orbit Determination using Atmospheric Density Calibration," *Journal of the Astronautical Sciences*, Vol. 46, No. 4, October-December 1998, pp. 395-409.
40. V. S. Yurasov, A. I. Nazarenko, "Atmosphere Density Tracking (Stage 1)," Report of progress prepared under an agreement with the Texas Engineering Experiment Station, Moscow, Russia, June 2007.
41. V. S. Yurasov, A. I. Nazarenko, "Atmosphere Density Tracking (Stage 2)," Report of progress prepared under an agreement with the Texas Engineering Experiment Station, Moscow, Russia, November 2007.
42. P. J. Cefola, "Summary Comments on the Atmosphere Density Tracking Study Stage 1 and Stage 2 Reports," *AIAA/AAS Astrodynamics Specialist Conference*, Honolulu, Hawaii, Aug. 18-21, 2008, AIAA-2008-6440.
43. V. S. Yurasov, A. I. Nazarenko, K. T. Alfriend, and P. J. Cefola, "Direct Density Correction Method: Review of Results," IAC-06-C1.5.02, *57th International Astronautical Congress*, Valencia, Spain, Oct. 2-6, 2006
44. V. S. Yurasov, A. I. Nazarenko, P. J. Cefola, and K. T. Alfriend, "Results and Issues of Atmospheric Density Correction," *Journal of the Astronautical Sciences*, Vol. 52, No. 3, July-September 2004, pp. 281-300.
45. V. S. Yurasov, A. I. Nazarenko, K. T. Alfriend, and P. J. Cefola, "Reentry Time Prediction Using Atmospheric Density Corrections," *Journal of Guidance, Control, and Dynamics*, Vol. 31, No. 2, March-April 2008, pp. 282-289.
46. A. T. Hiatt, "Deriving Atmospheric Density Estimates Using Satellite Precision Orbit Ephemerides," M.S. Thesis, University of Kansas, 2009.
47. C. Reigber, H. Lühr, P. Schwintzer (Eds.), *First CHAMP Mission Results for Gravity, Magnetic and Atmospheric Studies*, Springer-Verlag Berlin Heidelberg New York, 2003
48. R. Konig and K. H. Neumayer, "Thermospheric Events in CHAMP Precise Orbit Determination," *First CHAMP Mission Results for Gravity, Magnetic and Atmospheric Studies*, eds. C. Reigber, H. Luhr, P. Schwintzer, Springer, Berlin, 2003, pp. 112-119.
49. S. Bruinsma and R. Biancale, "Total Densities Derived from Accelerometer Data," *Journal of Spacecraft and Rockets*, Vol. 40, No. 2, pp. 230-236, March-April 2003.

50. S. Bruinsma, D. Tamagnan, and R. Biancale, "Atmospheric densities derived from CHAMP/STAR accelerometer observations," *Planetary and Space Sciences*, Vol. 52, 2004 , pp. 297-312.
51. D. E. Pavlis, S. Poulose, and J. J. McCarthy (2006), GEODYN operations manuals, contractor report, SGT Inc., Greenbelt, Md.
52. M. Torrence, and C. Noll, "Satellite Missions," International Laser Ranging Service Web Site, Last Accessed: April 21, 2010, http://ilrs.gsfc.nasa.gov/satellite_missions/list_of_satellites/
53. M. Torrence, and C. Noll, "Satellite GFO," International Laser Ranging Service Web Site, Last Accessed: February 23, 2010, http://ilrs.gsfc.nasa.gov/satellite_missions/list_of_satellites/gfo1_general.html
54. F. G. Lemoine, N. P. Zelensky, D. S. Chinn, B. D. Beckley, J. L. Lillibridge, "Towards the GEOSAT Follow-On Precise Orbit Determination Goals of High Accuracy and Near-Real-Time Processing," *AIAA/AAS Astrodynamics Conference*, Keystone, CO, USA, August 21-24, 2006, AIAA 2006-6402.
55. J. Lillibridge, W. Smith, D. Sandwell, R. Scharoo, F. G. Lemoine, and N. P. Zelensky, "20 Years of Improvements to GEOSAT Altimetry," *Symposium: 15 Years of Progress in Radar Altimetry*, Venice, Italy, March 13-18, 2006
56. F. G. Lemoine, C. M. Cox, N. P. Zelensky, S. B. Luthcke, B. F. Thompson, D. D. Rowlands, D. S. Chinn, and R. S. Nerem, "Gravity models from CHAMP and other satellite data," *EOS Trans. AGU*, 84(46), Fall Meeting Suppl., Abstract G32A-0730, 2003
57. M. Torrence, and C. Noll, "Satellite CHAMP," International Laser Ranging Service Web Site, Last Accessed: February 23, 2010, http://ilrs.gsfc.nasa.gov/satellite_missions/list_of_satellites/cham_general.html
58. M. Torrence, and C. Noll, "Satellite GRACE-A," International Laser Ranging Service Web Site, Last Accessed: February 23, 2010, http://ilrs.gsfc.nasa.gov/satellite_missions/list_of_satellites/graa_general.html
59. C. Dunn, W. Bertiger, Y. Bar-Sever, S. Desai, B. Haines, D. Kuang, G. Franklin, I. Harris, G. Kruizinga, T. Meehan, S. Nandi, D. Nguyen, T. Rogstad, J. B. Thomas, J. Tien, L. Romans, M. Watkins, S. Wu, S. Bettadpur, and J. Kim, "Instrument of GRACE: GPS augments gravity measurements," *GPS World*, 14(2), 16-28, 2003.
60. M. Torrence, and C. Noll, "Satellite ANDE-RR_Active," International Laser Ranging Service Web Site, Last Accessed: February 23, 2010, http://ilrs.gsfc.nasa.gov/satellite_missions/list_of_satellites/anra_general.html
61. A. C. Nicholas, J. M. Picone, J. Emmert, J. DeYoung, L. Healy, L. Wasiczko, M. Davis, and C. Cox, "Preliminary Results from the Atmospheric Neutral

Density Experiment Risk Reduction Mission," *Advances in the Astronautical Sciences,* Vol. 129, No. 1, 2007, AAS 07-265, pp. 243-254.
62. Pearlman, M.R., Degnan, J.J., and Bosworth, J.M., "The International Laser Ranging Service", *Advances in Space Research*, Vol. 30, No. 2, pp. 135-143, July 2002, DOI:10.1016/S0273-1177(02)00277-6.
63. M. Torrence, and C. Noll, "Satellite Stella," International Laser Ranging Service Web Site, Last Accessed: February 23, 2010, http://ilrs.gsfc.nasa.gov/satellite_missions/list_of_satellites/stel_general.html
64. J. G. Marsh, and R. G. Williamson, "Precision orbit computations for Starlette," *Journal of Geodesy*, Vol. 52, No. 1, pp. 71-83, March 1978.
65. G. Moore, "[Starshine] Project Description," Project Starshine Web Site, Last Accessed: February 23, 2010, http://www.azinet.com/starshine/descript.htm
66. G. Moore, "Project Starshine – Student Tracked Atmospheric Research Satellite," Project Starshine Web Site, Last Accessed: February 27, 2010, http://www.azinet.com/starshine/starshine2.html
67. G. Moore, "Project Starshine – Student Tracked Atmospheric Research Satellite," Project Starshine Web Site, Last Accessed: February 27, 2010, http://www.azinet.com/starshine/update111101.html
68. M. Torrence, and C. Noll, "Satellite GFZ-1," International Laser Ranging Service Web Site, Last Accessed: March 7, 2010, http://ilrs.gsfc.nasa.gov/satellite_missions/list_of_satellites/gfz1_general.html
69. T. S. Kelso, "Celestrak: NORAD Two-Line Element Set Format" CelesTrak web site, Last Accessed: March 16, 2010, http://celestrak.com/NORAD/documentation/tle-fmt.asp
70. J. M. Picone, J. T. Emmert, and J.L. Lean, "Thermospheric densities derived from spacecraft orbits: Accurate processing of two-line element sets," *Journal of Geophysical Research*, Vol. 110, A03301, 2005.
71. D. King-Hele, *Satellite Orbits in an Atmosphere: Theory and Applications*, Blackie, Glasgow, 1987
72 C. Förste, R. Schmidt, R. Stubenvoll, F. Flechtner, U. Meyer, R. König, H. Neumayer, R. Biancale, J. M. Lemoine, S. Bruinsma, S. Loyer, F. Barthelmes, and S. Esselborn, "The Geo Forschungs Zentrum Potsdam/Groupe de Recherche de Gèodésie Spatiale satellite-only and combined gravity field models: EIGEN-GL04S1 and EIGEN-GL04C," *Journal of Geodesy*, Vol. 62, No. 6, 2008, pp. 331-346.
73. R. D. Ray, "A Global Ocean Tide Model from TOPEX/Poseidon altimetry: GOT99.2," *NASA TM-1999-209478*, NASA Goddard Space Flight Center, September 1999.
74 M. P. Wilkins, C. A. Sabol, P. J. Cefola, and K. T. Alfriend, "Practical Challenges in Implementing Atmospheric Density Corrections to the

NRLMSISE-00 Model," *Spaceflight Mechanics 2006*, Vol. 124 of *Advances in the Astronautical Sciences*, Part I, 2006, AAS 06-170, pp. 1113-1130.
75. Carey Noll, "[SLR] Stations," ILRS Web Site, Last Accessed: March 17, 2010, http://ilrs.gsfc.nasa.gov/stations/index.html
76. D. A. Vallado, P. Crawford, R. Hujsak, and T. S. Kelso, "Revisiting Spacetrack Report #3," *AIAA/AAS Astrodynamics Specialist Conference*, Keystone, CO, 2006 August 21–24, AIAA-2006-6753.
77. Hoots, Felix R., and R. L. Roehrich. 1980. "Spacetrack Report #3: Models for Propagation of the NORAD Element Sets." U.S. Air Force Aerospace Defense Command, Colorado Springs, CO.
78. B. R. Bowman, F. A. Marcos, K. Moe, and M. M. Moe, "Determination of Drag Coefficient Values for Champ and Grace Satellites Using Orbit Drag Analysis," *Advances in the Astronautical Sciences*, Vol. 129, No. 1, 2008, AAS 07-259, pp. 147-166.
79. I.K. Harrison and G.G. Swinerd, "A free molecule aerodynamic investigation using multiple satellite analysis," *Planetary and Space Science*, Vol. 44, No. 2, 1996, pp. 171-180.
80. B. R. Bowman and K. Moe, "Drag Coefficient Variability at 175-500 km from the Orbit Decay Analyses of Spheres," *Advances in the Astronautical Sciences*, Vol. 129, No. 1, 2008, AAS 07-262, pp. 207-222.